Modeling Regional Variation of Cortical Spreading Depression: A Computational Study

A DISSERTATION
SUBMITTED TO THE FACULTY OF THE GRADUATE SCHOOL
OF THE UNIVERSITY OF MINNESOTA
BY

Austin Tuttle

IN PARTIAL FULFILLMENT OF THE REQUIREMENTS
FOR THE DEGREE OF
DOCTOR OF PHILOSOPHY

Yoichiro Mori

May, 2019

Acknowledgements

There are many people I would like to thank for their help, however small, to get me to where I am: Prof. John Mayberry for helping me discover and cultivate my love of math that sent me on this journey. The members of my cohort, without you I would not have made it through the first year of graduate school and beyond. My mom for supporting me all my life and driving me to do what I love. Prof. Yoichiro Mori for your advice and mentorship through our years working together. I have learned so much.

Lastly, my fiancee, you supported me throughout graduate school, putting up with my overly stressed states and distracted times of thought. You helped distract me from research and teaching.

Abstract

Cortical Spreading Depression(CSD) is a pathological phenomenon in the central nervous system in which normal cellular function is disrupted by a prolonged depolarization due to massive ionic fluxes. This spreads at a rate of millimeters per minute and is connected to with several medical conditions: migraine aura, stroke, traumatic brain injury, etc. In this thesis we present a multi-phasic continuum electrodiffusion model of spreading depression. The main result of this work is the efficient numerical simulation of 2D and 3D versions of this model. We make use of these simulations by focusing on the introduction of NMDA receptors and their effects on previous findings. From there, we investigate spatial variance of CSD in two ways. First, the natural occurrence of spiral wave patterns in a homogeneous domain. Second, we introduce spatial dependence of parameters to investigate how the varied structure of the hippocampus can impact CSD.

Contents

List of Tables

List of Figures

Chapter 1

Introduction

Cortical Spreading Depression (CSD) is a spreading depolarization in the brain (or central nervous system) that silences electrical activity for approximately 1 minute and travels at speeds of around 2-7 mm/min[10, 1]. CSD is characterized by massive ionic fluxes that make neurons unable to create action potentials during the duration of the spreading depolarization. Spreading depolarizations have been shown to appear during migraine and stroke. In migraine this phenomenon precedes headache symptoms by approximately 30 minutes before the headache of a migraine begins, in fact CSD appears to be the cause of the visual aura that some migraine sufferers report [39]. Spreading depolarizations have also been demonstrated in patients suffering from traumatic brain injury, ischemic stroke, subarachnoid hemorrhage, and intracerebral hematoma [23]. Since being first discovered by Leao [61], the details of the mechanisms behind CSD have been elusive[78, 102, 89].

- Chapter 2 briefly presents the biological background and modeling history of cortical spreading depression.
- Chapter 3 introduces our electrodiffusion model in a general form that can be expanded to included ions, compartments, and currents not included in this thesis.
- Chapter 4 describes the numerical method we use to solve our equations, our computational setup, and some convergence results.

- Chapter 5 introduces NMDA receptor and glutamate dynamics into our mathematical model.
- Chapter 6 analyzes the impact the addition of the NMDA receptor has on the dynamics of our model.
- Chapter 7 discusses and shows results of spiral wave patterns that naturally arise in our model in 2 dimensions.
- Chapter 8 introduces a full 3D simulation that includes a basic cortical layer structure and investigates the impacts this has on the dynamics.
- Chapter 9 presents a final discussion of the results presented in the thesis.

Chapter 2

Background

2.1 Physiology of CSD

CSD was first described by Leao in the 1940s. Leao discovered, while studying epilepsy, that brief, repetitive electrical stimulation cause a depression of electrical activity for 1-2 minutes. He also observed a large (in the range of -5mV to -15mV) shift in the extracellular voltage [61], we call this the DC shift. In addition to a voltage shift, CSD is characterized by massive ion fluctuations and cellular swelling. The ions of interest are potassium(K), Sodium (Na), Chlorine (Cl), and Calcium (Ca). Inside neurons, we see a sharp rise in sodium and a large drop in potassium. We also see a rise in chlorine and a small increase in calcium.

	Before	Peak
V_i	-70mV	0-10mV
$[K]_e$	2.7-3.5mM	30-60mM
$[Na]_e$	140-150mM	50-70mM
$[Cl]_e$	140-150mM	50-70mM
$[Ca]_e$	1.0-1.5mM	.2-.8mM

Table 2.1: Example extracellular ionic concentration ranges and neuronal voltage change. Data from [78]

These ion changes occur rapidly, they remain at the peak for an extended period with potassium beginning to recover first, but does so slowly. This leads the other ions

to return to normal levels very slowly in the extracellular space. As the ions return to homeostasis, the neurons re-polarize. However, even after voltage recovers, ions are not back to pre-CSD condition and normal brain function cannot continue until ions fully recover. In short, voltage recovers first, ions recover later.

Experimentally, CSD can be triggered in several ways: brief local increase in $[K^+]_e$ or glutamate, electrical stimulation, pinprick, or prolonged application of $[K^+]$[78]. Interestingly, different forms of initiations have different pharmacologies (respond differently to ion channel blockers). To add to the complexity, similar methods of initiation can lead to either CSD or prolonged seizures[89]. Initiation is caused by a feedback loop (summarized well in [78]'s flow chart). In the abstract, some stimulus causes an increase in the neuronal membrane voltage and extracellular potassium. This in turn opens voltage gated ion channels or NMDA receptors which allows further depolarization and ionic release. This feedback loop is mitigated by glial uptake, clearing extracellular potassium and glutamate. The key to this feedback loop is a large net-inward current[89]. Not only is the method of initiation unknown, but the mechanism behind the propagation of CSD is debated.

There are 4 main hypotheses[89] (broken up into two mechanisms). First there is the extracellular diffusion hypothesis. Some people say that potassium is the diffusing substance [38], while others say it is glutamate [42]. The second mechanism is gap junctions. These can be either neuronal or glial gap junctions. [89] Evidence leans towards the potassium hypothesis, however, all 4 likely have some effect in propagation[102]. The problem with Grafstein's hypothesis[38] of extracellular potassium causing the propagation of CSD is that TTX(tetrodotoxin) does not block CSD. Additionally, $[K]_e$ does not increase ahead of the depolarization, it follows. Van Harrevald's Glutamate hypothesis [42] has good merit. Glutamate does cause SD upon application and is released during SD. However, some opinions doubt it's role[71]. However, even those arguments still make mention of the role of NMDA receptors in spreading depression. Furthermore, while some glutamate receptor antagonists don't inhibit CSD, NMDA receptor antagonists do inhibit CSD [18]. So it seems the best explanation is that both glutamate(or at least NMDA receptors) and potassium play a role in the propagation, which is indeed

what Van Harrevald put forward 2 decades after his original hypothesis[97].

While cortical spreading depression is just the silencing of brain activity, there is a related phenomenon of this called spreading depolarization. It can be difficult to disentangle these two terms in the literature. The way we will discuss these topics is in regards to oxygen availability and the possibility of recovery. Cortical spreading depression is the more specific phenomena and can occur during normoxic and anoxic conditions[30]. Spreading depolarization is what the name implies, a depolarization that spreads. A depolarization can happen without massive ionic fluxes, this would allow the neuron to recover more quickly. However, if neurons lose a large amount of ions then this depolarization leads to a depression of activity. Because neuronal activity is linked to ionic gradients even if the membrane voltage recovers, the ions are not necessarily back to homeostasis, and thus action potentials won't be able to propagated until ions are recovered. This is a spreading depression.

Although one would suspect ischemia to be at play in CSD, that is not necessarily the case[89]. While a lack of oxygen can cause a spreading depression (the ion pumps do play a large role in preventing and recovering from CSD) neurons do not always lack for oxygen during SD[100]. The importance of oxygen during CSD is related to the massive amount of energy that must be invested in order to restore ionic gradients[59]. Indeed, in some models[99], available oxygen(and its use in ion pumps) is used as a parameter that is responsible for transitioning between 3 distinct behaviors from steady state into CSD into tonic firing.

Another important aspect people have researched is the role of calcium. For a time(early 1990s) people suggested that the calcium wave seen in astrocytes played in role increasing calcium in neurons[62]. One piece of evidence for this idea is that the glial calcium wave can be seen preceding the SD wave[10]. But much of this theory has been disproven or come into question[53]. It has been found that calcium channels in glia are unimportant, while calcium in glia rises sharply, the blocking of glial calcium channels shows no effect on the SD [10, 33]. Neurons however are more complicated, with CaV channels(voltage activated calcium channels) providing the impetus for the

release of glutamate, which in turn opens NMDA receptors allowing the flux of sodium, potassium, and calcium[78]. [94] found that CaV2.1 channels were necessary in order for brief potassium pulses to initiate CSD. However, prolonged potassium exposure still causes SD to be initiated regardless of a blockade of calcium channels[77, 78]. Interestingly, extracellular calcium [8] can be completely removed and SD will still occur, but the chances of recovery and it's reaction to hypoxia change. Suffice to say the main reason for the importance of calcium is its interaction with glutamate and the NMDA receptors [78].

Cortical spreading depression is tied to many neurological ailments. A healthy brain experiencing CSD will likely see no long term impact as the intense energy expenditure can be mitigated by increased blood flow [30]. However, in compromised tissue the reaction to CSD is a vasoconstriction instead, this can be very damaging. For example, in rats [31], a spreading ischemia was enough by itself to cause widespread necrosis. In a less damaging direction, CSD is intimately linked to migraine [60], it is known that the visual aura's some patients experience is caused by CSD, approximately 30 minutes after this aura is seen migraine onset occurs. However, migraines are not definitively caused by CSD, as not all migraine sufferers experience aura[19]. In addition to migraine, CSD is important in stroke, trauma and subarachnoid hemorrhage [78], these last issues being especially crucial as the tissue itself is compromised, with repeated spreading depressions this can lead to permanent damage[23, 81].

2.2 Modeling CSD

Many models of cortical spreading depression have been developed. Some models seek to model the dynamics at an abstract level of picking out a variable to model excitation and recovery [102, 23] or to describe bifurcations of neuron dynamics [99, 9, 50, 49]. Others seek a more biophysically faithful approach[85, 22, 53, 55]. Both of these approaches additionally breakdown into effectively ODE (single neuron/compartmental) models and PDE (continuum or network) models. Each of these has their strengths. Let's discuss some of these models. Several models are discussed further in [67].

In [99], they develop a single cell model that builds off of work by [96]. This model is a unification of ordinary neuron firing, epilepsy, and CSD. It tracks sodium, potassium, and chloride and uses only transient sodium, delayed rectifier potassium, NaK-ATPase, and some leak currents as a start. Onto this they add some basic oxygen dynamics and allow the strength of the ion pumps to change with the amount of available oxygen. They are then able to achieve different behaviors by varying the concentration of a potassium bath and an oxygen bath. However, they are only able to attain these behaviors by including oxygen. If they remove oxygen from the model they lose their unified behavior. This idea of epilepsy and cortical spreading depression being linked to the same underlying physiology is very compelling, and several other studies have shown both types of behavior. For example [55] shows tonic firing leading into a depolarization block, while not exactly CSD, it is related.

In [89], a very detailed review of CSD is given, however a model is also introduced. This is an compartmental ODE, where the compartments are the sections of a pyramidale neuron (cell body and dendrites). In this they showed that in ordinary circumstances of extended excitation the activity of Na-K ion pumps and glial potassium clearance kept the neuron functioning normally. But the decrease in activity of either of these mechanisms caused the depolarization to begin. In this paper an important insight, that we will use, is reached. CSD is ignited by a net inward current, that is slowly inactivating. This inward current arises from a feedback cycle (a very large diagram of this is in [40]). A general summary of this feedback mechanism is found in [78], where increasing membrane voltage or interstitial potassium leads to an opening of either NMDA receptors or voltage gated channels. Each of these will release more potassium, raising the voltage further and cycling back.

There are many other ODE models that investigate plenty of other effects around initiation and mitigation[22, 49, 54]

Then there are the spatial models. Starting with [95] and going forward, there are plenty of reaction diffusion models [79, 102, 23, 80]. Although these models provided some nice insights into the mathematics. They are phenomenological models,

they model abstract variables that are meant to be analogous to potassium or voltage. [86, 85] on the other hand melds together a diffusion equation with the ionic currents of the ODE models, while also tracking volume changes. These volume changes are an important addition as the volume changes during CSD are large, and should have a large effect on the ionic concentrations and voltages seen throughout SD's time course. A very important, albeit simple, finding of this is that the properties of the wave don't change with stimulus. CSD is a very robust phenomenon in experiments, and a model should reflect that. There are some issues with this model however, blocking gap junctions stops CSD. While this has an effect in vivo, it does not universally block CSD [78] (our model that we develop will not have this problem).

I'd like to list some other non-phenomenological reaction-diffusion type models that have been used before. A 5 compartment (neuron, dendrite, glia, extracellular, vasculature) model by Miura, et al [17] found the influence of blood flow and oxygen starvation during CSD to be an important indicator of speed and susceptibility. In [101], they develop a 2 compartment (neuron and extracellular space) diffusion model that tracks sodium, potassium, and chloride. With their ion channels, this model is very similar in conception to Prof. Mori's original paper [69], that this thesis is an extension of. Their main result is that cell swelling is not a big component. While we do not show this in the thesis, the 2 compartment version of our model would draw the much the same conclusions as [101].

Before we continue to the introduction of our model, we will discuss the journey of this model formulation. In Mori [69], this electrodiffusion model was introduced. It is a two compartment (neuron and extracellular) model that tracks sodium, potassium, and chloride ions. It integrates electrodiffusive gradients, osmotic forces, and ion channels into one large set of PDEs. In it are 4 passive ion channels and one active current. The 2 main aspects of note in this model, the first is the presence of a free energy identity. The second, and more important aspect, is the calculation of the extracellular voltage. This is the first paper in CSD to accurately calculate this critical aspect of CSD. The previous calculations of the DC shift relied on a formula that is only accurate in the absence of gap junctions.

After this the model was developed further by O'Connell and Mori in [73] and [72]. The primary addition is the glial compartment. The addition of this compartment has a very large impact on speed and the DC shift. Additionally, [73] gives some good insight into the Grafstein hypothesis that potassium comes before the CSD wave, it is shown that this can be true. The early DC shift is linked directly to the glial gap junctions and their relative potassium conductance. Furthermore, the 2D simulations are the end of [72] is the point where this thesis starts.

Chapter 3

Model

3.1 Electrodiffusion Model

Let Ω be our domain in $\mathbb{R}^n$(we will use n=1,2, and 3). Instead of dissecting the domain into regions of neurons, glia, and extracellular space, we treat it as a multi-phasic continuum. Suppose there are N compartments which we label with k, where $k = N$ will be the extracellular compartment. At each point in space we assign a volume fraction: α_k and impose:

$$\sum_{k=1}^{N} \alpha_k(x,t) = 1 \tag{3.1}$$

We can describe the change of volume fraction by looking at water flow due to osmotic pressure only:

$$\frac{\partial \alpha_k}{\partial t} = -\gamma_k w_k, \quad k = 1, \cdots, N-1 \tag{3.2}$$

$$\frac{\partial \alpha_N}{\partial t} = \sum_{k=1}^{N-1} \gamma_k w_k \tag{3.3}$$

γ_k represents the distance separating compartment k from N (the cell membrane). w_k is the water flow per unit area into each compartment k. The constitutive relations for

w_k involve osmotic and mechanical pressure differences:

$$w_k = \zeta_k RT \left(\frac{a_N}{\alpha_N} + \sum_{i=1}^{M} c_i^N - \frac{a_k}{\alpha_k} - \sum_{i=1}^{M} c_i^k \right)$$

where ζ_k is the hydraulic permeability and a_k is the amount of immobile ions in compartment k.

Next, we need to model the ionic concentration dynamics. Let c_i^k be the concentration of the ith ion in the kth compartment (we use Na^+, K^-, Cl^-, and glutamate as our ions) and ϕ_k be the voltage in compartment k. We assume that concentration changes due to electrodiffusive and inter-compartmental fluxes. For $i = 1, \cdots, M$, we have the following:

$$\frac{\partial(\alpha_k c_i^k)}{\partial t} = -\nabla \cdot f_i^k - \gamma_k g_i^k, \quad k = 1, \cdots, N-1 \tag{3.4}$$

$$\frac{\partial(\alpha_N c_i^N)}{\partial t} = -\nabla \cdot f_i^N + \sum_{k=1}^{N-1} \gamma_k g_i^k - D_i^N \left(\frac{c_i^N + c_i^{bath}}{2} \right) \left(\ln \left(\frac{c_i^N}{c_i^{bath}} \right) + \frac{z_i F}{RT} \left(\phi_N - \phi_{bath} \right) \right) \tag{3.5}$$

$$f_i^k = -D_i^k c_i^k \nabla \left(\ln \left(c_i^k \right) + \frac{z_i F}{RT} \phi_k \right), \quad k = 1, \cdots, N \tag{3.6}$$

D_i^k is the diffusion coefficient and depends on the volume fraction α_k. R is the ideal gas constant, T is temperature. z_i is the valence of the ith ion. F is the Faraday constant. We add an external bath that interacts with the extracellular space through electrodiffusion. g_i^k are the transmembrane ion fluxes, biophysically these are fluxes due to ion channels, transporters, and ion pumps. These are functions of intracellular and extracellular ions and voltages, the individual models of these will be described later.

Next, we need an equation for the electrostatic potential. Treating the cellular membrane as a capacitor, we have the following charge-capacitance equations:

$$\gamma_k C_m^k \phi_{kN} = z_0^k F a_k + \sum_{i=1}^{M} z_i F \alpha_k c_i^k, \quad \phi_{kN} = \phi_k - \phi_N, \quad k = 1, \cdots, N-1 \tag{3.7}$$

$$-\sum_{k=1}^{N-1} \gamma_k C_m^k \phi_{kN} = z_0^N F a_N + \sum_{i=1}^{M} z_i F \alpha_N c_i^N \tag{3.8}$$

C_m^k is the membrane capacitance per unit area between the kth compartment and Nth. Again, γ_k is the membrane separation. $z_0^k F a_k$ is the immobile charge density, z_0^k is the average valence and a_k is the amount of immobile ions in compartment k.

Now that we have all of the equations, we can scale the variables to cancel constants:

$$\frac{\partial \alpha_k}{\partial t} = -w_k \tag{3.9}$$

$$\frac{\partial \alpha_N}{\partial t} = \sum_{k=1}^{N-1} w_k$$

$$\frac{\partial (\alpha_k c_i^k)}{\partial t} = \nabla \cdot \left(D_i^k c_i^k \nabla \left(\ln \left(c_i^k \right) + z_i \phi_k \right) \right) - g_i^k \tag{3.10}$$

$$\begin{aligned} \frac{\partial (\alpha_N c_i^N)}{\partial t} = {} & \nabla \cdot \left(D_i^N c_i^N \nabla \left(\ln \left(c_i^N \right) + z_i \phi_N \right) \right) + \sum_{k=1}^{N-1} g_i^k \\ & - D_i^N \left(\frac{c_i^N + c_i^{bath}}{2} \right) \left(\ln \left(\frac{c_i^N}{c_i^{bath}} \right) + z_i \left(\phi_N - \phi_{bath} \right) \right) \end{aligned}$$

$$\epsilon C_m^k \phi_{kN} = z_0^k a_0^k + \sum_{i=1}^{M} z_i \alpha_k c_i^k, \phi_{kN} = \phi_k - \phi_N \tag{3.11}$$

$$-\epsilon \sum_{k=1}^{N-1} C_m^k \phi_{kN} = z_0^N a_0^N + \sum_{i=1}^{M} z_i \alpha_N c_i^N$$

The only new constant in the above is ϵ, which is the ratio between charge stored on the membrane and bulk ionic charge. Now we move to the descriptions of the microscopic dynamics. These equations will be referred to as volume(water flux) equations, concentration (electrodiffusion) equations, and voltage (charge-capacitance) equations.

3.1.1 Ion Channels

The transmembrane ion fluxes: g_i^k are a combination of fluxes from ion channels, transporters, and ion pumps. These different mechanisms for ion flow are the primary way through which we modify our model. Our current collection of channels in neurons is given by:

$$\begin{aligned} g_{Na} &= j_{NaL} + j_{NaP} + j_{NaT} + 2h_{NaK} + \frac{2}{3} j_{NMDA} \\ g_K &= j_{KL} + j_{KDR} + j_{KA} - 3h_{NaK} + \frac{1}{3} j_{NMDA} \\ g_{Cl} &= j_{ClL} \\ g_{Glu} &= j_{Ext} + j_{Glia} \end{aligned}$$

In Glia:

$$\begin{aligned} g_{Na} &= j_{NaL} + 2h_{NaK} + j_{Na}^{NaKCl} \\ g_K &= j_{KIR} - 3h_{NaK} + j_K^{NaKCl} \\ g_{Cl} &= j_{ClL} + j_{Cl}^{NaKCl} \\ g_{Glu} &= j_{Ext} + j_{Neur} \end{aligned}$$

Where NaL, KL, ClL are leak channels, NaP is the persistent sodium, NaT is the transient sodium, h_{NaK} are the active NaK ATPase pumps, KA is the transient potassium, KDR is potassium delayed rectifier, $NMDA$ is the NMDA receptor, KIR is the Potassium inward rectifier, and $NaKCl$ is the sodium-potassium-chloride cotransporter. Separate from all of these are the glutamate dynamics. These are made up of a voltage activated release from neurons, a passive uptake from neurons and glia, and a glutamate/glutamine-like cycle between glia and neurons which is described in Chapter 5.

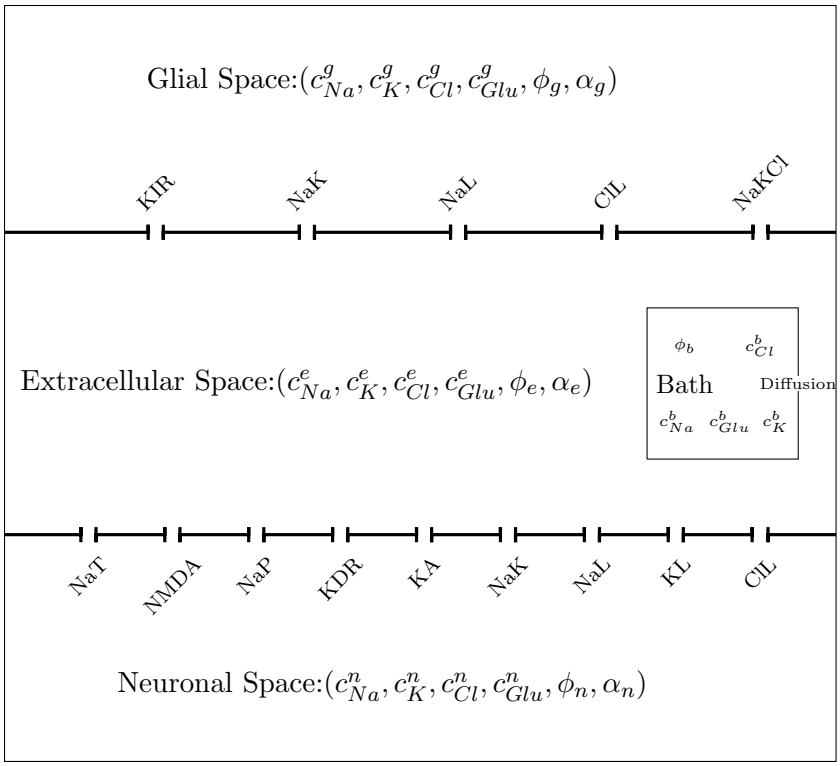

All of these fluxes have the form of:

$$j_{ion} = m^p h^q P_{ion} J(c^n_{ion}, c^N_{ion}, \phi_{nN})$$

where m and h are gating variables, P_{ion} is the permeability, J is either Hodgkin-Huxley (HH) or Goldman-Hodgkin-Katz (GHK) type of currents. Both of these currents depend on inter/extra cellular concentrations and the membrane voltage difference. Specifically these are:

$$J_{HH}(c^k_i, c^N_i, \phi_{nN}) = \phi_{nN} - \frac{RT}{F} \log\left(\frac{c^N_i}{c^k_i}\right)$$

$$J_{GHK}(c^k_i, c^N_i, \phi_{nN}) = \frac{z_i F \phi_{nN}}{RT} \left(\frac{c^k_i - c^N_i \exp\left(-z_i \phi_{nN} F/RT\right)}{1 - \exp\left(-z_i \phi_{nN} F/RT\right)}\right)$$

Every gating variable m and h has it's own ODE that is of the form:

$$\frac{ds_g}{dt} = S(\phi_{kN}, s_g)$$

Where S is some linear function in g with typical Hodgkin-Huxley type relations for opening and closing of ion channels that depends on membrane voltage. In Table 3.1 is a list of each set of parameters for the channels we use in the model. (Values come from [101],[99],[53])

Paramater	Value
General	
m_K	2×10^{-3} mmol/cm^3
m_{Na}	7.7×10^{-3} mmol/cm^3
Neurons	
P_{NaT}	0 cm/s
P_{NaP}	2×10^{-5} cm/s
P_{KDR}	1×10^{-3} cm/s
P_{KA}	1×10^{-4} cm/s
P^*_{NaL}	$6.2737560407 \times 10^{-9} cm/s$
P_{KL}	7×10^{-2} mS/cm^2
P_{ClL}	10×10^{-2} mS/cm^2
I^*_{max}	$1.5971645540 \times 10^{-7}$mmol/cm^2/s
Glia	
P_{KIR}	0.13 mS/cm^2
P_{NaKCl}	9.1806×10^{-10} mmol/cm^2/s
P^*_{NaL}	$2.1290277618 \times 10^{-9} cm/s$
P^g_{ClL}	5×10^{-2} mS/cm^2
I^*_{max}	$7.588971664 \times 10^{-8}$ mmol/cm^2/s

Table 3.1: Ion channel parameters that come from [101],[99],[53]. The values with a $*$ are calculated in order to start the system at steady-state. These are sodium leak and the NaK pump strength in both neurons and glia.

3.2 Ion Channel Details

3.2.1 Neurons

Currents	Type	P_{ion}	Gates($m^p h^q$)	Voltage-Dependent rate constants
I_{NaT}	GHK	100×10^{-5}	$m^3 h$	$\alpha_m = 4\varphi(.25\phi + 12.975)$ $\beta_m = 1.4\hat{\varphi}(.2\phi + 4.978)$ $\alpha_h = .128\exp(-(0.056\phi + 2.94))$ $\beta_h = \frac{4}{1+\exp(-(.2\phi+6))}$
I_{NaP}	GHK	2×10^{-5}	$m^2 h$	$\alpha_m = \frac{1}{6(1+\exp(-(.143\phi+5.67)))}$ $\beta_m = \frac{\exp(-(.143\phi+5.67))}{6(1+\exp(.143\phi+5.67))}$ $\alpha_h = 5.12 \times 10^{-8}\exp(-(.056\phi + 2.94))$ $\beta_h = \frac{1.6\times10^{-6}}{1+\exp(-(.2\phi+8))}$
I_{KDR}	GHK	1×10^{-3}	m^3	$\alpha_m = 0.08\varphi(0.2\phi + 6.98)$ $\beta_m = 0.25\exp(-(0.25\phi + 1.25))$
I_{KA}	GHK	1×10^{-4}	$m^2 h$	$\alpha_m = 0.2\varphi(0.1\phi + 5.69)$ $\beta_m = 0.175\hat{\varphi}(0.1\phi + 2.99)$ $\alpha_h = 0.016\exp(-(0.056\phi + 4.61))$ $\beta_h = \frac{0.5}{1+\exp(-(0.2\phi+11.98))}$
I_{NaL}	HH	6.2738×10^{-9}	None	
I_{KL}	HH	7×10^{-2}	None	
I_{ClL}	HH	10×10^{-2}	None	

where $\varphi(u) = u/(1 - \exp(-u))$ and $\hat{\varphi}(u) = u/(\exp(u) - 1)$. Now, the NaK ATPase is modeled by the h_{NaK}, we explicitly compute this as:

$$h_{NaK} = \frac{\hat{I}_{max}}{(1 + m_K/c_K^e)^2(1 + m_{Na}/c_{Na}^i)^3}$$

where, $\hat{I}_{max} = I_{max}/F$, $I_{max} = 13\mu A/cm^2$, $m_K = 2mmol/l$, $m_{Na} = 7.7(mmol/l)$.

3.2.2 Glia

Next, we move onto glial ion channels. While glia possess different ion channels they share several with neurons: sodium and chloride leak currents and NaK-ATPase. The two new channels are the potassium inward rectifier(replacing the potassium leak current) and the NaKCl cotransporter which transports sodium, potassium, and chloride. Both of these channels do not readily fit the format used above.

Currents	Type	P_{ion}	Gates($m^p h^q$)	Voltage-Dependent rate constants
I_{NaL}	HH	2.1290×10^{-9}	None	
I_{ClL}	HH	5×10^{-2}	None	

Potassium inward rectifier (KIR):

$$\hat{g}_K^{g,IR} = \sqrt{\frac{c_K^e}{3}} \frac{1+\exp(18.5/42.5)}{1+\exp((\phi_{ge}-E_K^g+18.5)/42.5)} \frac{1+\exp((-118.6-85.2)/44.1)}{1+\exp((-118.6+\phi_{ge})/44.1)}$$

$$J_K^{g,IR} = \left(\phi_{ge} - E_K^g\right)$$

$$P_K^{g,IR} = 1.34736 \times 10^{-7} mSmol/cm^2 C$$

$$j_{KIR} = P_K^{g,IR} \hat{g}_K^{g,IR} J_K^{g,IR}$$

E_K^g will be the Nernst-Potential in the glial compartment for potassium. $\hat{g}$ is the percentage of channels open. For neuronal channels, these were equal to $m^p h^q$.

Na^+/K^+ ATPase:

NaK ATPase is the same, with a different I_{max}

$$h_{NaK} = \frac{I_{max}^g}{(1+m_k/c_K^e)^2(1+m_{Na}/c_{Na}^k)^3}$$

$$j_K^{NaK} = 3h_{NaK}$$

$$j_{Na}^{NaK} = -2h_{NaK}$$

Constants are:

$$m_K = 2 \times 10^{-3} mmol/cm^3$$

$$m_{Na} = 7.7 \times 10^{-3} mmol/cm^3$$

$$I^g_{max} = 7.5890 \times 10^{-8} mmol/cm^2/s$$

Sodium, Potassium, Chloride cotransporter:

$$h_{NaKCl} = P^{NaKCl} \ln \left(\frac{c^g_{Na} c^g_K (c^g_{Cl})^2}{c^e_{Na} c^e_K (c^e_{Cl})^2} \right)$$

$$j^{NaKCl}_{Na} = h_{NaKCl}$$

$$j^{NaKCl}_{K} = h_{NaKCl}$$

$$j^{NaKCl}_{Cl} = 2h_{NaKCl}$$

where, $P^{NaKCl} = 9.1806 \times 10^{-10} mmol/cm^2/s$.

3.3 Constants

Definition of various constants that we make use of:

Name	Symbol	Value
Gas Constant	R	8.314472×10^6nJ/K/mmol
Temperature	T	$(273.15 + 37)$ kelvin
Faraday constant	F	$9.64853399 \times 10^7 \mu$C/mmol
Tortuosity	λ	1.6 $(1.2 - 2.4)$ [70]
Sodium Ion Diffusion	D_{Na}	1.33×10^{-5} cm^2/sec
Potassium Ion Diffusion	D_K	1.96×10^{-5} cm^2/sec
Chloride Ion Diffusion	D_{Cl}	2.03×10^{-5} cm^2/sec
Membrane Capacitance	C_m	0.75×10^{-3} mF/cm^2[53]
Cell Surface Area	Sa	1.586×10^{-5} cm^2[53]
Intracellular Volume	Vol_i	2.16×10^{-9} cm^3[53]

Extracellular Volume	Vol_e	$0.15Vol_i$ cm^3[53]
Avg. Membrane Seperation	ell	$(Vol_i + Vol_e)/SA$ cm[53]
Hydraulic Permeability	ζ_k	5.4×10^{-5} cm/sec/(mmol/cm^3) [85]
Sodium Bath	c_{bath}^{Na}	.140mmol/cm^3
Potassium Bath	c_{bath}^{K}	3.4×10^{-3}mmol/cm^3
Chloride Bath	c_{bath}^{Cl}	.120mmol/cm^3
Glutamate Bath	c_{bath}^{Glu}	1×10^{-8}mmol/cm^3
Bath Voltage	ϕ_{bath}	$0mV$
Extracell. Immobile anions	a_o	5×10^{-4}mmol

Table 3.2: Constants and parameters used throughout the model, with citations.

3.3.1 Excitation and Initiation

We need a well defined method of initiation. The common method used, increasing potassium concentration via a diffusion from a bath or some outside source, will not be suitable for us as it takes too long to initiate a wave. We will use an abstraction of the trigger of CSD that accomplishes the same thing: a large net inward current. So, we add an artificial ion channel that we call P_{exct}, this channel has the same affect of turning on the persistent sodium channel. It will be on for a brief period and turn off. We define it as follows:

$$P_{exct} = p_{max} \sin\left(\pi \frac{t}{t_{exct}}\right)^2 \frac{RT}{F^2}, \quad t < t_{exct}$$

This is then added to the total ion flux of every ion (sodium, potassium, chloride, and glutamate) using a Hodgkin-Huxley current-voltage relation. This effectively just increases the leak permeability of each of these ions. We can then choose where to place this excitation, for the most part we place this excitation on the boundaries (either a whole boundary, or a portion of it). If, we excite a region(for example, a circle) in the middle of the domain, we would use a $\cos^2(\pi/2r/L)$ term that would allow us to have a

continuous and differentiable excitement that peaks at 1 in the center of the circle and falls to zero at its boundary.

Chapter 4

Computational Model and Simulation

4.1 Discretization

We simulate our equations via a mixed implicit-explicit finite volume routine. For ease of notation we will only discuss the numerical scheme in $\mathbb{R}^2$, $\mathbb{R}^3$ follows the same pattern. Let $\alpha^n_{k,lm}, c^{kn}_{i,lm}, \phi^n_{k,lm}$ be the evaluation of our variables at position: $(x, y) = (l\Delta x, m\Delta x)$ and time $t = n\Delta t$. For easier reading we will denote the evaluation at (l, m) to be simply: $\alpha^n_k, c^{kn}_i, \phi^n_k$. Define the discrete operators:

$$D^+_{grad} u_{l,m} = \frac{u_{l+1,m} - u_{l,m}}{\Delta x}\hat{x} + \frac{u_{l,m+1} - u_{l,m}}{\Delta y}\hat{y}$$

$$D^-_{div}(v^x_{l,m}\hat{x} + v^y_{l,m}\hat{y}) = \frac{v^x_{l,m} - v^x_{l-1,m}}{\Delta x} + \frac{v^y_{l,m} - v^y_{l,m-1}}{\Delta y}$$

$$A^+(v^x_{l,m}\hat{x} + v^y_{l,m}\hat{y}) = \frac{v^x_{l+1,m} + v^x_{l,m}}{2}\hat{x} + \frac{v^y_{l,m+1} + v^y_{l,m}}{2}\hat{y}$$

In order to make the involved matrix more uniform along the diagonal we take the time derivative of the voltage equations. This gives us a system of PDEs with only 1 algebraic condition (the extracellular volume fraction). Performing the discretization we get:

Volume Equations:

$$\alpha_k^{n+1} - \alpha_k^n + \Delta t w_k^{n+1} = 0, \quad k = 1, \ldots, N-1 \tag{4.1}$$
$$\alpha_N^n = 1 - \sum_{k=1}^{N-1} \alpha_k^n$$

Concentration Equations

$$\alpha_k^{n+1} c_i^{k,n+1} - \alpha_k^n c_i^{kn} - \Delta t f_i^k + \Delta t g_i^{k,n+1} = 0, \quad k = 1, \ldots, N-1, i = 1, \ldots, M \tag{4.2}$$
$$\alpha_N^{n+1} c_i^{N,n+1} - \alpha_N^n c_i^{Nn} - \Delta t f_i^N - D_i^N \left(\frac{c_i^N + c_i^{bath}}{2} \right) \left(\ln \left(\frac{c_i^N}{c_i^{bath}} \right) + z_i \left(\phi_N - \phi_{bath} \right) \right) -$$
$$\Delta t \sum_{k=1}^{N-1} g_i^{k,n+1} = 0, i = 1, \ldots, M$$
$$f_i^k = D_{div}^- \left(D_i^k A^+ \left(c_i^{kn} \right) D_{grad}^+ \left(\ln \left(c_i^{k,n+1} \right) + z_i \phi_k^{n+1} \right) \right)$$

Voltage Equations

$$\epsilon C_m^k \left(\phi_{kN}^{n+1} - \phi_{kN}^n \right) - \sum_{i=1}^{M} z_i \Delta t \left(f_i^k - g_i^{k,n+1} \right) = 0, \quad k = 1, \ldots, N-1 \tag{4.3}$$
$$- \epsilon \sum_{k=1}^{N-1} C_m^k \left(\phi_{kN}^{n+1} - \phi_{kN}^n \right) - \Delta t \sum_{i=1}^{M} z_i \left(f_i^N + D_i^N \left(\frac{c_i^N + c_i^{bath}}{2} \right) \left(\ln \left(\frac{c_i^N}{c_i^{bath}} \right) + z_i \left(\phi_N - \phi_{bath} \right) \right) \right) -$$
$$\Delta t \sum_{i=1}^{M} \sum_{k=1}^{N-1} g_i^{k,n+1} = 0$$

These sets of equations are nonlinear, so we used Newton's method to solve them. In addition to the macroscopic state variables the gating variables need to be solved/updated. These are solved in a separate update step as:

$$s_g^{n+1} = s_g^{n+1} + \Delta t S(\phi_{kN}^{n+1}, s_g^{n+1})$$

Since S is linear in g we can easily solve these. Before we move to more in depth parameter analysis, Figure 5.1 shows time profiles of an example 1D simulation. We can see the depolarization, the extracellular DC shift, the extracellular volume shrinkage,

and the huge ionic fluctuations.

4.2 Algorithms

We will be using with 4 ions/molecules (Na, K, Cl, and Glutamate) and 3 compartments (Neurons, Glia, and Extracellular) from now onwards. This gives us 17 total macroscopic variables. Additionally, we have 10 gating variables: NaT activation and inactivation, NaP activation and inactivation, KDR activation, KA activation and inactivation, and NMDA activation, desensitization 1 and 2. We will utilize a split scheme where we solve the macroscopic variables separately from the gating variables. Additionally, due to the slow changes of volume, it will be separated from concentrations and voltage. A simple schematic for our algorithm is:

1. Update α_k(nonlinear).
2. Update c_i^k and ϕ_k(nonlinear).
3. Update gating variables(linear).

4.2.1 Solvers

The equations we need to solve are very large, nonlinear, and nonsymmetric. Using the software package PETSC[5][6][7], we use Newton's method as our nonlinear solver, with a preconditioned Krylov Subspace iteration(KSP) as our linear solver. We have found 2 setups that lead to relatively fast performance on serial computer:

1 Smaller grid or not power of 2.

   a. Nonlinear: Newton Line Search
   b. KSP: deflated GMRES
   c. Preconditioner: incomplete LU

2 Power of 2 bigger than 32×32.

   a. Nonlinear: Newton Line Search
   b. KSP: Flexible GMRES

c. Preconditioner: W-Cycle Multigrid:

   i. SubKSP: Richardson

   ii. SubPreconditoner: SOR.

4.3 Convergence Study

We performed a convergence study of the model in 2 dimensions. We initiated a large depolarization on a circle of radius $0.15cm$ in the center of a domain of size $(0.5cm) \times (0.5cm)$. We performed 12 simulations of this setup with $N_x = N_y = 32, 64, 128, 256$ and $\Delta t = 0.01, 0.005, 0.0025$ seconds and allowed it to run until 30 seconds.

We see the expected convergence rate of 2 in space and 1 in time. For a propagating wave we can see that the l_∞ norm suffers due to the difference in propagation

Vars	l_2 space	l_∞ space	l_2 time	l_∞ time
c^n_{Na}	2.652340	1.372628	0.827744	0.717851
c^n_K	2.645715	1.358864	0.826925	0.715618
c^n_{Cl}	2.900286	1.754658	0.890492	0.878489
c^n_{Glu}	2.912111	1.858918	0.879499	0.877977
c^g_{Na}	2.895549	1.833247	0.876704	0.877024
c^g_K	2.893778	1.866245	0.869456	0.806521
c^g_{Cl}	2.931924	1.793115	0.897486	0.877109
c^g_{Glu}	2.851757	1.714351	0.889808	0.893874
c^e_{Na}	2.600553	1.371666	0.829394	0.712736
c^e_K	2.594958	1.385203	0.829491	0.714999
c^e_{Cl}	2.752381	1.459150	0.858175	0.769786
c^e_{Glu}	2.890538	1.735678	0.878921	0.874742
ϕ_n	2.379721	0.839017	0.618567	0.359324
ϕ_g	2.708053	1.945447	0.882969	0.839519
ϕ_e	2.627927	1.617569	0.856773	0.792548
α_n	2.916831	1.632008	0.904519	0.897103
α_g	2.910650	1.708667	0.900307	0.899290

Table 4.1: Convergence rates for increasing spatial and temporal resolution of a 2D circular wave.

speeds that occurs for the different spatial discretization sizes. The shape of the curves are all similar, it is mainly their displacement in time that changes. Additionally, we can see the small membrane capacitance that makes our equations stiff manifests itself in the smallest l_∞(and l_2) convergence time appearing the the neuronal voltage equation. Looking at time profiles (for example fig. A.6) of the voltages for smaller grid sizes has small oscillations that occur every time the wave advances to the next grid point. This surge appears in each of ϕ_n,ϕ_g, and ϕ_e. However, this surge effect disappears when looking at the membrane voltage $\phi_n - \phi_e$ and $\phi_g - \phi_e$, as the surge is caused by a small amount of ions drawing a change in voltage, but since charge/ions is/are conserved in our discretization this behavior is invisible in the membrane voltage.

4.4 Time Splitting

There are several more advanced computational techniques that we could employ: grid coarsening or time adaptive methods. Instead we will take some inspiration from multi-rate time stepping of [83] and alternating direction implicit methods. We can formulate this as the idea of predictor-corrector schemes for ODEs. The predictor seeks to adaptively update in time only where needed on a point by point basis on the grid. This is important as the (some) gating variables change rapidly at the front edge and back edge of a spreading depression wave and the voltage adjusts rapidly to small ionic changes. The corrector in this case is our original method

In the full solve, each point depends on it's four neighbors. This leads to a large matrix where each coordinate changes with all $N_x N_y$ points. To speed this up we choose each point and update it in reference to only it's four neighbors as if we were solving the same problem on only a 3×3 grid (or any generally smaller grid).

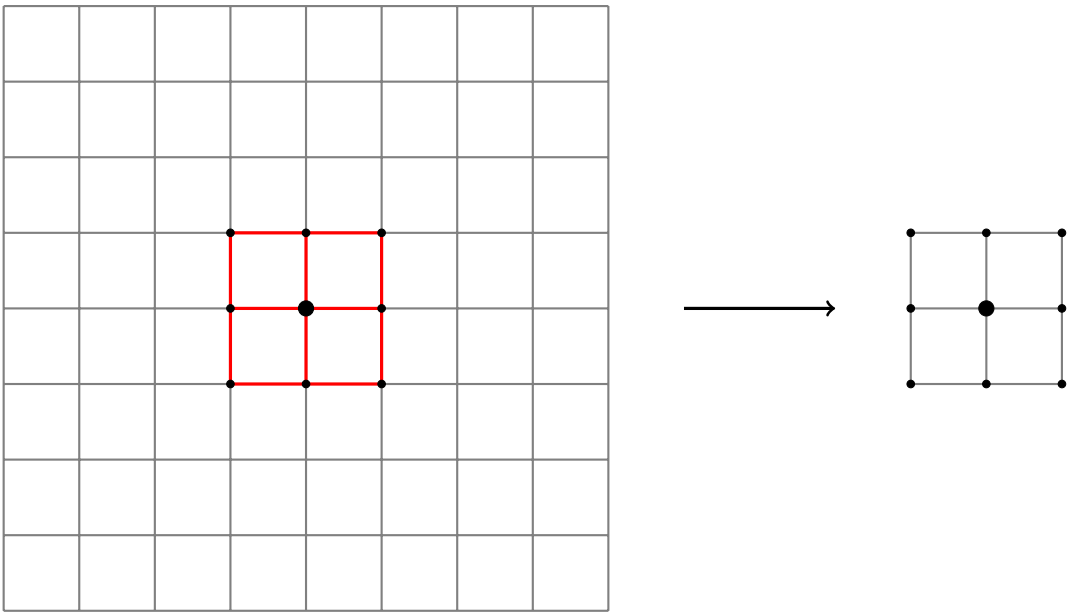

On this small problem we take advantage of the fact that CSD waves are localized. We cycle through all the grid-points and update only the ones that have had a voltage change in the previous step over a threshold. Then, we attempt to update each point one by one (note on the boundary we just copy the closest grid value so the small problem is still 3x3.). We adaptively refine the time according to the number of newton iterations (keeping them less than 3 for example). At the end of the adaptive solve we save only the center point's value. We then use these approximations for c, ϕ, α , and all the gating variables to solve our full set of equations. So, the algorithm for the update goes like the following:

```
for(x=0;x<Nx;x++){
        for(y=0;y<Ny;y++) {
            if  |vm_new-vm_past|>threshhold  {
                // Load new gridpoint
                Load_Grid(data, x, y);
                //Update new grid (adaptive time steps)
                Update_Grid(x, y, t, data);
                //Save the held variable
```

```
                Unload_Grid(data, x, y);
            }
        }
    }
```

This method of updating on small grid's is a PDE solver in it's own right. However, it is inconsistent. For the 1D heat equation this inconsistency is given by the following multiplication of the diffusion coefficient(for a standard method this is 1):

$$\frac{1}{1+3D\frac{\Delta t}{\Delta x^2}}$$

So the predictor becomes more accurate for smaller diffusion coefficients and less accurate for smaller grids. Because of this we choose to solve the equations using the algebraic form of the voltage equations and not the derivative form. Additionally, for greater stability we solve c, ϕ, and α all together, while still keeping the gating variables separate. All together in pseudocode our algorithm looks like:

```
for(t=0;t<Time;t+=dt){
//Predict:
    for(x=0;x<Nx;x++){
       for(y=0;y<Ny;y++) {
           if  |vm_new-vm_past|>threshhold  {
              // Load new gridpoint
              Load_Grid(data_old, x, y);
              //Update new grid (adaptive time steps)
              // c,phi,alpha simultaneous. And algebraic voltage.
              Update_Grid(x, y, t, data_guess,data_old);
              //Save the held variable
              Unload_Grid(data_guess, x, y);
           }
       }
    }
    //Update volume
```

```
    Update_Volume(data_new,data_guess,data_past);

    //Update c,phi (with derivative phi)
    Update_c_phi(data_new,data_guess,data_past);

    //Update Gating variables:
    Updating_Gating_variables(data_new,data_past);

}
```

By it's incorporation with the previous method it is not any less accurate. However, it does cost added computational time. When transient sodium is turned off (which is true for many of our results), it is not worth the cost. But, when transient sodium is active it does add some accuracy. For example, take for ground truth $\Delta t = 0.001$, the unpredicted method. Then then we can test both the predicted and unpredicted methods for $\Delta t = 0.01$. The predictor leads to a very modest improvement of the relative l_2 norm from 0.0711 to 0.0702., but the main differences between these two waves and the finer Δt wave is in velocity. The wave profiles are very similar, they are just shifted in time/space. If we correct for this time shift (about .2 seconds), then the difference is much more dramatic: 0.01995 to 0.01313. All of this difference occurs in the small, rapid oscillations that happen near $-50mV$ right when the spreading depression wave arrives at any given point. After these rapid oscillations the neuron depolarizes and the differences among all 3 simulations becomes negligible as diffusion takes over.

Method	Time	Newton Iterations	KSP Iterations
With Predictor	13.36min	6330	201003
Without Predictor	6.76min	6371	183191

We can also compare the computational details of this method. We performed a test with a 30 second simulation on a 32x32 grid with $\Delta t = 0.01$(3000 time steps). The table above gives the results with the predictor and without. The short of it, is that the predictor makes the simulation take about twice as long while lower the number of newton iterations. This is to be expected as we are increasing the accuracy, but this accuracy is only gained on the front and tail of the wave. So this method should only

be used to get a better idea of the onset of CSD when fast ion channels are activated.

Chapter 5

NMDA Receptor Dynamics

5.1 NMDA Receptor and Glutamate

N-methyl-D-aspartate receptors (NMDAR) are closed in the absence of glutamate (and other agonists). When glutamate is released 2 glutamate molecules bind to the receptors, thus opening them. This allows the flux of sodium, potassium, and calcium. During a normal conditions magnesium will move to block the channel [51], however as the neuronal voltage increases the magnesium will become dislodged allowing the channel to become open.

Glutamate is the primary neurotransmitter in the brain. When a neuron receives a stimulus glutamate is secreted from synaptic vesicles into the synaptic cleft. There, they bind with the NMDA receptors on neighboring dendrites which allows an influx of sodium and calcium and efflux of potassium. After release glutamate is then taken up by both neurons and glia, although glia do most of the work. The glutamate that is taken by the glia is detoxified by turning it into glutamine. The glutamine is then transported back into neurons via the extracellular space where it is transformed back into glutamate. This process is the glutamate-glutamine cycle and it is ATP-dependent [26]. While it is ATP-dependent, during ischemia (and other free energy starved conditions) glia can continue to uptake glutamate [103], they just won't be able to transform glutamate into glutamine.

The behavior for sodium, potassium, and chloride is well understood and modeled in the context of CSD. The same cannot be said of glutamate. The role of glutamate and it's role in action potential propagation are well known; however, it's role and behavior during CSD is much debated. While many people believe extracellular potassium diffusion is the mechanism of propagation [38], there is evidence that this does not give a full picture of CSD [102]. A different hypothesis is that glutamate diffusion is behind propagation, this is Van Harrevald's hypothesis [42]. However, 20 years after Van Harrevald retracted this assertion slightly [97] stating that both potassium and glutamate could play roles. Even modern detractors of glutamate propagation push forth the important role of NMDA receptors in CSD [71].

Despite these disagreements, no model that we know of (save for a recent one [22]) include glutamate dynamics. Instead previous models have modeled the NMDA receptor activation as being tied to extracellular potassium concentration [53] or neuronal membrane voltage [86]. Since there has been more evidence recently about the importance of glutamate diffusion and NMDA receptor driven glutamate release [104], we will investigate the influence of glutamate diffusion. To do so, we will introduce a model of glutamate dynamics and NMDA receptor activation that will allow us to investigate the difference in behavior in NMDA receptor driven propagation and persistent sodium driven propagation. These two modes of propagation are driven by extracellular glutamate or extracellular potassium release, respectively.

5.2 NMDA and Glutamate Model

5.2.1 Glutamate Dynamics

Only one previous paper that we know of tracks glutamate as a part of it's model [22]. Many other models use the extracellular potassium model of Kager, Wadman, and Somjen[53] as a stand-in for glutamate in NMDA receptors. Another alternative is the voltage driven activation of Shapiro [85]. For our glutamate dynamics, we seek to have a model that as voltage increases glutamate is released from neurons. This glutamate then flows back into neurons and glia. In the glia it is then cycled back into neurons by

being transformed into glutamine, we will assume that glutamate is not directly released by glia [41](this is the opposite of [22]). The simplest set of equations that have this behavior are:

$$g^e_{Glu} = A\frac{c^n_{Glu}}{c^n_{Glu}+\varepsilon}\tilde{c}_e(\phi_{ne}) - B_e\left(c^e_{Glu} - R_e c^g_{Glu}\right) \tag{5.1}$$

$$g^n_{Glu} = -A\frac{c^n_{Glu}}{c^n_{Glu}+\varepsilon}\tilde{c}_e(\phi_{ne}) + \nu B_e\left(c^e_{Glu} - R_e c^g_{Glu}\right) + B_g\left(c^g_{Glu} - R_g c^n_{Glu}\right) \tag{5.2}$$

$$g^g_{Glu} = (1-\nu)\,B_e\left(c^e_{Glu} - R_e c^g_{Glu}\right) - B_g\left(c^g_{Glu} - R_g c^n_{Glu}\right) \tag{5.3}$$

we borrow the expression for glutamate release (the term with the A) from [12]. We use a fit from their supplemental materials to enforce the "correct" amount of extracellular glutamate that is released.

$$\tilde{c}_e(V_m) = (0.76mM)e^{-0.0044(V_m-8.66)^2} \tag{5.4}$$

A is the release rate for glutamate modified by a current response curve that enforces 0 glutamate release when there is none to release and quickly saturates to 1 for moderate amounts of glutamate. B_e and B_g are the reabsorption rate and glutamate-glutamine cycle rate. ν is a fraction that allows a portion of glutamate to flow back into neurons. R_e and R_g are constants that are chosen to set the desired steady state fraction of glutamate. That is:

$$c^g_{Glu} = R_g c^n_{Glu}$$

$$c^e_{Glu} = R_e c^g_{Glu} = R_g R_e c^n_{Glu}$$

We opt to have a simplified glutamate-glutamine cycle that does not track the glutamine and makes no use of ATP to maintain the rate. For a prolonged depolarized neuronal membrane (like what happens during CSD) this release mechanism will constantly dump glutamate from neurons as fast as it is replenished. So a decline in the rate of this cycle would not impact our model much.

Our parameter choices are detailed in Table 5.1. We should note that our value of A is $50mM/s$ instead of the $500mM/s$ in [12], this is because for our system of equations $500mM$ results in a peak extracellular glutamate value of $2.4mM$. If we look at the

Parameter	Description	Value
ν	Reabsorbtion Rate Percent	0.2 (arbitrary, but near 10%[25]))
A	Release Rate	$50mM/s$(chosen)
B_e	Extracellular Decay Rate	$(42s)^{-1}$[82]
B_g	Cycle Rate	$(84s)^{-1}$(arbitrary)
R_g	Glial fraction	10^{-3} (goal is around $10\mu M$[45])
R_e	Extracellular fraction	10^{-3} (goal is $.01\mu M$[56])
ε	Saturation Constant	$22.99\mu M$[14][75]
D_{glu}	Glutamate diffusion	$0.05 - 0.41\mu m^2/msec$[76]/$6.67 \times 10^{-6} cm^2/sec$[20]

Table 5.1: Parameters for the glutamate dynamics

supplement of [12] at $-10mV$(our maximum membrane potential value) we should have an extracellular glutamate value of $.14mM$. We can get this value by adjusting the release rate to be $50mM/s$. Additionally, while our decay rate comes from [82], our cycle rate is arbitrary. We chose it to be 1/2 the rate into the glia so that the glia could sequester glutamate away from the neurons. A more accurate description of this cycle could be formed using the data and model from [87], however we want to keep our glutamate dynamics simple in this initial study.

5.2.2 NMDA Receptor

While previous CSD models have included NMDA receptors, they all model the glutamate dynamics as being a simple function of either voltage [85] or extracellular potassium [53]. One model included glutamate dynamics [22], however in this model the glutamate is released from the astrocytes and not neurons. During ischemia, glutamate is mainly released via reversed uptake [82, 93] (of both neurons and glia), since the uptake is reversed there is no mechanism to clear the glutamate away besides extracellular diffusion. During this glutamate release, if we use the 2 state model of the NMDA receptor used in [85, 12, 28] or the 5 state model of [29] for a fixed large concentration of glutamate, we'd see that the NMDA receptors would never close. And since the voltage would be raised there could be no Mg block and the neuron would never recover. Perhaps this is just cell death. However, without a strong enough uptake mechanism this would happen regardless of ischemia. This leads to 3 possible conclusions:

NMDA receptors and glutamate have no major role in CSD propagation, there is some un-modeled glutamate uptake/clearance mechanism that remains active during energy starvation, or the NMDA receptors become desensitized to glutamate over time.

Our model is one that takes the last path, if we assume the 4 state model of [82], that has the NMDA receptor go through stages of desensitization, we can have neurons recover. There is evidence for this assumption. Zn provides a partial block that is weakly voltage dependent unlike the full, strong block from Mg[91].

We say that when glutamate is bonded to the receptor it rapidly opens ([75]). It then goes through a period of desensitization before becoming inactivated (eventually) due to glutamate removal. It can then slowly recover to a state that can be reactivated. Thus our gating variables are a system of equations:

$$\begin{aligned}
\frac{O}{y} = \frac{O}{O+C} = F_{Glu} &= \frac{(c^e_{Glu})^{1.5}}{(c^e_{Glu})^{1.5} + (2.3\mu M)^{1.5}} \\
\frac{dy}{dt} &= k_2 D_1 - k_1 F_{Glu} y \\
\frac{dD_1}{dt} &= k_1 F_{Glu} y + k_4 D_2 - (k_2 + k_3) D_1 \\
\frac{dD_2}{dt} &= k_3 D_1 - k_4 D_2
\end{aligned}$$

where the variables are fractions of channels in either: Closed (C), Open (O), Open+Closed (y), Desensitized 1(D_1), Desensitized 2(D_2). The desensitized states are (mildly) arbitrary. In [82] they used 33% and 16% conductance respectively. We need the second state to be a smaller value (5% or less) in order to achieve recovery in our simulations.

We will just denote these d_1 and d_2. We then form the channel conductance as:

$$j_{NMDA} = P_{NMDA}\,\hat{g}_{NMDA}\left(\frac{2}{3}J_{Na}^{k,NMDA} + \frac{1}{3}J_{K}^{k,NMDA}\right) \tag{5.5}$$

$$J_i^{n,NMDA} = \frac{F\phi_{ne}}{RT}\frac{c_i^n \exp\left(\frac{F\phi_{ne}}{RT}\right) - c_i^e}{\exp\left(\frac{F\phi_{ne}}{RT}\right) - 1}, \quad i = Na, K \tag{5.6}$$

$$\hat{g}_{NMDA} = G(\phi_{ne})\left(y(t, c_{Glu}^e) + d_1 D_1(t, c_{Glu}^e) + d_2 D_2(t, c_{Glu}^e)\right) \tag{5.7}$$

$$G(\phi) = \left(1 + 0.28\exp(-0.062\phi)([Mg^{2+}]_e/3.57)\right)^{-1} \tag{5.8}$$

The NMDA receptor is blocked by magnesium. This scales as given the equation $G(\phi)$[51], we will set magnesium to a fixed value of $2mM$, but the range is anywhere between $1mM$ and $2mM$. Additionally, the flux into the NMDA receptor is 2 thirds from sodium and 1 third from potassium. While calcium also flows through the NMDA receptor, it only contributes to 5% or less of the current for extracellular calcium concentrations seen during CSD[52].

Parameter	Description	Value
P_{NMDA}	NMDAR Permeability	0.0 - 5×10^{-5} cm/sec
Mg^{2+}	Magnesium Concentration	1-2mM
d_1	First Desensitize Percent	0.1-0.33(chose .1)
d_2	Second Desensitize Percent	0.0-0.05(chose .01)
k_1	$y \to D_1$	$3.94s^{-1}$
k_2	$D_1 \to y$	$1.94s^{-1}$
k_3	$D_1 \to D_2$	$0.0213s^{-1}$
k_4	$D_2 \to D_1$	$0.00277s^{-1}$

Table 5.2: Parameters for the NMDA receptor. We vary permeability over a large region.

5.3 Example Simulation Results

Quickly we will show the detailed time evolutions of all of the state variables of the model in Figure 5.1. This is a 1D simulation of a wave, time plots are taken at a point

in the middle of the domain. We can see the telltale DC shift (the extracellular voltage becoming negative), we see the neurons depolarize with the glia following. We see a massive release of potassium from neurons and the subsequent uptake of sodium. We see the slow recovery of the neuron even after the extracellular space has (appeared) to recover. Harder to see is the neurons(and glia) swelling with the extracellular space shrinking.

5.4 NMDA Receptor Models in the Literature

Before we proceed into our results, lets first discuss in greater detail how previous models have used the NMDA receptor. We will discuss these with an eye towards the possibility of glutamate or NMDAR driven propagation. The primary method of argument for which substance drives propagation is to see which variable begins to rise first. So if potassium rose before glutamate, this implies potassium drives propagation.

Most paper's cite back to Kager, Wadman, and Somjen's model [53] of glutamate activation that is controlled by extracellular potassium. This model naturally has glutamate rise in tandem/after potassium is released. So it would not allow for glutamate driven propagation. It would however serve an intermediate result of NMDAR driven propagation. They do cite a result of having either NMDAR or persistent sodium driven initiation. They mention in the discussion that it has been shown that a cocktail blocking both persistent sodium and NMDA receptor conductances stops CSD. Blocking only one or the other reduces but does not eliminate CSD [53].

An alternate to the potassium driven approach of NMDAR activation is the purely voltage driven activation of Shapiro [85].

Two previous models use glutamate directly. [22] and [72]. [72] is the previous iteration of our electrodiffusion model. In this work O'Connell made use of the NMDA receptor(a 2 state model) and glutamate model from [12], with some slight modifications to limit the amount of glutamate released. A key component she added was glutamate "decay" into glia. Over the course of a simulation the glia sequestered and kept excess

glutamate. This permanent clearance is how she managed to attain recovery for larger values of NMDA receptor permeability. Because we wanted to include glutamate in the same way the other ions are modeled, and we wanted to allow for multiple spreading depolarizations, we had to modify this model into the one introduced above.

The other paper that uses glutamate in its NMDAR model is Terman, et al's paper [22]. In this paper they use a model of the Na-Glu transporter (EAAT2) to make glia release glutamate by reverse uptake (in line with [93]). We attempted this model as our glutamate release mechanism, but we found that it did not release enough glutamate to allow for NMDAR driven propagation. This is in line with their [22] results about glutamate being able to initiate CSD but not propagate it. Switching our glutamate release dynamics to the neuron driven model of [12] and using the NMDAR permeability that [22] used, we still do not achieve propagation. However, if we use a value of NMDAR permeability that is an order of magnitude larger (in line with other models[53]), we do achieve NMDAR driven propagation. My interpretation of these results, glial glutamate release is not a precursor to CSD, however, neuronal release of glutamate may be.

On the experimental side, we can look at [34] experiment (mentioned by [22]) as recent proof that interstitial potassium diffusion is behind the propagation of CSD and not glutamate diffusion. It shows that extracellular glutamate increased after the neuronal calcium wave but before the astrocyte calcium wave. And all of these happened after the DC shift, which looked to arrive just after the extracellular potassium increase. However, it should be pointed out that the NMDA receptor activates for very small concentrations of glutamate (picture a log scale). So, even if NMDA receptors are the drivers of the wave, it might be possible that glutamate rise is not apparent at the leading edge of that wave. Indeed if you create the plots seen in this paper with our model, it appears that the DC shift arrives just before potassium rise and glutamate rise happens significantly after (fig.5.2). However, if one looks at a log scale for the concentrations, we can see that the initial rise in glutamate causes the voltage shift to become more pronounced. This is how our model is designed when the persistent sodium is turned off: glutamate is released in response to voltage, this opens NMDA receptors releasing potassium. Additionally, it is worth mentioning, neuronal calcium

is expected to increase when NMDA receptors open. And since calcium increases by a much smaller amount it's increase might be noticed more quickly than potassium.

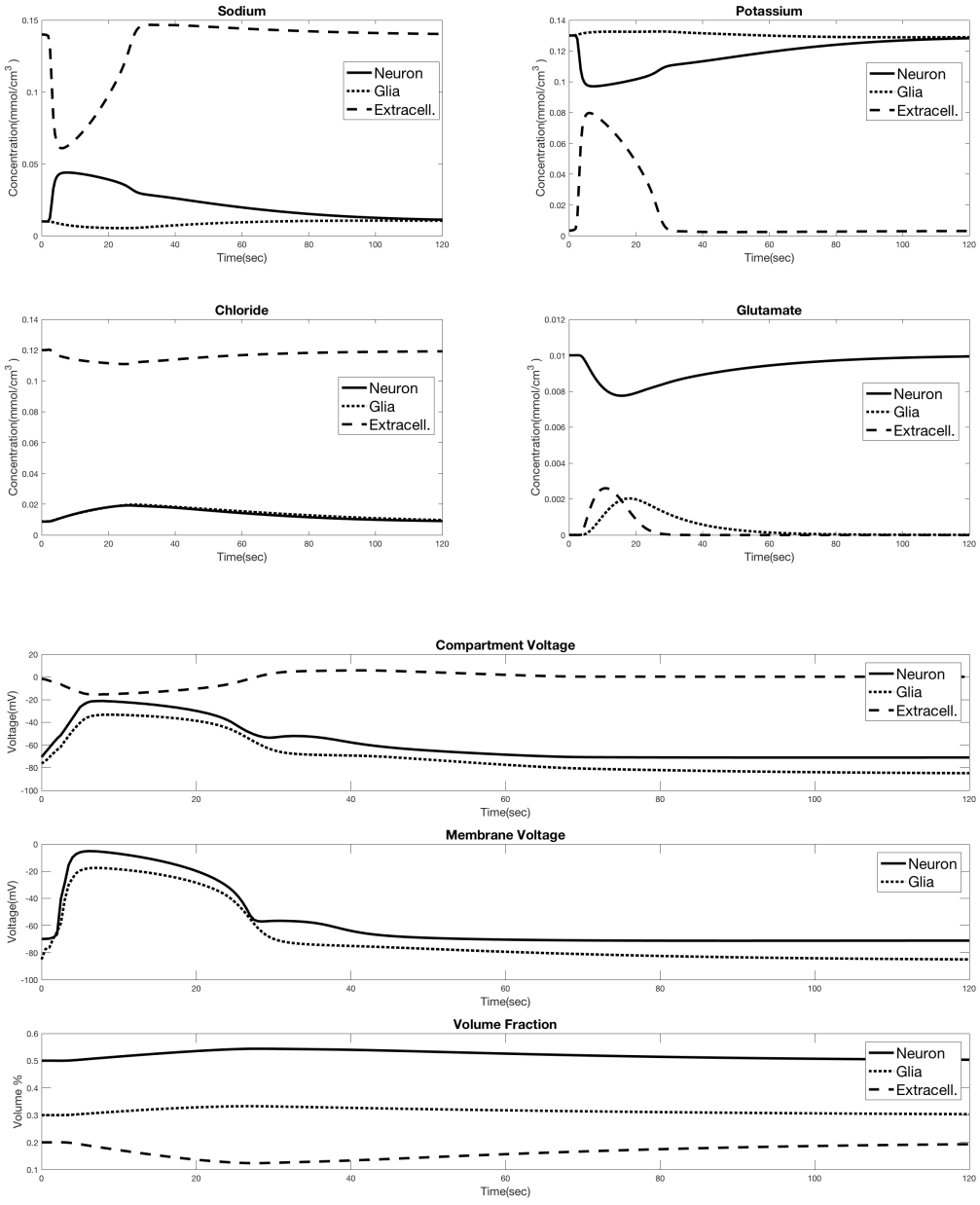

Figure 5.1: Full variable detailed time plots from a 1D simulation with $P_{NMDA} = 1 \times 10^{-5} cm/s$ and $P_{NaP} = 2 \times 10^{-5} cm/s$. These time plots are evaluations at some point in the middle of the domain as a wave passes.

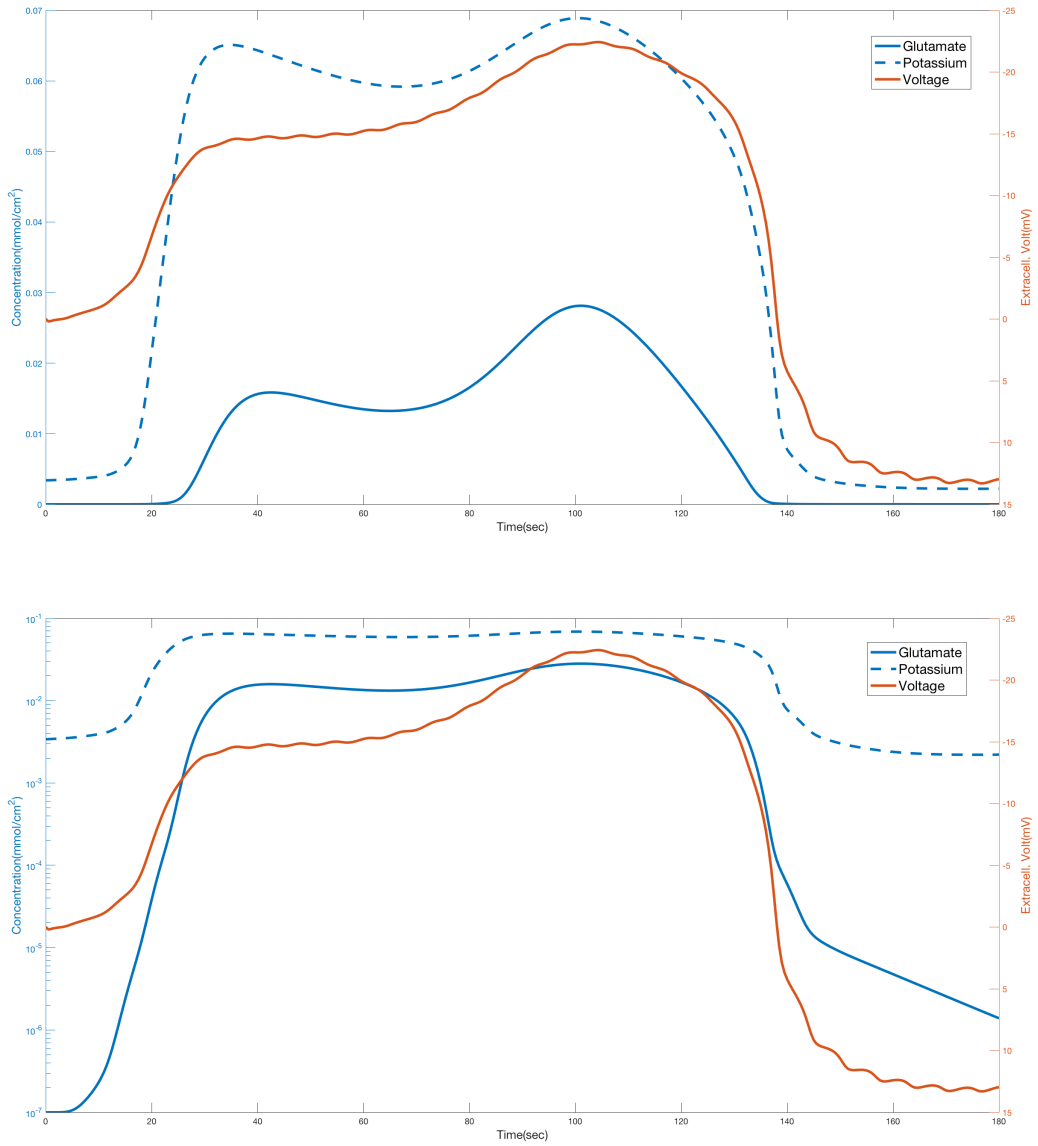

Figure 5.2: Looking at extracellular glutamate(scaled up by a multiple of 10 for ease of visibility), potassium, and voltage(axis is flipped). First graph is a standard scale. Second has concentrations on a log scale. From the first graph it looks like potassium leads glutamate. However, the log plot shows that it is glutamate that rises before extracellular voltage.

Chapter 6

One Dimensional Dynamics

6.1 NMDAR as a Means of Propagation

We previously mentioned that there are several theories of propagation. The two we focused on are both driven by extracellular diffusion, one through potassium, the other through glutamate. In our model there are two vehicles for propagation: the persistent sodium channel and the NMDA receptor. These have been identified as the methods of propagation in other models [89] and the difference between them has been used to explain certain behaviors in the resulting depolarization. The results of our simulations put forth 2 types of propagation. The first is persistent sodium driven propagation that relies on potassium diffusion. The second is NMDA driven propagation that requires glutamate diffusion, with potassium assisting. However, these 2 kinds of propagation lay on a spectrum, there is a whole middle ground where both of these mechanisms work in concert to create spreading depolarizations.

First, we should look at the behavior of the velocity and duration of CSD as we vary NaP(persistent sodium) and NMDARs and allow glutamate to diffuse, Figure 6.1. We can see that increased expression of both channels correlates with increased velocity. However, persistent sodium has a significantly greater impact on speed; purely NMDAR driven propagation has a speed 20% that of purely NaP driven propagation. This observation is in line with other models [85]. In addition, the opposite is true of the duration. As NMDAR increases we see an initially small increase in duration, then

once we get to a certain level the duration quickly increases from around 30 seconds to upwards of 100 seconds. This observations fits with experiments in the hippocampus [44], where the duration in the dendrites(stratum radiatum) is longer (about 2-3 times longer) than the duration in the somata(stratum pyramidale). Next, we can contrast these results with simulations where we set glutamate diffusion to zero, Figure 6.2. We can see that while the NMDA receptor has some effect on propagation (most noticeably, allowing propagation to occur with slightly less persistent sodium expression), its effect is significantly reduced.

This observations allows our model to fit nicely within the observations of the difference between normoxic and anoxic spreading depolarizations. Normoxic SD is blocked by NMDAR antagonists, while anoxic SD is either not impacted or delayed by NMDAR antagonists but not stopped[89]. Therefore, our model with more NMDAR expression fits a model of normoxic CSD, whereas less NMDAR expression fits a model of anoxic spreading depolarizations more closely. However, that view is too simplistic as the effects of NMDAR blockers change depending on age and brain region[68, 78], our model allows us to investigate all of these effects in one unified framework, as age and brain region differences can be explained by the difference in ion channel expressions.

Going back to which substance drives propagation. We can conclude that if NMDA receptors are driving propagation, then the propagation is influenced by glutamate diffusion regardless of the presence of persistent sodium channels. When persistent sodium and NMDARs are working in tandem it is the action of both potassium and glutamate diffusion that pushes the wave along. In fact, in the absence of persistent sodium channels, potassium diffusion has little effect on the propagation speed(from simulations where we lower potassium diffusion).

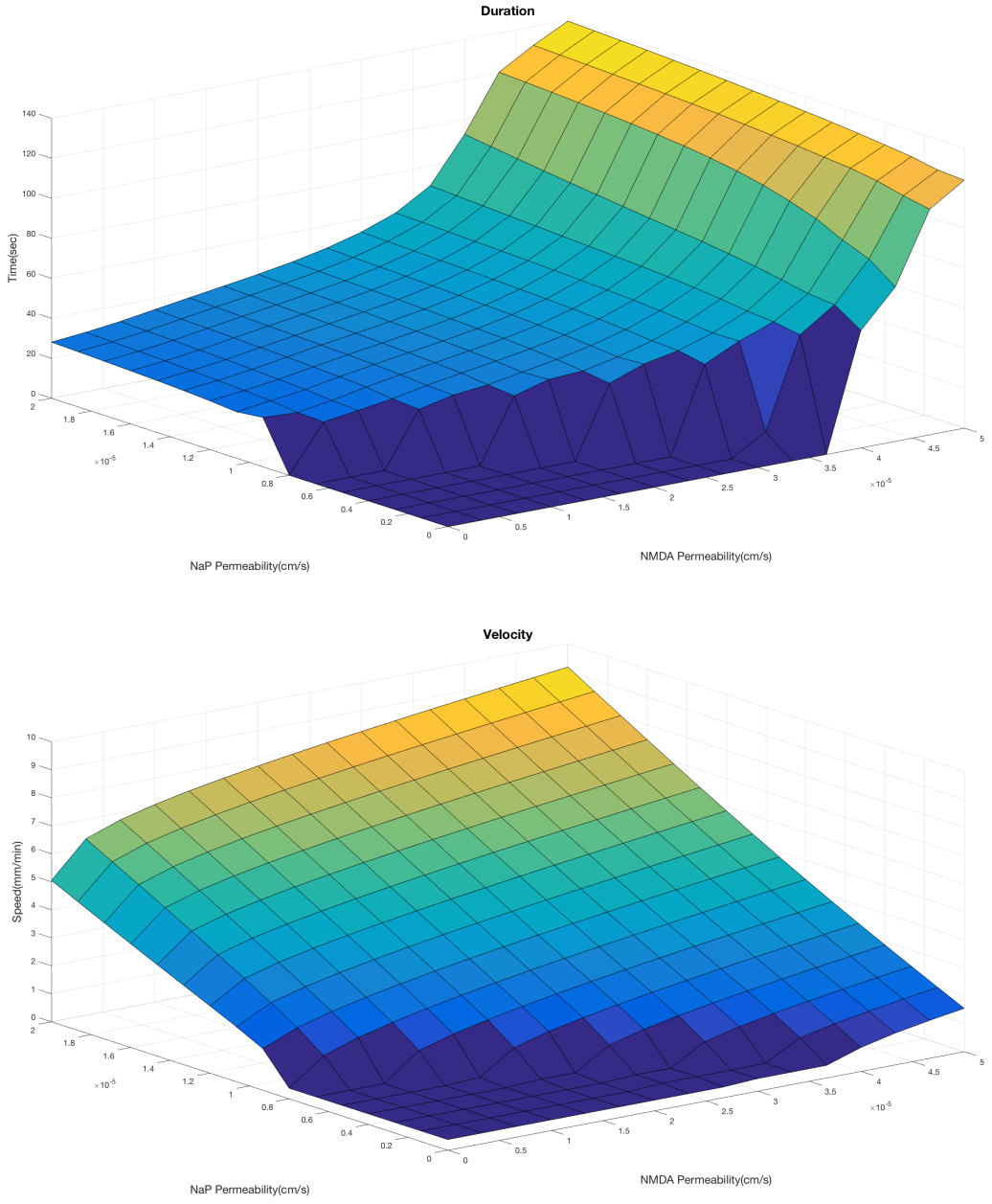

Figure 6.1: Duration and Velocity of spreading depression over a range of P_{NaP} and P_{NMDA}.

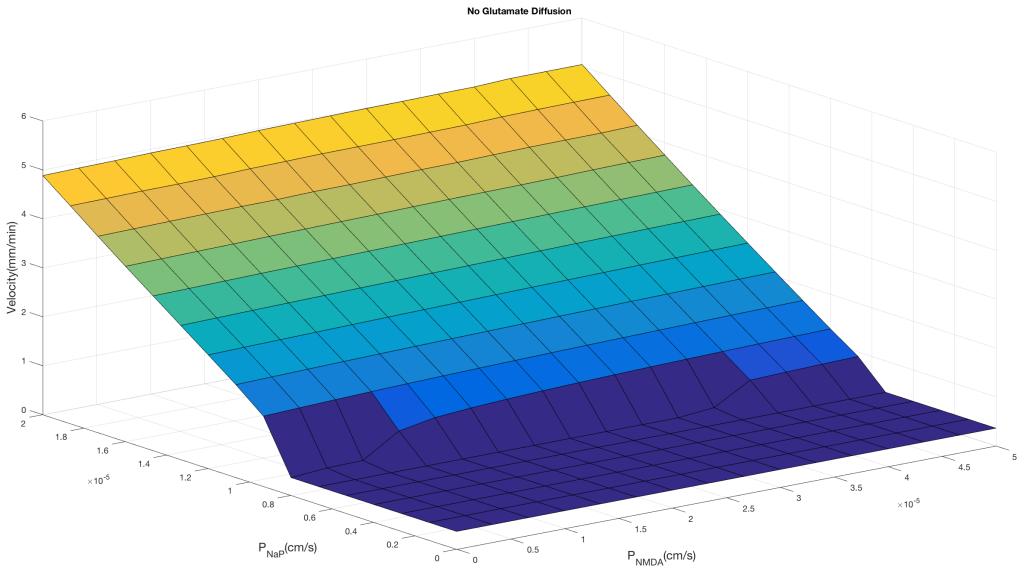

Figure 6.2: Velocity of spreading depression when there is no glutamate diffusion.

6.2 Voltage and DC Shift Influenced by NMDAR

NMDAR's presences impacts more than just duration and velocity. The time course of the depolarization changes with NMDAR as well. In figure 6.3, we can see a secondary depolarization of the neuron. This secondary bump is not coming from the neurons own voltage, but actually from the DC shift. While our model has a DC shift in the absence of NMDAR, the NMDA receptor has modified its behavior. As evident in figure 6.4, we see a second (greater) negative shift. The initial DC shift (as well as the lone DC shift under purely NaP dynamics) reaches a minimum of $-15mV$, this secondary shift goes below $-20mV$, nearing $-25mV$. This is consistent with some experiments [44, 89], and can be explained by experiments that show that the DC shift changes depending on where the measurements were taken [78, 16] or if the NMDA receptor is blocked [44]. Measurements taken near the dendrites show this secondary hump, whereas measurements taken near the soma lack it. This fits a hypothesis where our model with NMDA receptors (and NaP channels) represents a model of the dendritic layer and our model without NMDA receptors represents a somatic layer or anoxic spreading depolarization. Indeed, the existence of this two valley behavior is due to the persistent sodium channel. As the persistent sodium channel deactivates, we get an initial recovery, and this recovery is cut short by the NMDA receptor taking over, which fits with observations that in [89]. Another interesting observation is as NMDAR increases and persistent sodium decreases we see an increasing positive polarization in the extracellular voltage. In fact, for a fixed persistent sodium permeability, Figure 6.3, at around the halfway point of NMDAR permeability in we can see the disappearance of the 2nd hump accompanying an appearance of an increasing hyper-polarized recovery, curiously this is seen in [44] in their partially blocked NMDA-receptor experiment.

Related to these observations, we see interesting behaviors of other variables. We see that extracellular potassium has an appearance of a second hump when NMDAR permeability is high enough (fig .A.2), the partially weakened NMDA behavior of this graph looks very similar to the experimental results of potassium concentration in [44]. In the same figure, we have a very strange slow increase in sodium that reaches a quick peak that dips back down towards steady state (notably, very different from those same

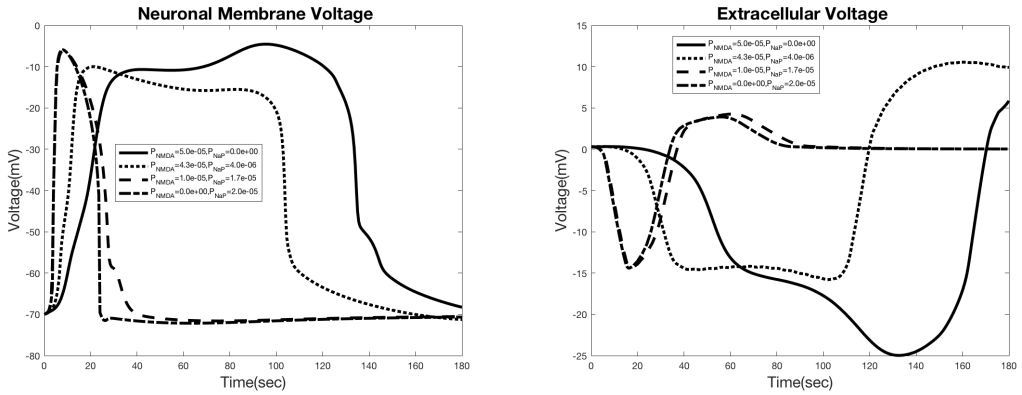

Figure 6.3: Time profiles of neuronal membrane voltage and extracellular voltage. Sampled are 4 different pairs of NaP and NMDAR permeabilities. 2 of these have strong NaP permeability and weak NMDAR permeability. The other 2 have strong NMDAR but weak NaP.

results in [44]). For our model, this quick peak comes from the sudden recovery of the extracellular volume (fig. 6.5). Also seen here, is the increased shrinking of the extracellular space that follows from having a higher NMDAR permeability. We transition from having a minimum of 12% extracellular volume fraction to nearly 2%. This new volume shrinkage is very important because volume influences concentrations.

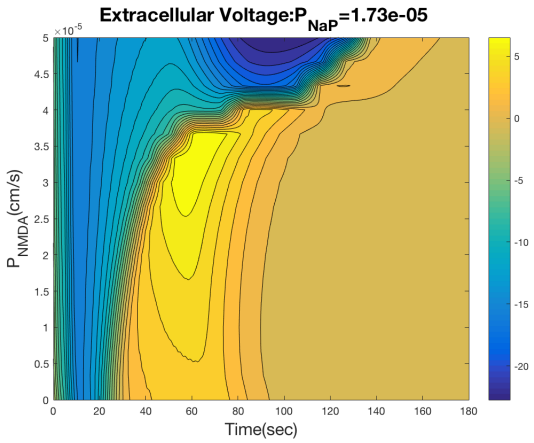

Figure 6.4: Time profiles with extracellular voltage as NMDAR permeability is varied.

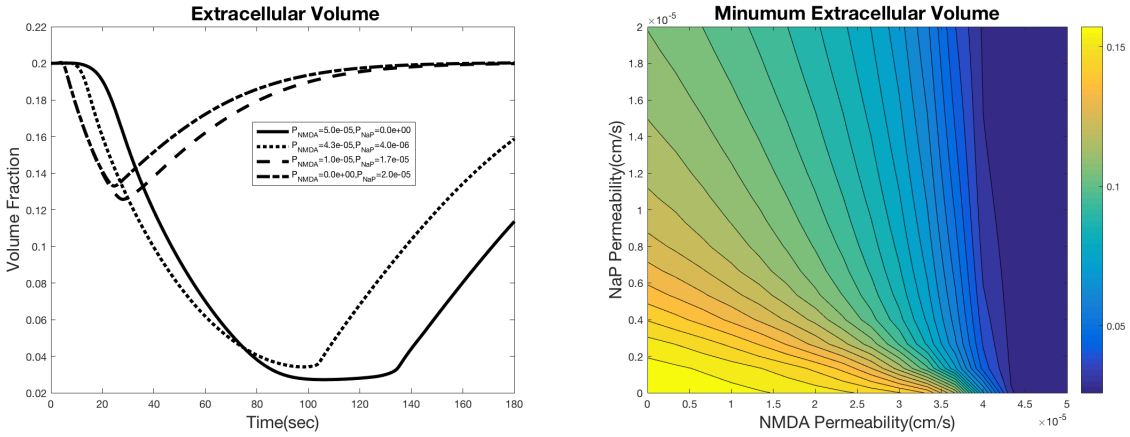

Figure 6.5: Time profiles of extracellular space for 4 samples of NaP and NMDAR permeability. Also the minimum extracellular volume as it depends on both NaP and NMDAR.

6.2.1 Interaction of Volume and NMDA Receptors

We can investigate the role volume changes have in our model. In some models cellular swelling had almost no effect [101], but in others it was necessary for propagation [85]. Our model conforms with neither of these. We can adjust the effect of volume changes by changing the hydraulic permeability coefficient. Without NMDA receptors, this has almost no effect besides reducing the expansion of neurons and glia. But, with NMDA receptors we can see an effect(see figures 6.6 and 6.7). For large enough NMDA receptor permeability we see the 2 DC shift humps, but as the neurons and glia are swell less these humps disappear. While NMDA permeability needs to be a certain level to see the second depolarization, it interacts with the constriction of the extracellular space in a surprising way. Because glutamate is released during depolarization at a constant rate and reaches an equilibrium after being absorbed back into the glia, the total amount of glutamate stays at a constant (heightened level, see Figure 6.8), however, the slower inactivation of the NMDA receptor causes the neurons and glia to swell more. This constricts the extracellular space making the concentration suddenly spike. Since NMDA receptors are activated by the concentration of glutamate and not the amount, we see a second reactivation of NMDARs. This behavior cannot be attained with voltage gated ion channels and can only be achieved with a ligand-gated channel.

We can summarize all of the mechanics of the persistent sodium channel and NMDA receptor in the diagrams of Figures 6.9 and 6.10. When persistent sodium drives depolarization neuronal swelling has no direct impact on further depolarization. We see extracellular potassium being the substance that drives the wave forward. When NMDA receptors help drive the depolarization neuronal swelling assists with further depolarization, causing prolonged duration and a second DC shift. Propagation becomes the joint effort of extracellular potassium and glutamate.

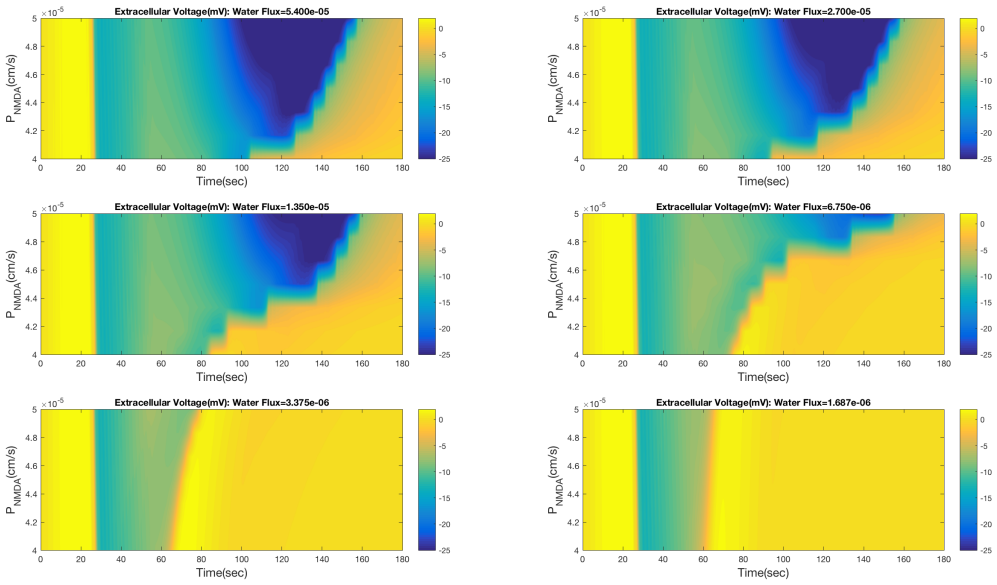

Figure 6.6: Time profiles of extracellular voltage. We vary NMDA receptor permeability between $4-5\times10^{-5}$cm/s along the y-axis. Each panel has a different value for hydraulic permeability(water flux). For small enough hydraulic permeability, the wave looks no different than a persistent sodium driven wave with no/little NMDA receptor activity.

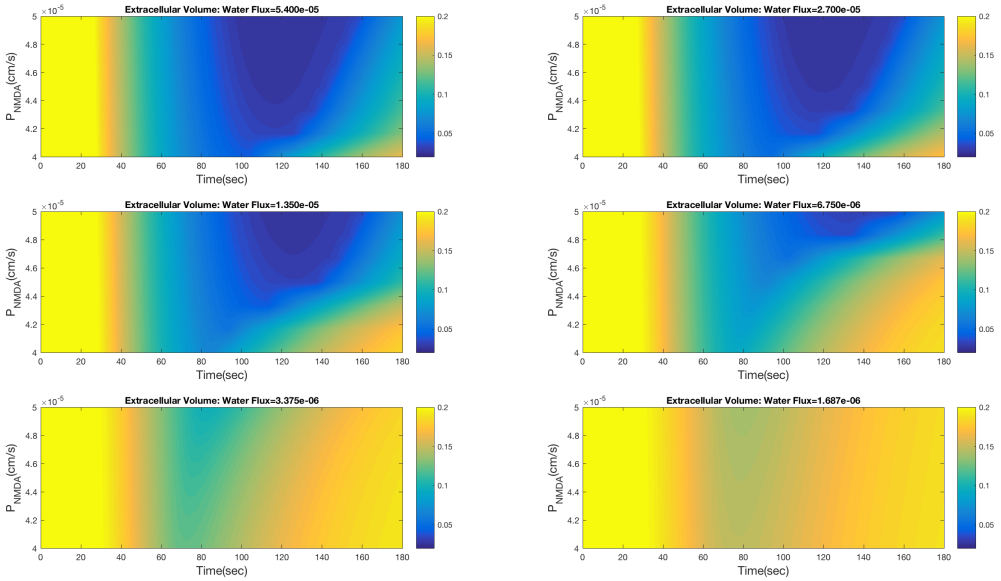

Figure 6.7: Time profiles of extracellular volume. We vary NMDA receptor permeability between $4-5\times10^{-5}$cm/s along the y-axis. Each panel has a different value for hydraulic permeability(water flux). We can see the decreasing change of volume as we vary the hydraulic permeability.

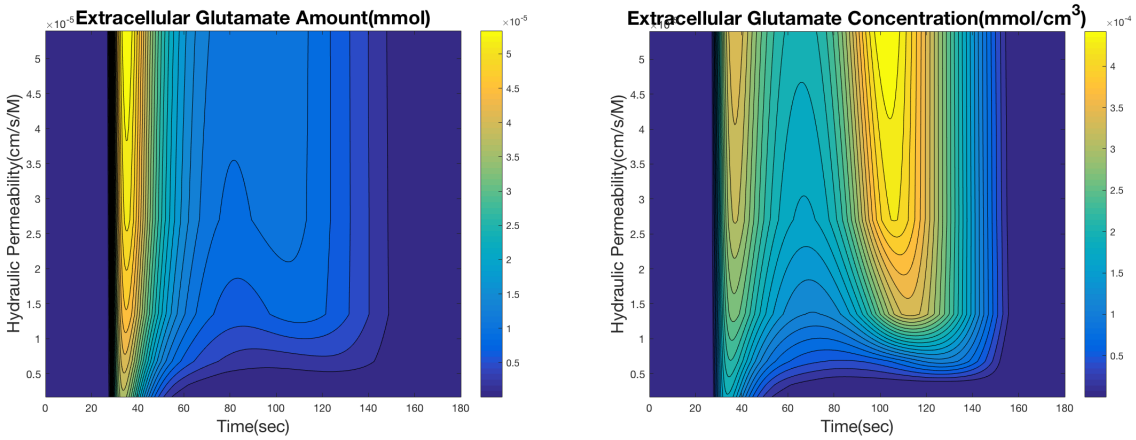

Figure 6.8: Effect of varying hydraulic permeability on extracellular glutamate. This shows the difference between the amount of glutamate(concentration times volume) and just concentration.

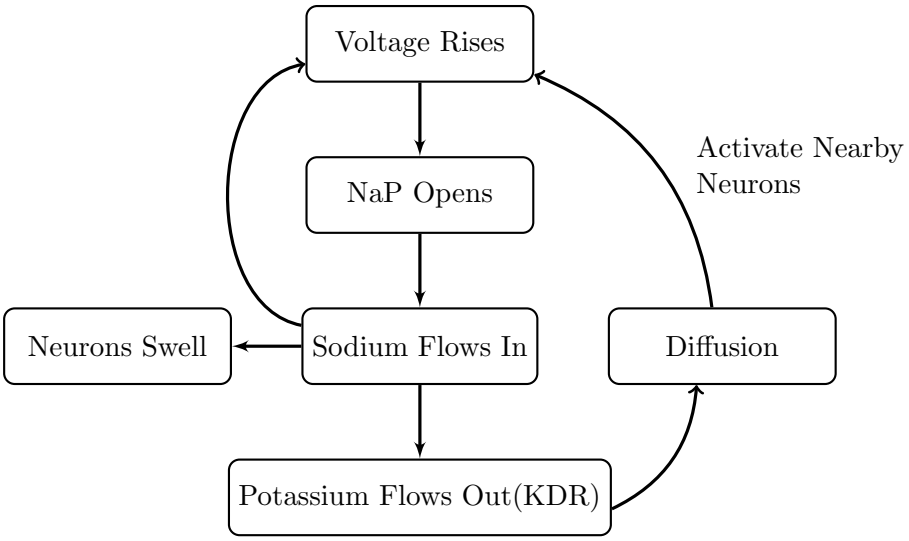

Figure 6.9: Summary of Initiation and Propagation due to the persistent sodium channel activation and interstitial potassium diffusion.

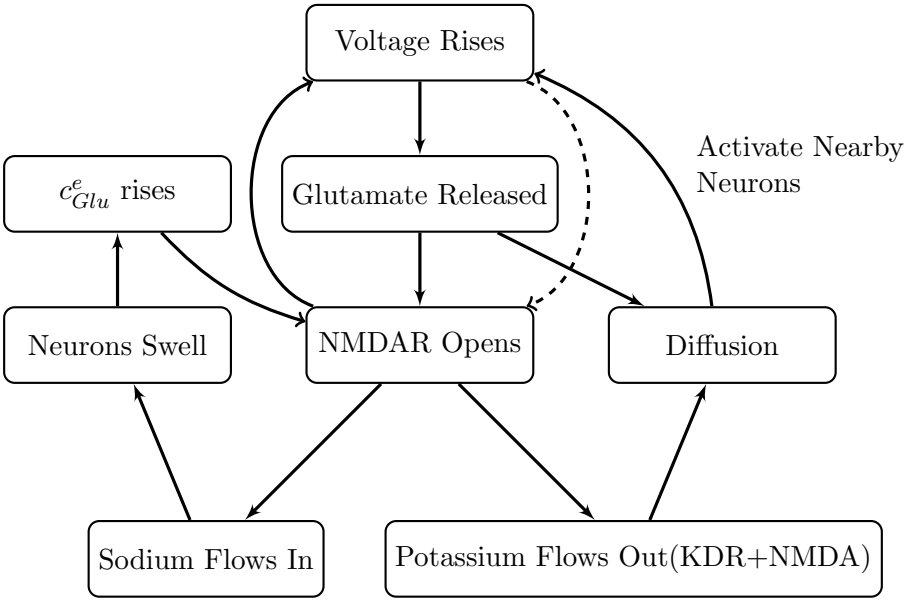

Figure 6.10: Summary of CSD dynamics of our model. Initiation due to NMDA receptor with propagation caused by the combination of interstitial glutamate and potassium diffusion. Neuronal swelling causes prolonged activation of NMDA receptors.

6.3 Recurrent Spreading Depressions

It is of clinical importance to understand the impact of recurrent spreading depressions, repeat CSDs facilitate dendritic damage[81], can impact oxygen availability after subarachnoid hemorrhage[15], and lead to cell death [30]. Experiments have shown that recurrent spreading depression behave differently than a single wave. For example,[37] found that the time between excitations impacted the subsequent speed of the waves. [43] found that repeat depolarizations influenced the duration, amplitude, and latent period in odd ways. They additionally found that during long exposures an unstable form of CSD would form, one where there would be smaller regular amplitudes that shifted into larger amplitudes. We can investigate these behaviors within our model. While Chapter 7 will investigate self-sustaining recurrent SD, here we will look into the dynamics and transitions that occur due to an exterior(outside the region) influence.

First, lets look at the velocity of repeated excitations. There are many ways to repeatedly excite the domain. We will use two in this section. Using our excitation defined in Chapter 3, we can just remove the cutoff so that it just oscillates for all time on a boundary point. The effect of this is that the left boundary is a permanent state of depolarization and causes waves to periodically spread across the rest of the domain as soon as it is able. The second method of excitation we use is a rapid excitation that cuts off quickly but recurs. For example a pulse that activates for $50ms$(using the same excitation as Chapter 3) then remains off for $5s$. This method allows a longer refractory period.

Taking the first method of excitation we can cause waves to propagate as frequently as the model allows. We can use this to investigate the interplay between velocity and latency period. Consider Figure 6.11, we can see that there is a very close relationship between the latency period and the velocities. Just like [37] found, when we re-initiate CSD we see the velocity drop sharply (from the initial $5.5mm/min$ to $3.3mm/min$ with a period of recovery of 81 seconds). We also can see that once the latent period reaches near 60 seconds, it takes a longer subsequent period before the neurons recover enough to depolarize again. This longer time allows more time for the whole domain

to recover, thus the velocity becomes faster again. When we look at the time profile near the boundary we can see why this transition happens (Figure 6.12), on the 6th excitation the neuron only depolarizes to $-50mV$, in the model this point is normally an unstable steady state, however because of the distress of the previous 5 CSDs, this point now doesn't get passed to a higher voltage. This small wave does not penetrate into the domain. So, the remaining sections of the domain are allowed a longer time to recover.

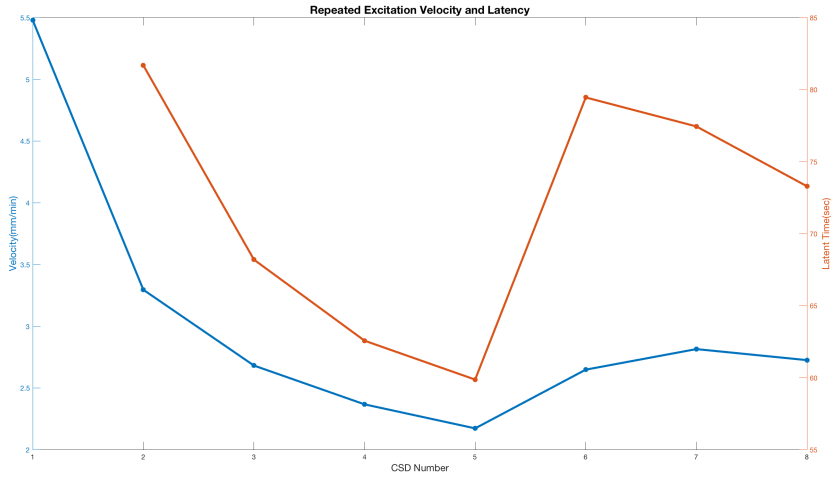

Figure 6.11: Repeated excitations for 12 minutes. Allowing 8 waves to spread through the domain. Here we see the velocity of the 8 waves and the 7 latency periods between them.

Next, we look at the results using the second type of activations: periodic, short pulses. The only difference this presents is in the side of the domain that touches the boundary, the rest of the behavior is the same as if we did a prolonged pulse. We will look at the effect varying parameters has on these repeated CSDs. Figure 6.13 shows that for certain parameter changes the second wave that passes through the domain is delayed as a nice continuous function. But there are certain points where a transitions occurs, and a small change in the parameter causes a much longer waiting period. After the second wave passes we can see that this process repeats in a nonintuitive way. While for each specific KIR value the duration of each wave is nearly constant the latent period

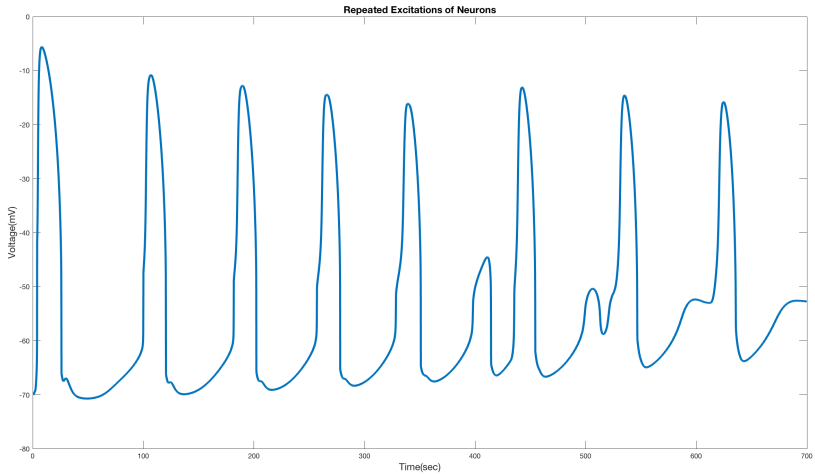

Figure 6.12: Repeated excitations, the boundary is constantly excited. This is a time profile of a point close to it.

changes on the range of 10 seconds to 100 seconds. We can see these transitions more easily by measuring the latent period between each wave(Figure 6.14). Looking at this latent period, we can clearly make out the smooth decrease in latency that occurs for increasing KIR. Then at some point near 1.7(and 1.95) we see a sharp transition. We can see that these transitions happen more readily for the 3rd wave (measured by the second period). The 3rd and 4th periods are even more jagged.

These bifurcations are quite robust. Changing persistent sodium or NMDA causes the same behavior to occur. The same transitions happen for different frequencies of excitement and different amplitudes. These sharp transitions can help explain the results of [43], where adjacent cells did not depolarize at the same time. These cells could have different expressions of ion channels, and as we showed, even a small difference can cause a huge difference in the time the depolarization occurs. Additionally, this odd irregular depolarization that we see (Figure 6.12) fits well with the unstable behavior they found in the stratum radiatum[43] (and the behavior in the stratum pyramidale fits well with our results in Chapter 8). And the observations that the two hippocampal layers switched their order of excitation after subsequent waves could fit with the observations in Figure 6.15, where the first wave occurs simultaneously, the second has

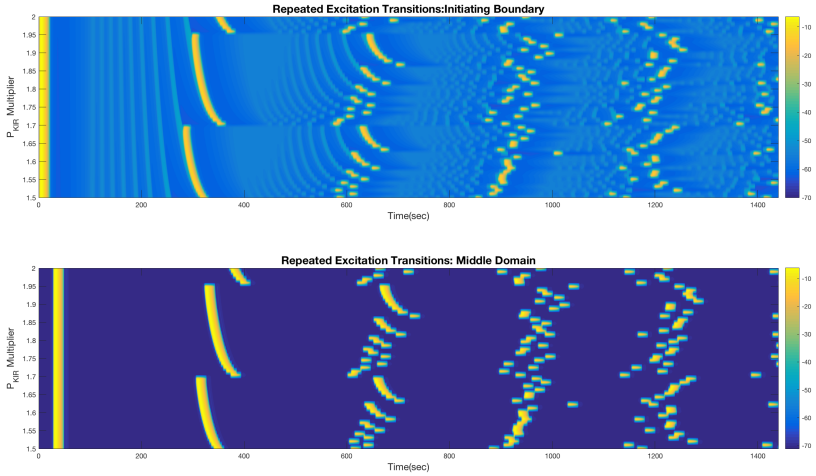

Figure 6.13: Periodic excitations for 24 minutes. Effect of changes in KIR permeability has on the propagation/initiation. Top panel is the boundary point that is excited. Bottom panel is .25cm into the domain.

red leading, where the 3rd, 4th, and 5th have blue leading.

This type of resonance could be very important in the complicated interaction between sections of the brain. With their different ion channel expressions and underlying geometry a circular feedback between different regions could be initiated or canceled with the help of these transitions. It appears that they happen when the displacement from the resting state reaches a certain level. And while in this section we forced these repeated excitations, they can naturally occur if a self-sustaining CSD wave or an ischemic region is interacting with a region away from itself.

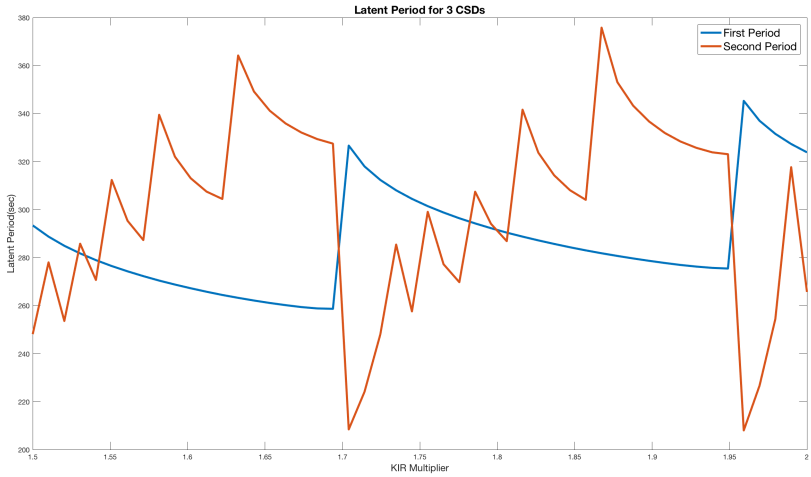

Figure 6.14: Latent period for different values of KIR. Blue curve is the latency between the 1st and 2nd wave. The red curve is the latent period between the 2nd and 3rd.

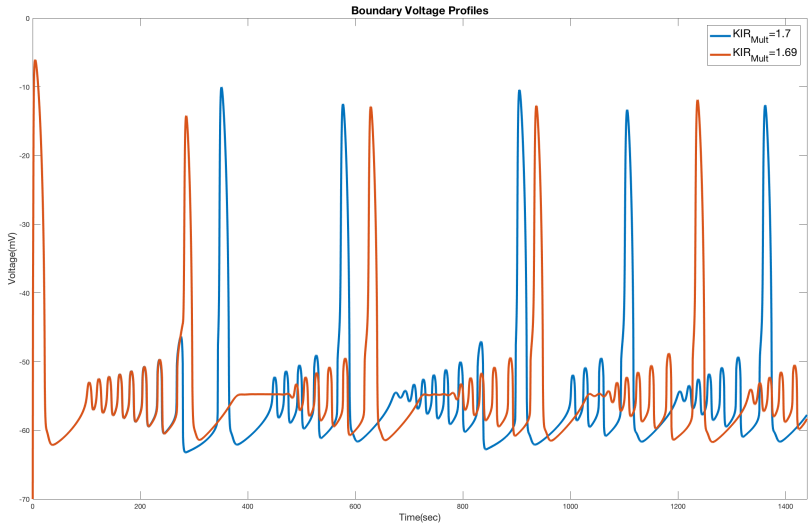

Figure 6.15: Time profiles of the boundary that is excited for two KIR multiple values that are near each other.

Chapter 7

Spirals

7.1 Spiral Patterns

Moving up to 2 dimensions allows us to have more interesting dynamics (spirals/recurrent spreading depolarizations). We create a spiral by temporarily inhibiting neurons in a section of tissue. This allows a wave to propagate around it. We then slowly allow the region to recover. Once this regions fully recovers we are left with a self sustaining spiral. This is how spirals can be formed in a laboratory setting [23]. Due to how we formed the spiral(and because of the discrete grid size) it is not a perfectly stable spiral shape, the center has some regions that are out of sync with the spiral, figure 7.1 shows 4 time samples of a spiral that we formed. Other papers have discussed spiral formation of CSD, but they have used nonlocal coupling in phenomenological models to achieve their spirals [23]. For computational reasons we limit the size of the domain to a .5 cm by .5 cm square, because of this there are slight edge effects, but these only impact the waves we show near the edge.

In addition to the voltage, we can see how different the other state variables look during a spiral in Figure 7.2. We can see how the two main drivers of the wave have the most crisp spiral shapes (extracellular potassium and glutamate). Neuronal sodium has a pronounced recovering edge of the spiral. It is also clear how glia act as potassium buffers as the entire right hand side of the domain has a very prolonged wake, with the minimum only occurring near the spiral center. Looking at volume, we can see that

it appears the cellular volume shrinks just before the spiral arrives, however, that is actually the volume getting nearly back to steady state levels before being disrupted by the next rotation of the spiral. We can compare these resulting time profiles of a point to the plane wave case, the summary of this comparison is that the duration of either increase or decrease of each variable is shortened by the influence of the onset of another depolarization. Tied to this duration change, some variables see slightly less of a rise or fall (for example peak neuronal membrane voltage is -5mV in a plane wave, but -10mV in a spiral), the difference is likely due to the system not being allowed to fully reach steady state before each excitation.

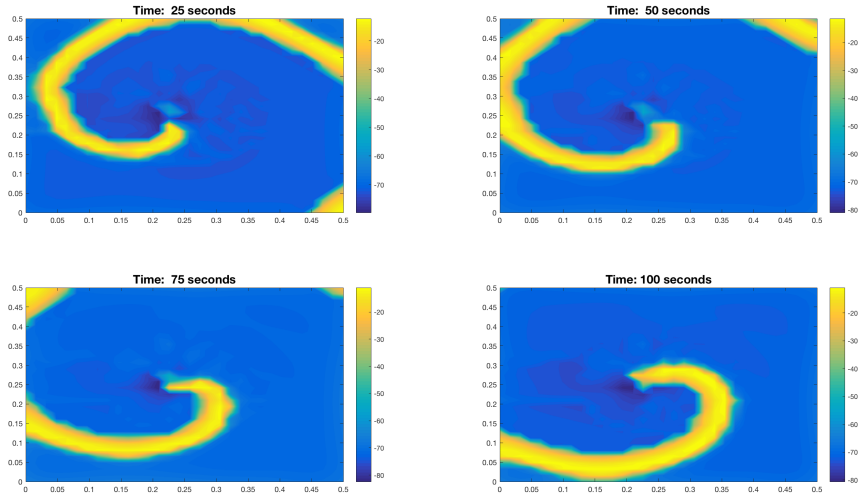

Figure 7.1: Example Spiral. Showing neuronal membrane voltage.

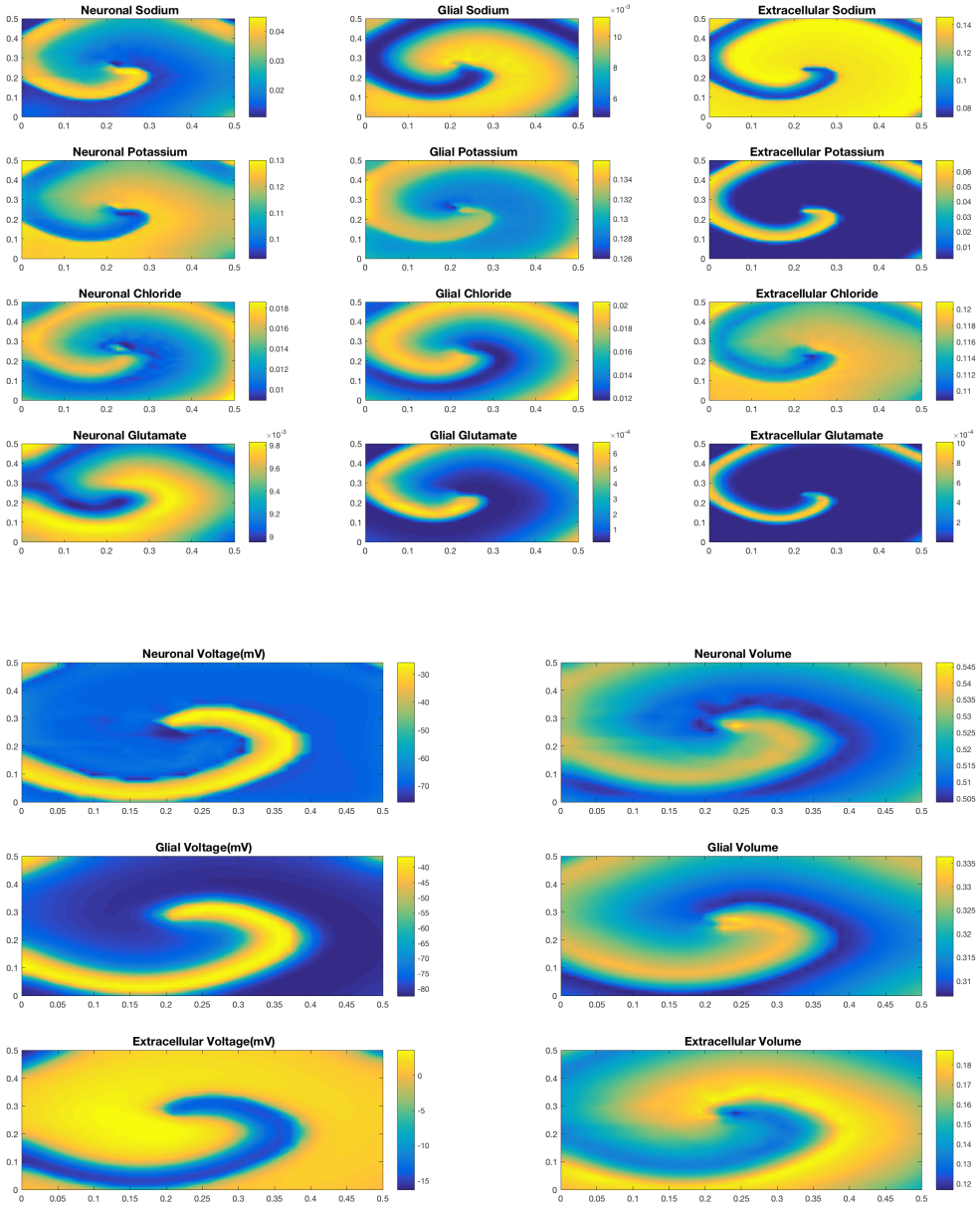

Figure 7.2: Examples of the values of each of the major variables during a spiral. Notice the counter balancing ions (Chloride, extracellular sodium, and glial potassium) have very wide arcs that the main drivers do not have (neuronal sodium/potassium, extracellular potassium, extracellular glutamate).

7.2 Spiral CSD as a Regulator

The formation of a spiral causes several interesting changes from the plane wave/1D case to arise. The non-uniform nature of a spiral causes the center and the outer region to behave different. The central region sees very irregular depolarizations (the exact center shows this the most, never being allowed to get below -50mV), whereas the outer region sees regular periodic depolarizations.

Just like the 1D case, we can look at the velocity of the wave (for details on how we calculated the 2D velocity see the appendix). Because we have a spiral, different points in the domain experience different velocities, Figure 7.3. The speed increases as we move away from the center, with the center moving at a speed near $0.5mm/min$ and the near-boundary moving no faster than $3.5mm/min$. This maximum speed is a near 50% decrease in speed when compared to a plane wave traveling with the same set of parameters. This same behavior has been observed in experiments [37, 24](chicken retina). There it is explained that the speed loss correlates with the length of the recovery period of repeated CSD initiation, and the reported speed loss was 49% in [24]. We can look at the period/frequency of excitation as well, Fig. 7.4, and see that away from the core the period between excitations decreases.

Now, we can investigate how this change in behavior carries over to the transition from persistent sodium driven propagation to NMDAR driven propagation. We can see (in Fig. 7.5) that since the spiral limits its own propagation speed, we do not see the same speedup as in 1 dimension. Previously, along the $P_{NaP} = 2 \times 10^{-5} cm/s$ line, the NMDA receptor caused a nearly 2-fold increase in speed, for the spiral it only caused a 25% increase. Additionally, consider the duration (Fig. 7.6), the duration appears to look like the 1D duration but shifted to the right. The sharp transition upwards has gone away, the recurrent nature of the spiral has influenced the duration making it nearly 25% the plane wave value. However, the sharp increase will reappear if $P_{NMDA} > 5 \times 10^{-5} cm/s$, canceling out the spiral. Additionally, we can infer from this that propagation for a smaller value of P_{NaP} does not occur like in 1D due to the increase in duration that occurs. Once duration gets too large the recovering edge of

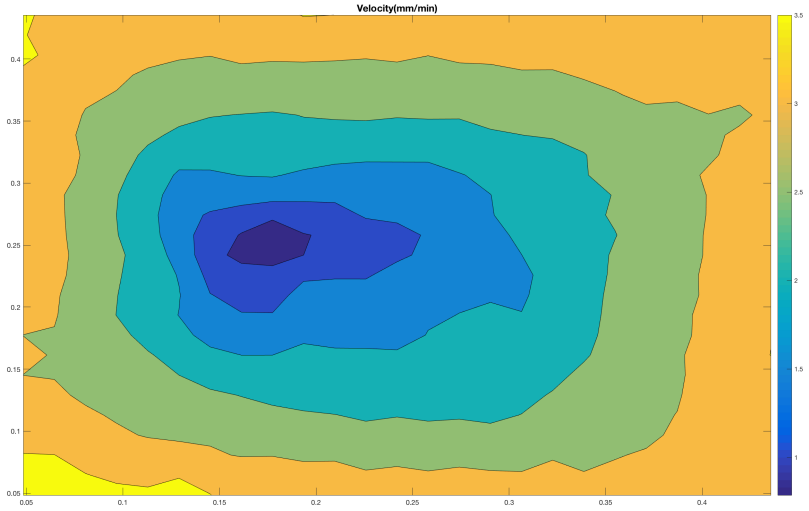

Figure 7.3: Speed of the spiral wave calculated at each point in the domain (edges removed because of edge effects from the velocity calculation).

the spiral will inhibit the initiating edge of the wave causing the wave to dissipate as the whole region becomes depolarized for a long time($\approx$ 3minutes).

Because of the geometry of the spiral, the inner core rotates more slowly than the outer core (Fig. 7.3). In connection with this, the frequency of excitation and recovery period is different (Fig. 7.4). One, not immediately obvious, consequence is that the duration of depolarization is different as well. The central area has a shorter duration because that region is not allowed to fully recover before becoming depolarized again. Recall that as we increased NMDA receptor permeability we saw the creation of a second depolarization (and an increase in duration). If, for different NMDAR permeabilities, the period of excitation was the same, then this increase in duration would cause a decrease in the recovery time(this is simply a statement that Period=Duration+Recovery). As [37] found in experiments, our model shows a decrease in speed with a decrease in allowed recovery time. The combination of the initially lower velocity in the center, duration increase with NMDA receptors, and recovery time scaling leads to some none trivial reactions to an increase in NMDAR permeability on the spiral(as shown in the

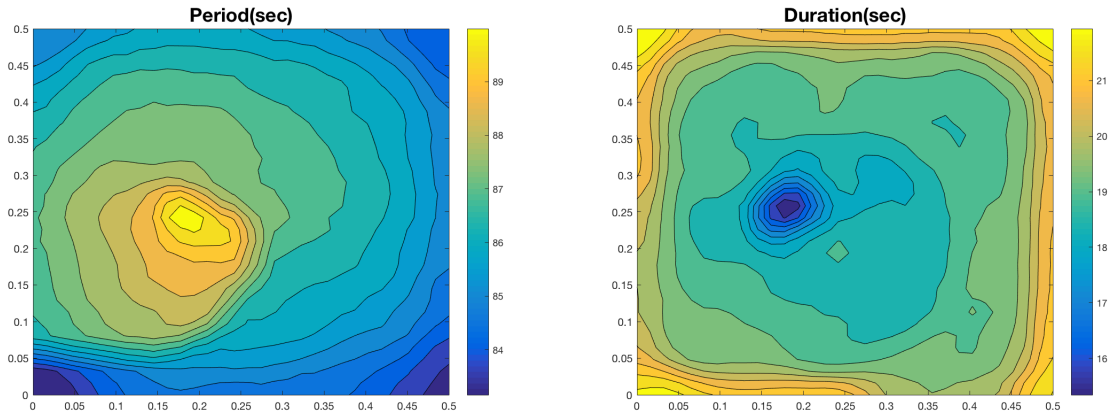

Figure 7.4: Time between each depolarization for each point in the domain as well as duration. Filtered out is the exact center, as it behaves wildly differently than the points around it.

first image in Fig.7.7).

For example, in our simulations, for lower NMDAR values we see larger recovery times for the whole domain, these times decrease as we increase NMDARs. For the outer portion we go from $\approx 50sec$ to $\approx 20sec$, for the center we go from $\approx 30sec$ to $\approx 15sec$ seconds. These unequal recovery time changes lead to a difference in behavior of the velocity of the center and outside as NMDAR changes (Fig. 7.7 and 7.8). The away from center portion sees an asymptotically decreasing speed. On the other hand, the center sees an initial increase in speed, but once the duration reaches a certain level the resulting decrease in recovery time causes a sharp decline in velocity(remember $P = D + R$, since duration is increasing and period stays the same, recovery must decrease). The reason for this decrease in speed is because the second partial depolarization caused by the NMDA receptor increases the duration and makes the recovery period shorter. This behavior is especially prominent near the center.

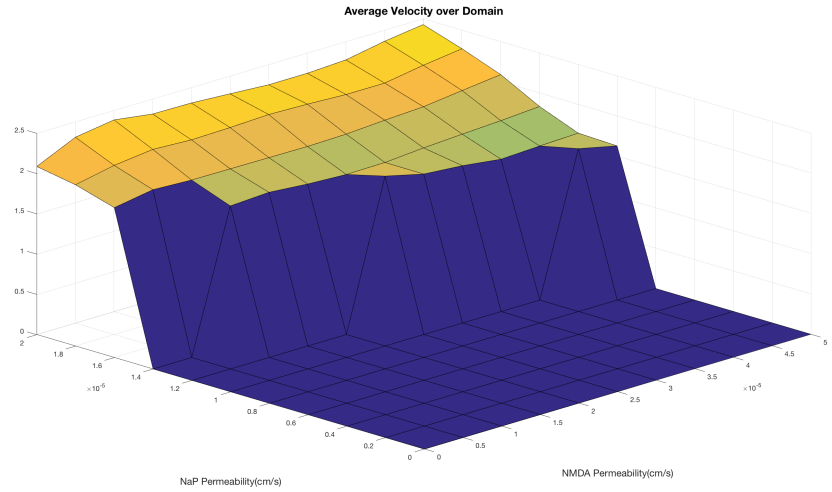

Figure 7.5: Dependence of the speed of spirals on NMDAR and NaP. Calculated by taking an average away from the center.

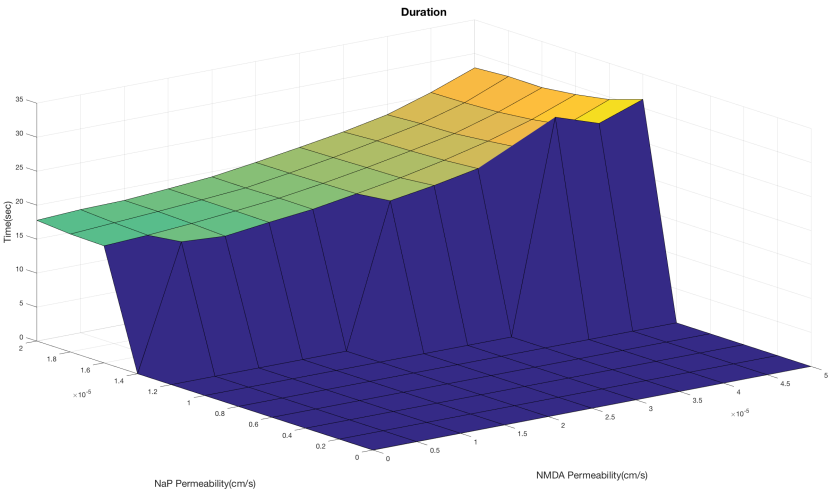

Figure 7.6: Dependence of duration on NMDAR and NaP. The zero sections are regions where the spiral dies off due to a lack of propagation. Beyond 5×10^{-5} the duration spikes quickly preventing the spiral from recurring.

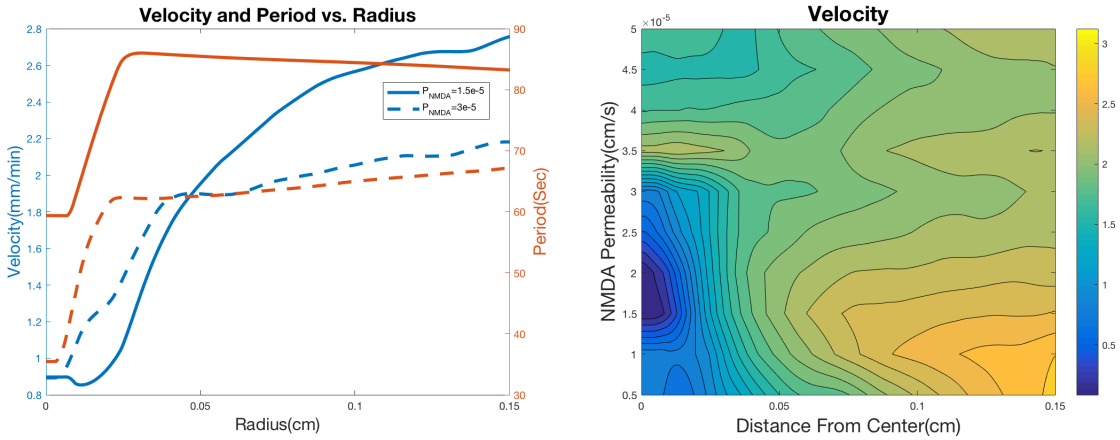

Figure 7.7: Velocity and Period as measured by averaging around circles of different radii for two different NMDA receptor permeabilities. Also, how the velocity changes with increasing NMDA receptor permeability along the domain.

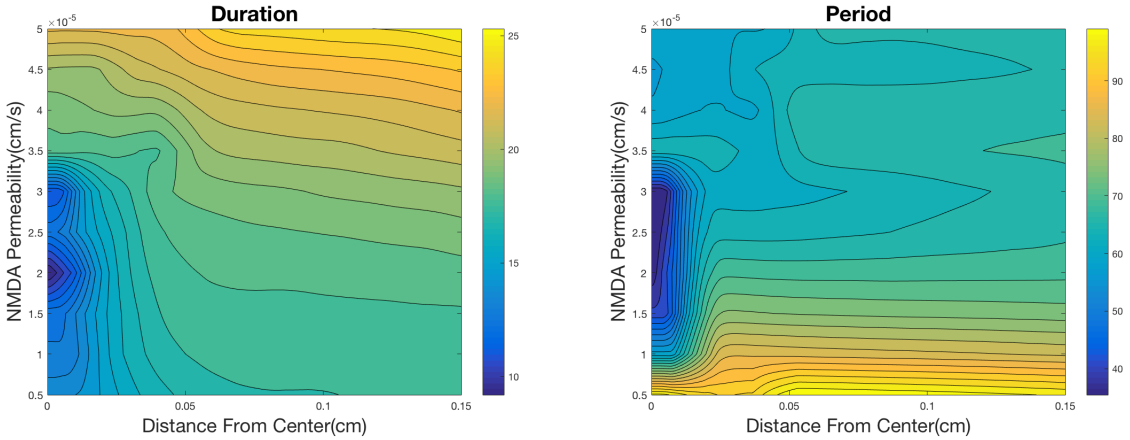

Figure 7.8: Duration and period as measured by averaging around a circle of a given radius. For small enough values there is a large spatial difference. This difference disappears when NMDA is increased.

7.3 Rotational Movement

We saw that the rotational movement of the spiral had a big influence on velocity and duration. We can attempt to quantify this rotational behavior by looking for the angular velocity/speed. In order to calculate the rotational velocity we need to first find the center of the spiral, and then fine its rotational speed, we can do this simultaneously in an optimization problem described in the appendix. It is evident that the center of the spiral moves over time, so we can perform this calculation continuously as the spiral evolves.

First let's talk about this temporal evolution. The spiral does not turn at a constant rate, for certain parameter choices it is evident that the spiral speeds up on one side of its spin. This speedup is a result of an asymmetric time these regions have been allowed to recover. This semi-periodic rate can be seen in the angular velocity over time, Figure 7.9. The rotation is nearly periodic, but sees some small deviation(with larger NMDA showing more deviation). The lower NMDA receptor permeability shows a large variation, but it is centered around a slower average. We can look over the whole range of NMDAR and NaP values we sampled and calculate an average rotational speed over time.

We can see (in Fig. 7.10) that since the spiral limits the propagation speed of itself we do not see a continual increase in angular speed. We do get an initial increase for increased NMDA, but eventually it starts to decrease back down. We see the more significant impact persistent sodium has on rotation, just like speed. To understand why the angular velocity decreases above a certain value we can look at all of the spirals for the maximum value of persistent sodium (Fig. 7.11). For the first 6 panels it is evident that the spiral is getting more tightly wound, but after the 6th panel it starts to stagnate. This is happening because at the center of the spiral the wake of the wave lasts long enough to interrupt the upcoming part of the spiral(as shown in the duration plot of Fig. 7.8). Each of these panels also has a different spiral center. Figure 7.12 shows that the point where the angular velocity is the largest is also the first graph where the path breaks it's closed loop-type trajectory. After this point increasing NMDA receptor

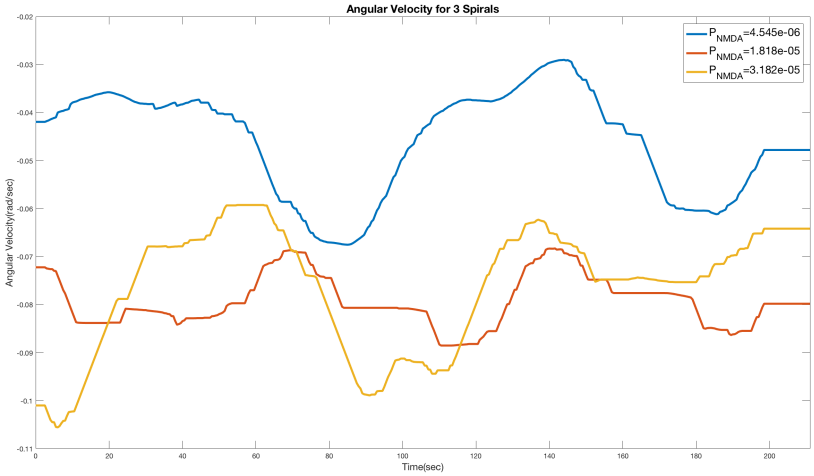

Figure 7.9: Angular Velocity over time for 3 NMDA samples.

expression makes the loop more and more open as the spiral starts to meander more. However, looking at the zoomed out picture we can see that it does not meander very far over the whole domain. The last two NMDA values move the furtherest, at about 1 mm. This extra movement helps explain the decrease in angular velocity, as it is moving it's angular velocity can no longer be as high.

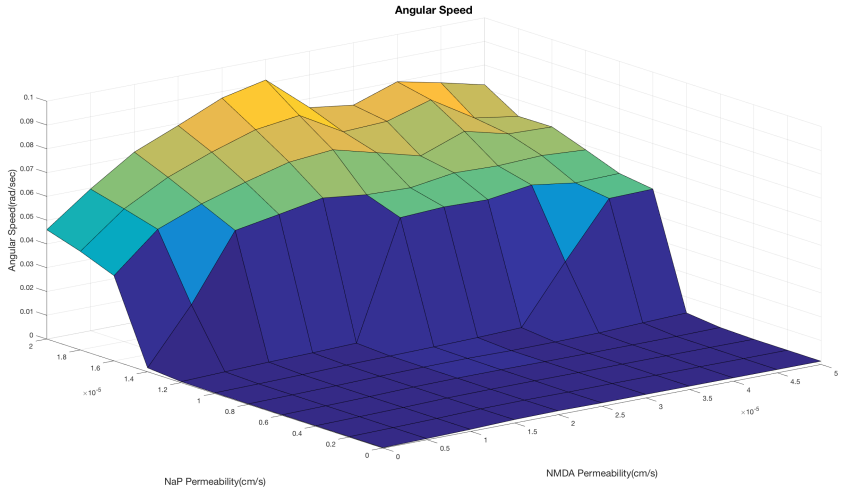

Figure 7.10: Dependence of angular speed of spirals on NMDA and NaP.

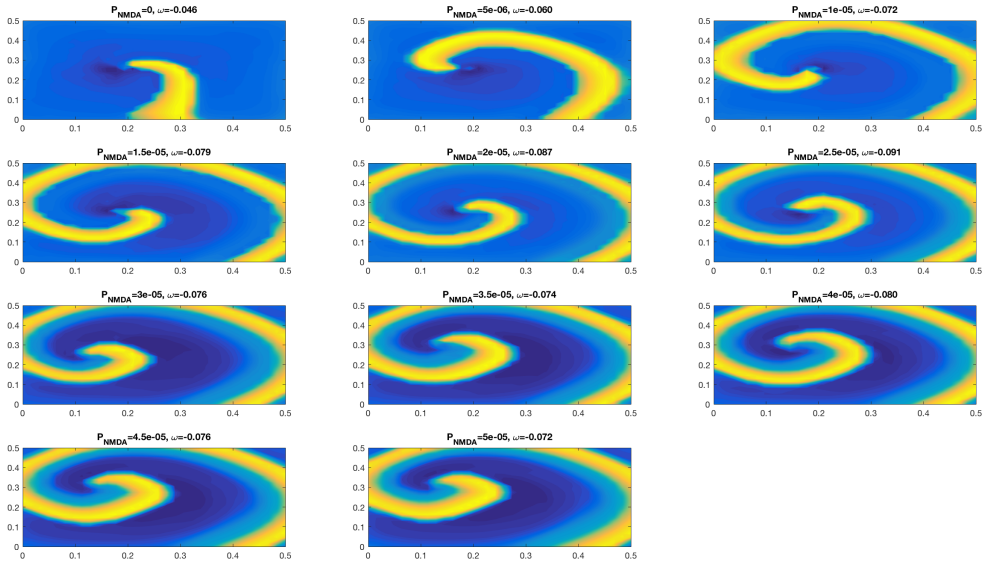

Figure 7.11: Spirals for different values of P_{NMDA}. We set the value of $P_{NaP} = 2 \times 10^{-5} cm/s$. The value of angular velocity is printed in the title of each. The 6th plot, $P_{NMDA} = 2 \times 10^{-5}$ is the turning point where angular velocity no longer increases. It can be seen that in the plots that come after this the center of the spiral has a more pronounced wake. This wake causes the spiral to slow down in the center of the spiral as it waits for the wake to subside.

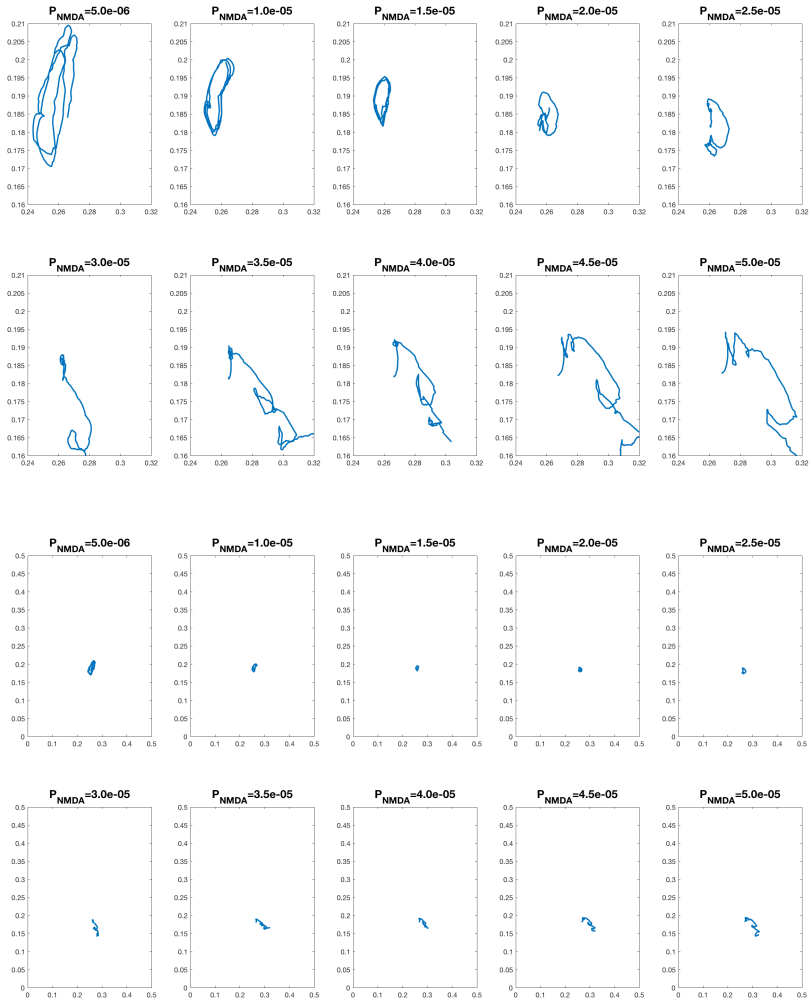

Figure 7.12: The trace of the calculated spiral centers for each of 10 different NMDA values. The top right plot ($P_{NMDA} = 2.5 \times 10^{-5}$), is the point where angular velocity is maximal. The top 10 graphs are zoomed in, the bottom 10 show the size of the whole domain.

7.4 Energy Consumption

The energy expended during spreading depression is a crucial component in patients suffering from stroke or traumatic brain injury[32]. One benefit of our model is that we can derive a free energy identity(see [69] for details or the appendix for just the equations). This energy is broken up into elastic energy, free energy from ions, and energy stored in the membrane as a capacitor. The free energy is allowed to change via work done via diffusion and work done by ion transport across membranes. This work is all passive save for the ion pumps (NaK-ATPase in neurons and glia). During CSD there is a free energy starvation as ions are moved away from their homeostatic state. Ion pumps would ordinarily work to against this free energy decrease, but, there is a lack of ATP during CSD. New ATP cannot be formed due to a lack of glucose available during CSD [92]. We can calculate the work done by the ion pumps during a spreading depression wave; Figure 7.13 shows the work due to the ion pumps during a spiral. At the front of the wave the pumps work hard to balance ions and ultimately fail and cease working as the depolarization happens. Then, when the ions passively start to recover the pumps activate and help restore homeostasis. There is a location dependence of this process on the spiral, as seen by the center behaving erratically. We can see this dependence clearly by looking at the maximum work and average work done versus the distance from the center in Figure 7.14. The average work done by the center of the spiral is significantly greater than that done by the periphery. The maximum while decreasing with distance, does so for smaller range of values. Much like the work, the total free energy sees the same type of behavior.

The intense localization of this work can be mitigated via decreasing activation of the NMDA receptors. Seen in Figure 7.15, increasing the NMDA receptor permeability increases the amount of work done as a whole. However, most of this increase is concentrated around the center of the spiral. The reverse occurs for glia, increasing NMDA receptor expression lessens the burden on their ion pumps. This does not mean that glia uptake less potassium, because this ignores the uptake due to KIR.

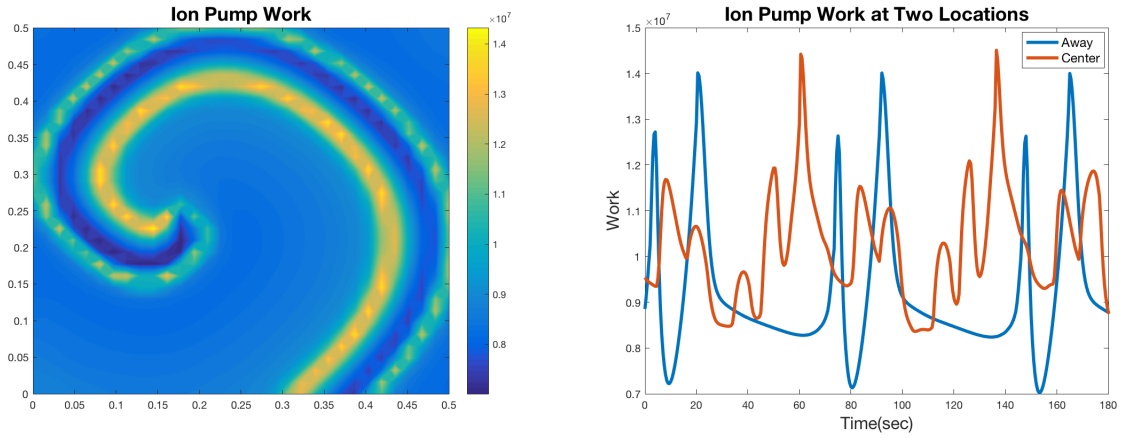

Figure 7.13: We can calculate the work done by the ion pumps. At the front of the wave we see a sharp increase that quickly decreases below the steady state value. In the wake of the wave we see a sharper rise that then recovers more slowly. In the center we see this same behavior but it is erratic.

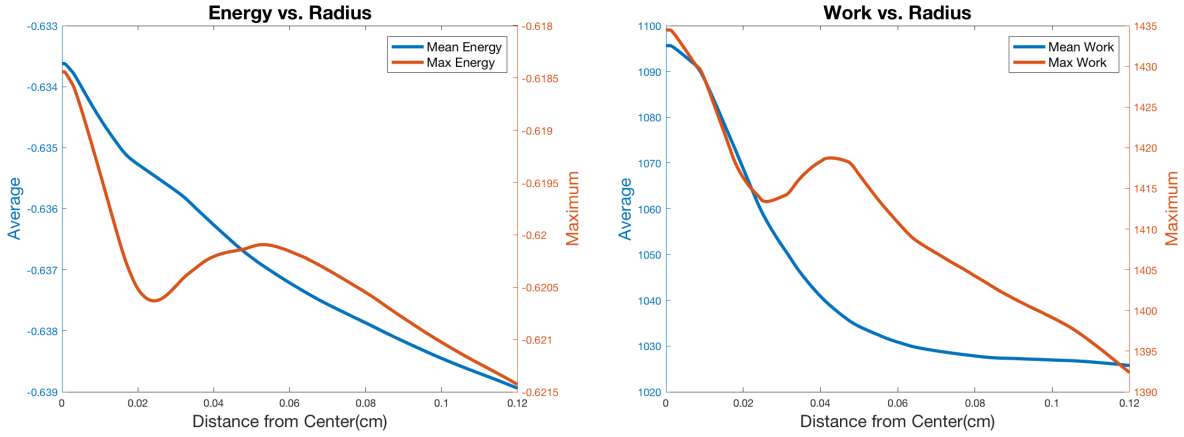

Figure 7.14: Maximum and time average of the work done by both neuronal and glial ion pumps(over 3 minutes), as measured by averaging around the spiral center. The center of the spiral does significantly more work, both over time and as a maximum.

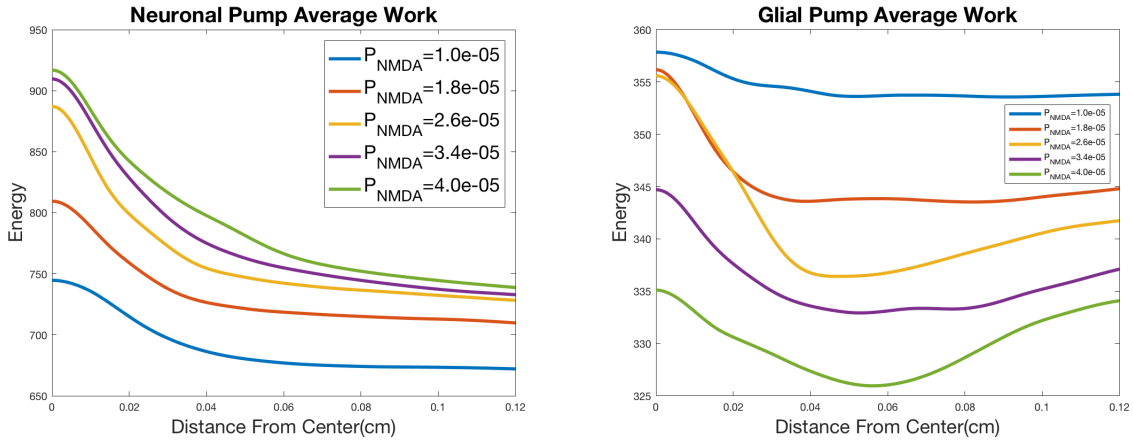

Figure 7.15: Average work done by ion pumps, in both the neurons and glia, versus radius. We show increasing values of NMDA permeability.

Chapter 8

Layer Model

8.1 Homogeneous CA1 Layer Model

The expression of ion channels is dependent on innumerable factors: brain region, age, neuron type, position on the neuron, etc[36]. However, there are some general structures and patterns that are followed within the same brain regions. We will focus on one of these, Hippocampus CA1 region. This region has a particularly interesting morphology, most of the neurons run in parallel directions and act as messengers between other layers. Because they are just messengers, there are very few connections amongst themselves, for this reason it is a good fit for our model as action potentials will not propagate in the transverse plane. A simple ODE model of one of these neurons is described in [90, 55, 53], a regional diagram for this is shown in Figure 8.1.

That is, for our 3 compartment model, we create 3 different regions for the neuron: Apical dendrite, soma, and basal dendrite. These neuronal sections fall into distinct layers in the CA1 region: stratum radiatum(containing apical dendrites), stratum pyramidale(containing soma), stratum oriens(basal dendrites and axon). Each of these regions are where the majority of each structure are located. In the apical dendrite we have synaptic and extra-synaptic NMDA receptors. In the soma we have the transient currents for potassium and sodium (KA/NaT). Then in both of these persistent sodium (NaP), potassium delayed rectifier (KDR), sodium-potassium ATPase (NaK), and leak

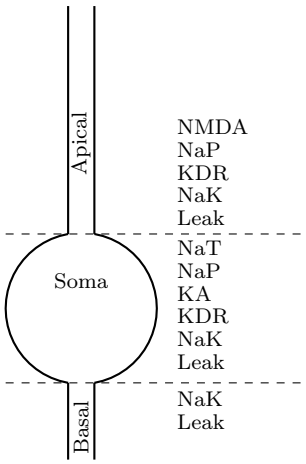

Figure 8.1: Homogenous layer model copying regions from [55]. Not shown is a small transition layer at the proximal region of the apical dendrite with no NMDAR.

currents are found. Lastly, the basal dendrite only has NaK-ATPase and leak currents.

The apical dendrite (for [55]) was divided into 6 segments, with 5 segments totaling to a length of $400\mu m$ and a last segment of $200\mu m$. We will ignore the 6th segment and treat the remaining 5 segments as one region. The closest segment to the soma (D0), doesn't have a NMDA receptors(which is not shown in our diagram, but is in the results we will show). The basal dendrite is a single segment of length $100\mu m$ and the soma is a single segment of length $30\mu m$. Hence, a total length of this neuron is $0.53mm$.

Each of these segments has a different volume and surface area which impacts the distribution of ion channels and the effective membrane capacitance. We took values from [53] which are uniform across each compartment/region(seen in Table:8.1):

Region	Surface Area(cm^2)	Neuron Volume (cm^2)	Membrane Separation(cm)
Soma	1.586×10^{-5}	2.16×10^{-9}	15.66×10^{-5}
Apical	16.408×10^{-5}	3.852×10^{-9}	2.6998×10^{-5}
Basal	10.324×10^{-5}	1.762×10^{-9}	1.9627×10^{-5}

Table 8.1: Surface area and volume constants dependence on region. Where membrane separation is calculated as: $(Vol_{neuron} + Vol_{ext})/(SurfaceArea)$, with $Vol_{ext} = 0.15Vol_{neuron}$.

Lastly, the important change to the model in the jump from 2D to 3D. Since this layer consists of groups of neurons extending upwards (henceforth the direction of the layers will be the z direction). Then we must have neuronal diffusion. Previously, we had assumed no neuronal diffusion (neurons do not have much spatial extent or gap junctions). However, now that the layer is short enough to contain single neurons we will have diffusion in one direction. All of our diffusion coefficients are calculated with the formula:

$$D_{ion}^{comp} = D_{ion}\alpha_{comp}/\lambda^2 \vec{D}_{comp}^{mult}$$

where D_{ion} is that ions diffusion coefficient, α_{comp} was the volume fraction(for neurons and glia this fraction is the fixed resting fraction .5 and .3 respectively), λ is the tortuosity. Finally, the most important (and arbitrary) piece, the diffusion vector multiplier. This is how we can introduce anisotropy. For all of the simulations up to this point this has been(in their 1/2D counterparts):

$$D_{neuron}^{mult} = (0, 0, 0)$$

$$D_{neuron}^{mult} = (0.25, 0.25, 0.25)$$

$$D_{neuron}^{mult} = (1.0, 1.0, 1.0)$$

Since we are now allowing neurons to have more spatial extent, we modify this to be:

$$D_{neuron}^{mult} = (0, 0, 0.5)$$

(Modeling note, if we added x-y direction diffusion, the soma compartment could pass action potentials at fine time scales)

8.1.1 Homogenous Results

When we simulate these layers we see the same basic dynamics we saw in the 1D simulations. Regions with increased NMDA see an extended duration, more pronounced potassium release, and a large DC shift (Figure 8.2). These are modified slightly to be stitched together among the sharp transitions between compartments. The most interesting interaction comes from the relatively inert basal layer. This layer provides a

mitigating effect thanks to interlayer diffusion (neuronal, glial, and extracellular diffusion acting in concert). For the extracellular voltage this causes a pronounced positive shift (10mV).

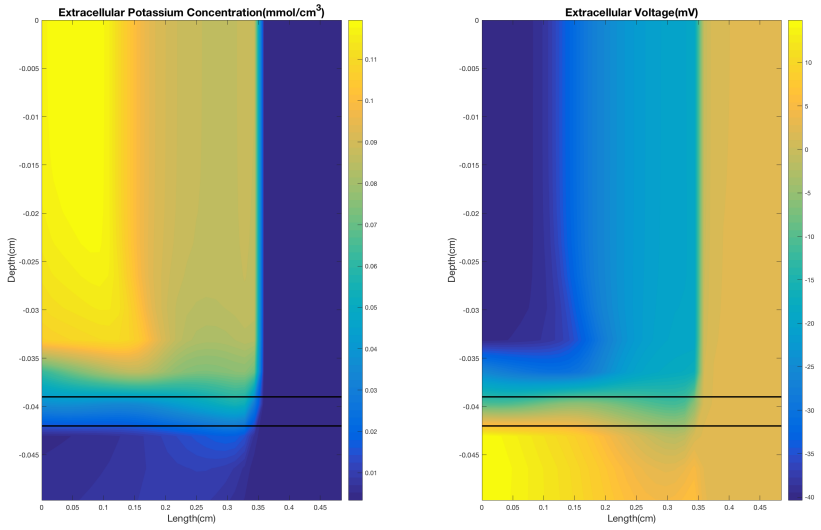

Figure 8.2: Extracellular potassium and voltage wave propagating to the right across the layers.

The impact of neuronal diffusion is very evident in the potassium uptake, both in neurons and glia. For neurons, because of the absence of other ion channels in the basal layer, the dendrites can uptake potassium through NaK-ATPase pumps. Though, this change isn't as noticeable, and provides less mitigation than glia. While, Glia have always played a mitigating role during CSD, clearing excess glutamate and potassium from the extracellular space attempting to halt the feedback loop that causes neurons to depolarize, in the basal layer their role has been magnified. In Figure 8.3, since there is almost no potassium released within the basal layer itself, the glia here uptake potassium released from the somatic layer above it. But, since the duration of CSD is significantly shorter in the soma, after the it recovers potassium is allowed to slowly pass through from the proximal apical dendrites(immediately above the soma). However, when considering concentrations, something we must keep in mind is that the

upper layers expand much more in volume than the bottom ones. On the apical side we see an expansion from a volume fraction of 0.3 to 0.37., whereas the basal compartment only goes from 0.3 to 0.31. So, there are significantly more potassium ions (in amount/moles) in the upper layers, but the basal layer does still play a large role in moving potassium.

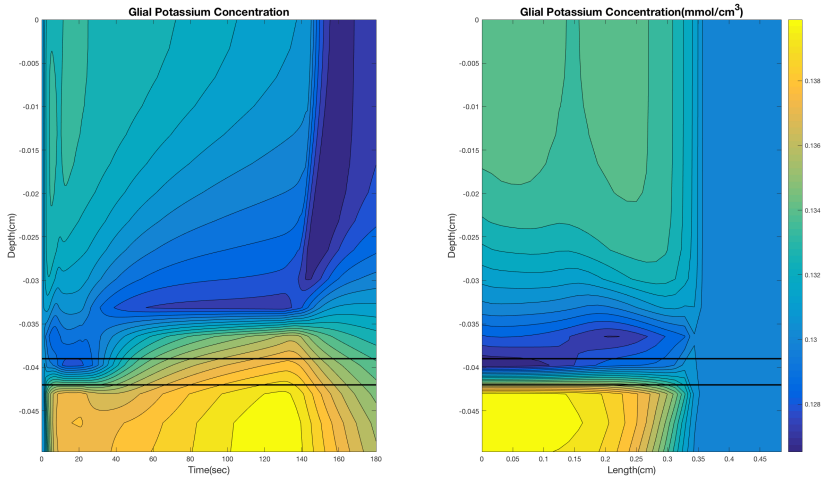

Figure 8.3: Glial potassium concentration. Left: Depth and time contours evaluated near initiating boundary. Right: Depth and Length contours showing the wave traveling to the right.

8.1.2 Diffusion Impacts

One question we should investigate is: What is the impact of neuronal diffusion? What does it add or modify from the results above. To investigate this we varied the neuronal diffusion multiplier over a range of values from 0 to 0.5. While the extracellular potassium concentration remains essentially the same for any value, the inclusion of diffusion influences the extracellular voltage. For near 0 neuronal diffusion the minimum value of the apical dendrite's extracellular voltage is -43mV, at this time the basal layer only has an extracellular voltage of 2mV. When we increase diffusion back up towards .5,

we see a change back to the -54mV and 6mV pairing visible in Figure 8.2. Neuronal diffusion also plays a large part in the glial potassium uptake. Figure 8.4 shows us that the large amount of glial potassium that we saw in the past section was directly tied to the presence of neuronal diffusion. When there is no diffusion we do see a small amount of potassium uptake in the basal layer glia, but increasing diffusion gives us a very large amount. This increase comes from two mechanisms. First, the expanded extracellular space, when there is little diffusion the basal layer contracts much like the rest of the domain(going down near 8%), but for increased neuronal diffusion it contracts much less (near 18%). This increased extracellular volume has equal contributions from neurons and glia, since the glia are less big their concentration can be higher while still containing the same amount of ions.

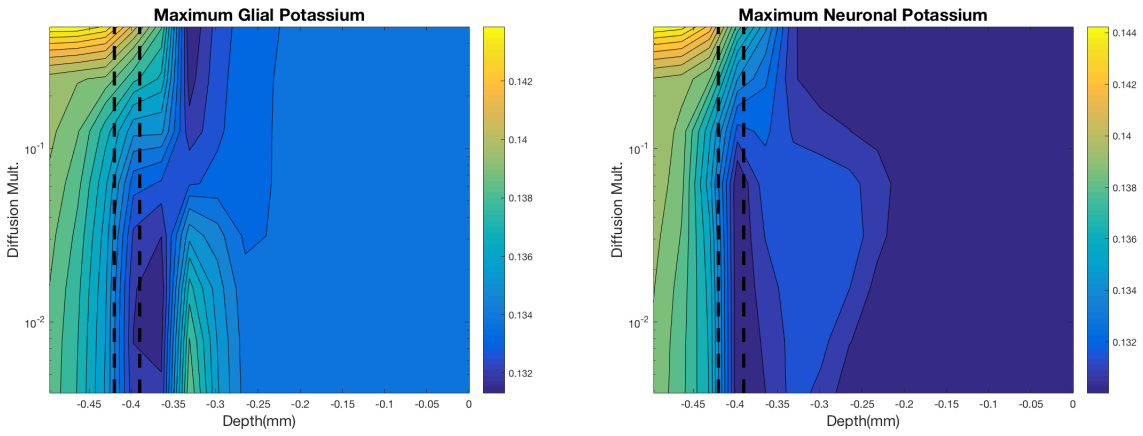

Figure 8.4: Maximum(over time) Glial and neuronal potassium concentration for various values of neuronal diffusion. Since potassium ordinarily decreases in neurons, the maximum is constant in apical dendrites.

The second, more interesting, reason for this extra potassium is the neuronal NaK pumps. The basal neurons only have leak currents and NaK ATPase, since these take up potassium the neurons help clear extracellular potassium. This clearance is shown in Figure 8.4, neuronal potassium actually increases in the basal layer. But the neurons are communicating with the somatic layer above them, since this layer lacks neuronal potassium the potassium in the basal dendrites can diffuse upward and become dumped

again). This potassium can then by taken up by the glia near the layer of soma or it can diffuse down and be split into neurons and glia in the basal layer, the glial potassium slowly rises during this loop(seen in Figure 8.5). This extra potassium movement from neuronal diffusion is likely why there is a minimum just above the soma in the glial potassium in Figure 8.4.

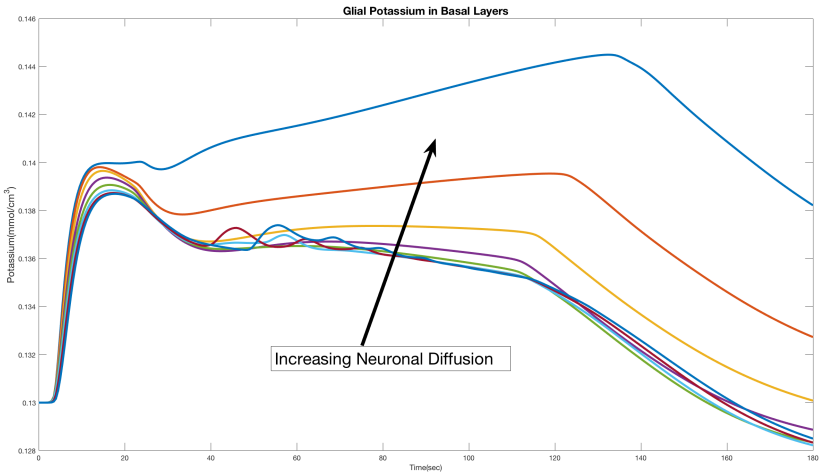

Figure 8.5: Glial Potassium in the bottom basal layer over time for each of the diffusion simulations. The larger the neuronal diffusion, the larger the slow buildup after the first excitation is.

This feedback loop in the neurons when neuronal diffusion is high causes a large buildup of extracellular sodium. In Figure 8.1.2, we can see this happen (at the top of the extracellular sodium graph). The sodium builds up slowly over time in the extracellular space. At the same time potassium builds up in both the neurons and the glia(high diffusion case of Figure 8.7). The current that is flowing in this loop is what causes the extracellular voltage to become positive.

Looking for the same feedback when neuronal diffusion is low, we can see that the soma acts as a barrier(low diffusion case of Figure 8.7). The immobility of the ions in the neuronal compartment causes an increasing neuronal voltage (Figure 8.1.2, bottom of half of neuronal voltage). This slight depolarization of the basal compartment

occurs just before the extracellular potassium reaches a maximum(the point where the neuronal ion pump start to become stronger). After this potassium flood, we can see the activation of the ion pumps because of the quick rise of extracellular sodium(Fig. 8.1.2). These effects become mitigated by increasing neuronal diffusion, we identify the transition as the point the neuronal voltage increases earlier(right near the 10^{-1} mark on Fig.8.1.2). This portion of the graph of extracellular potassium and neuronal voltage at the 20sec mark have an inverse relationship with diffusion, increasing diffusion lowers the value seen for potassium while increasing the neuronal voltage.

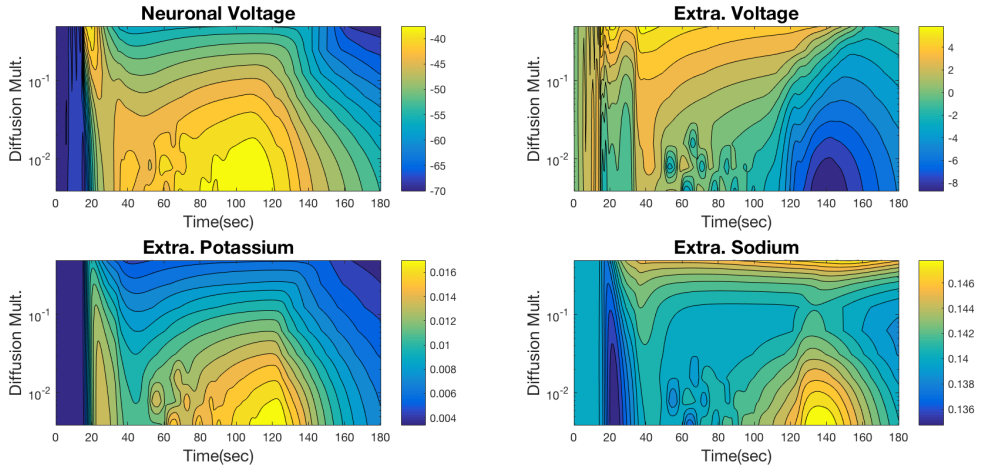

Figure 8.6: Basal layer Neuronal voltage and extracellular voltage,potassium, and sodium time profiles compared with different neuronal diffusions.

8.1.3 Inter-regional Interactions and Transitions

Outside of the results for these specific parameter choices. The impact that hard layer transitions can have on the wave is massive. For certain parameter regimes the apical layer can cause the somatic layer to go through multiple spreading depolarizations while the dendrites are depolarized (see Figure 8.8). The excess ions that build up in the basal layer can cause the somatic layer to trigger one more time after the apical dendrites have recovered, causing a second (more quickly recovered) wave to propagate through the whole domain one last time. So a single initiating event can cause multiple

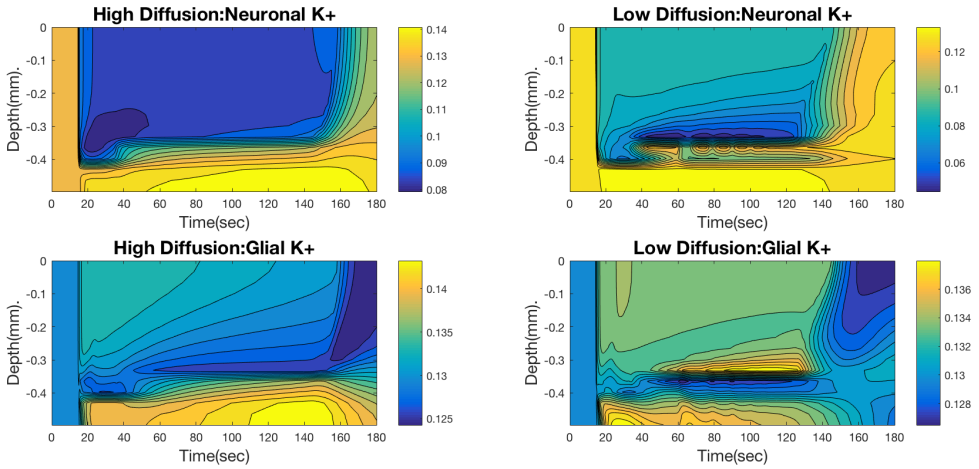

Figure 8.7: Depth and time profiles of high diffusion(0.5 times) and low diffusion(2^{-9} times) of potassium in neurons glia.

spreading depressions due to the heterogeneity of the region it spreads through. While this is a consequence of the hard transitions within our layers in this simple toy model of the CA1 layer. These types of transitions can occur in real brains, instead of being a transition from dendrites to cell bodies, these transitions exist among brain regions (think CA1 feeding into CA3[43, 1], or other the hippocampus into the neocortex). In one simulation we managed to see a spreading depression wave travel forward in the top layer and initiate a wave further along in the somatic layers causing a wave to travel both forward and backward in that layer. While this chaotic behavior, for that simulation, was due to odd initial conditions(initiating a wave while one was already traveling) it is an actual behavior seen in hippocampus slices [43].

Lastly, before we introduce a more detailed layer model. We should show some result that actually requires 3D (specifically making use of 2 dimensions on each layer). We can take the initial condition of the spiral we formed and investigated in Chapter 7 and copy that to each layer in this model. After letting this run for a time (around 1-2 minutes), a new stable recurring pattern develops (Figure 8.9). The interaction between the layers caused the single spiral arm to transform into 2 spiral wings that rotate in opposite directions. Periodically we get a central island of depolarized tissue

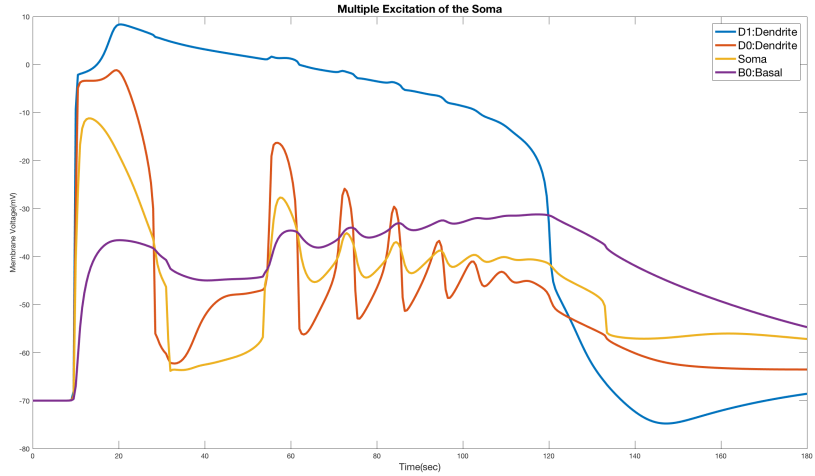

Figure 8.8: Neuronal membrane voltages when neuronal diffusion is low. The prolonged depolarization caused by NMDA in the dendrites causes the soma and proximal dendrite region(that lacks NMDA receptors) to encounter multiple depolarizations.

surrounded by recovering areas. The soma layer cancels itself out every rotation, but the activity in the dendrites above reactivates it. This simulation is of a 0.5x0.5x0.053 region broken up into a 32x32x16 grid, it is run for 360 seconds with 36,000 time steps. It took 45 hours to run on a single core processor. The large time increase from the 2D spirals (which took ≈ 1 hour to run) is not just from the increased simulation size, but from the addition of neuronal diffusion, which modified the jacobian. This modification, with the major differences among layers, causes the jacobian to be less regular on the matrix blocks representing the z direction diffusion on the far off diagonal.

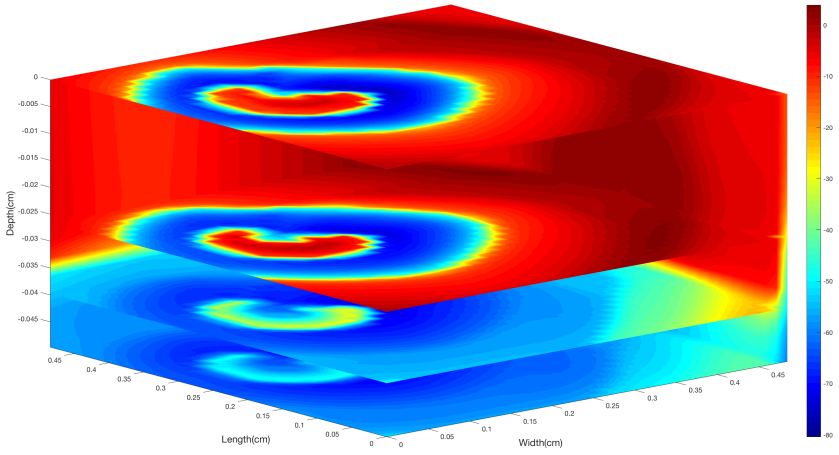

Figure 8.9: Layered spiral wave snap shot. This is a 32x32x16 simulation that took 45 hours to run, displayed are 4 layers. The bottom of the basal layer, the soma layer, and 2 apical layers.

8.2 Heterogeneous CA1 Layer Model

The ion channel distribution along a neurons length is not a simple binary, present or absent, distribution. We can take the previous simplified model of the compartmentalization of a CA1 neuron and build on top of it. By modifying the distribution to fit more closely with observed neurons, we will construct an initial model of the layer dependent structure of this region. A good summary of the ion channel distributions of this region can be found in [66] and [13].

We are constructing our model with the view that for in the CA1 region the primary neurons spread upward. This region is split into further subregions. We will pay attention to 3: stratum oriens, stratum pyramidale, and stratum radiatum. We make the assumption that the cell body is prominently concentrated in the stratum pyramidale (though some can be found within $100\mu m$ of the stratum oriens [3]). The apical dendrites extend into the stratum radiatum and branch much further away from the cell body. The basal dendrites are found in the stratum oriens and begin to branch much closer to the cell body. We will make the correlation that NMDA receptors increase with spine density, and since the spine density of the apical dendrite increases with distance from the soma, we say that the NMDA receptor become more expressed as we get further from the soma.

The CA1 layer receives signals from CA3 pyramidal neurons[3]. A consequence of this is that CA1 neurons have a very small number of connections amongst themselves (the probability two neurons are connected is about 1%[57]). Furthermore, these connections tend to occur on basal dendrites, where the connection is made with axon collaterals. Since we do not model outgoing signals, we ignore the axon, but include the axon initial segment. All of this combined means that we do not allow neuronal diffusion in the transverse plane (no gap junctions). We do allow diffusion in the z-direction, along the dendrites. A note for the future, there are interneurons that act as inhibitors to the pyramidal neurons in the stratum oriens. An approximation to this (since we do not distinguish neuron types), would be to allow a small amount of diffusion in the stratum oriens.

Now we discuss channel distribution. [64] shows that sodium channel distribution is uniform, however this figure does vary based on age. More recent results [63], show a sharp decrease in Nav1.6 channels from the axon initial segment (AIS) to the dendrites. We will take a combination of these, introduce a sharp decline in the transient sodium channel along the apical dendrite, while keeping the persistent sodium channel constant along this portion. For the basal dendrite, we will have no transient sodium. But, the persistent sodium channel will be modified. First, while we do not explicitly model it, the axon initial segment (AIS) is in this region, and [4, 27] found that persistent sodium in this segment must be significantly higher. While specifically about the axon [35] found that the first $35 - 50\mu m$ of the AIS must be 3 times higher that the soma, but also found that the concentration in the basal dendrites had to be $10 - 30\%$ higher than the soma. This agrees with [48], where a nice linear rise in NaV1.6 intensity in this region, from 0.2 to 0.6, so a linear rise in this region with a cap would seem to be accurate.

For potassium channels, we have to manage two of them. First, [47] says that the recorded density of the transient component increased linearly with distance (showed about a 4 times increase). Since we do not fully model the dendritic branches and likely overestimate the amount of neuronal space in the stratum radiatum, we will change this to a more moderate 14% rise in transient potassium (KA). For the non-inactivating component [47] found a mostly constant density along the dendrites, so ours will be constant. On the basal dendrite, we do not have any sources. However, [84, 27] found that in order to match with experiments, their simulation needed the axon to have 3-5 times KDR density of the soma. More crucially this value changes with distance along the axon. We will interpret this as a small 50% rise compared to the soma. We will also assume there is no transient potassium in the basal dendrites.

Last among the channels, the NMDA receptor. The distribution of this is more complicated because there are multiple different NMDA channel types, and the channels move and change very readily[3]. The specific type of NMDA receptor we model is of type NR2, and in this region the predominant type is NR2B. This type preferentially chooses the apical dendrite over the basal. While, we associate these receptors

Channel	Basal	Soma	Apical
NaT	0	5×10^{-5}	$5 \times 10^{-5} (1 - d/L_a)^3$
NaP	$1.5385 \times 10^{-5} (1 + 0.3(d/L_b))$	1.5385×10^{-5}	1.5385×10^{-5}
KDR	$(2/3) \times 10^{-3} (1 + 0.5(d/L_b))$	$(2/3) \times 10^{-3}$	$(2/3) \times 10^{-3}$
KA	0	0.8772×10^{-4}	$0.8772 \times 10^{-4} (1 + 0.14(d/L_a))$
NMDA	$5 \times 10^{-5} (d/L_b)$	0	$5 \times 10^{-5} (d/L_a)$

Table 8.2: Channel Permeability in cm/s. d is distance from the soma. L_a is the length of the apical dendrite. L_b is the length of the basal dendrite. Values for KDR and KA lead to maximum values equal to what we used previously.

with synapses, NMDA is quite often found in extra-synaptic locations [74]. In basal dendrites, AMPA receptors increase in expression whereas NMDA receptors decrease [65]. This does however depend on whether they are perforated or not, and regardless the change is not large. While we do not model AMPA receptors, we can use NMDA receptors as a crude stand-in. In accordance with this, we will be increasing the NMDA receptor permeability from 0 to 5×10^{-5} along both the apical and basal dendrites.

We can summarize this as follows. The transient sodium channels will be active in the soma and decrease quickly(we use a cubic) along the apical dendrites. We will have a fixed amount of persistent sodium along the soma and apical dendrite, but have a linear 30% increase back along the basal dendrite. Transient potassium will be inactive in the basal dendrites, then increase by 14% along the apical dendrites. The KDR channel will be constant along the apical dendrite and increase 50% along the basal dendrite. For the NMDA receptors we make the simple assumption that it is not expressed on the soma and increases as we move away from the soma(both in the apical and basal dendrites). While this is not wholly accurate, we must keep in mind we are modeling a whole continuum of space (neurons, glia, and extracellular space), so even if we mention the idea of specific dendrite regions, we are talking about a small part in a larger scheme. For a schematic of this see Figure 8.10 or detailed equations see Table 8.2.

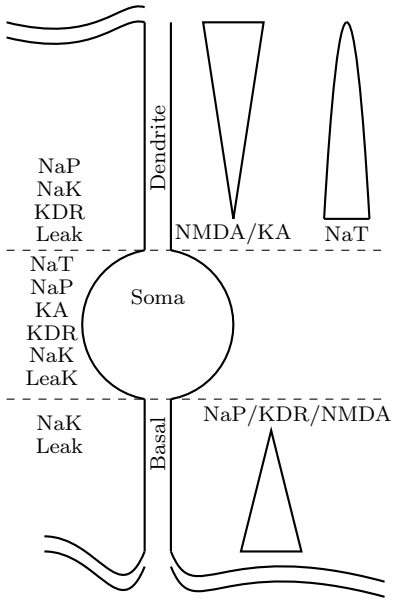

Figure 8.10: Schematic for more heterogenous CA1 model. The ion channels on the right of the figure have shapes that represent their increase or decrease with position. The ones on the left are constant in that region.

8.2.1 Heterogeneous results

Similar to the homogeneous results we see the same basic behavior, however the continuous shifting of parameters has made differences between compartments smoother and more distinct at the top and bottom of the domain. Figure 8.11 shows the time course of the extracellular potassium and voltage over the layers (evaluated about .01cm from the left boundary). Now that the basal layer has ion channels it sees a similar ionic shift to the apical dendrites. In fact, even though the wave was initiated in the top left of the domain, the maximum of the potassium is reached first in the basal layer. However, there is an initial jump up that is nearly simultaneous among the layers. As seen in [98], in different compartments you can see largely different extracellular potentials(in their case sources and sinks). The apical dendritic region sees a much stronger negative DC shift. And thanks to the addition of NMDAR into the basal dendrites, we see a two hump negative DC shift as well (Figure 8.12). Interestingly however, it is much less pronounced and much shorter duration than its apical counterpart. Additionally, we can see that the proximal basal layer(basal layer closest to the soma) sees an early positive polarization, while the other basal layers see a more pronounced positive shift compared apical regions.

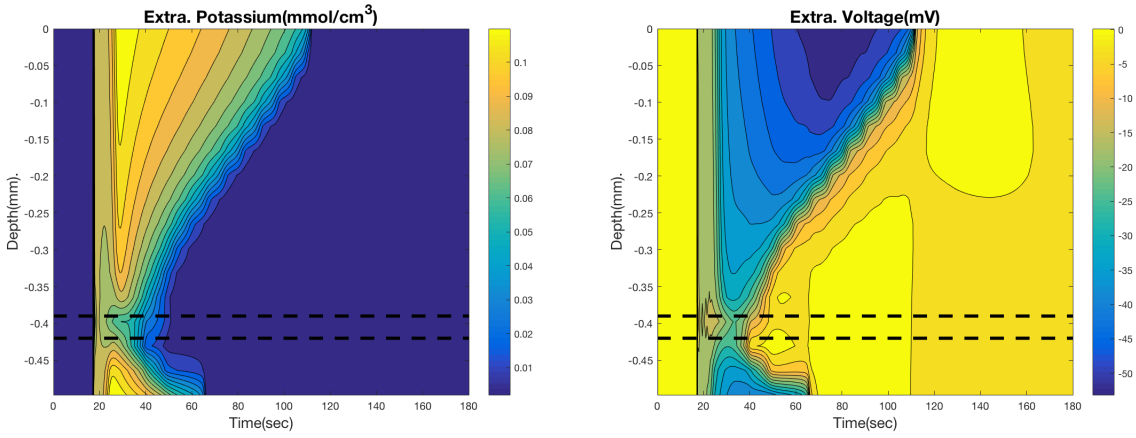

Figure 8.11: Extracellular potassium and voltage wave propagating across the layers in the heterogeneous model. Black lines show the division between regions.

Moving onto glial potassium uptake, we see an initially large uptake of glia in the somatic layer near the wave front. This then decreases slightly and remains elevated

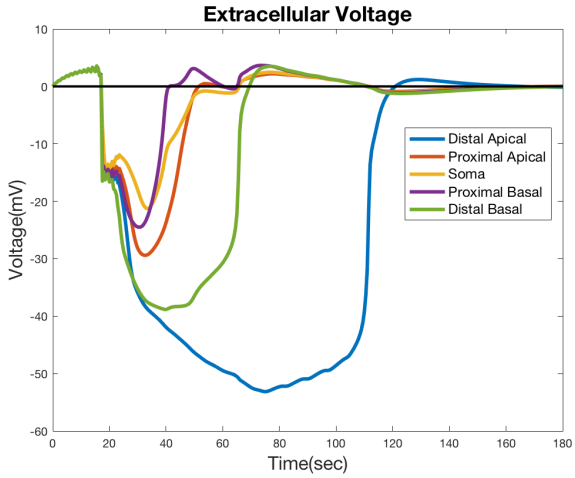

Figure 8.12: Extracellular voltage profiles at 5 choice regions.

above steady state for the duration of the wave. We see the proximal basal region slowly uptake to a peak a large amount of potassium. Around the time of that second peak is when the neurons in the soma region have recovered most of their potassium. We can see that the very top apical region loses much of its potassium to the lower layers causing the glia in this area to actually go below steady state concentrations(Fig.8.14). Looking at the concentration across layers after 3 minutes (Figure 8.15), we can see that for all apical dendrites above -.2mm, there is a lack of potassium in all compartments. This means that these concentrations must recover via diffusion from the bottom regions and not ion channels. While the other ions show these similar gradients, each of them has at least the neurons or extracellular space having a higher concentration, meaning they can recover from the combined effort of ion channels and diffusion gradients.

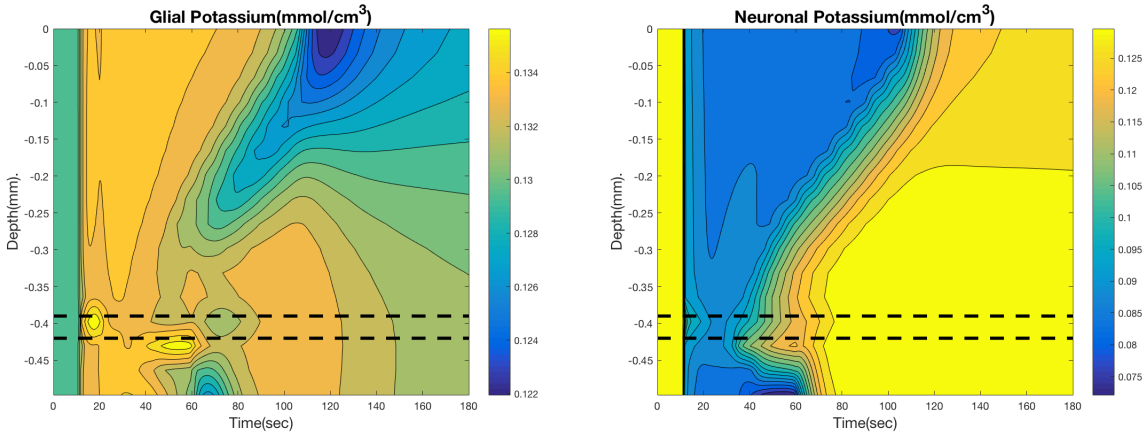

Figure 8.13: Glial and neuronal potassium time profiles across layers. Notice the larger glial uptake in the region surrounding the soma that happens even after neuronal potassium recovers.

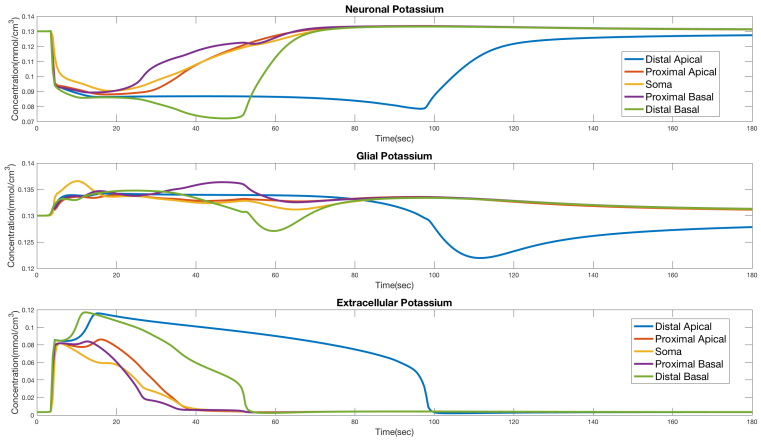

Figure 8.14: Potassium profiles for 5 choice layers. It is very evident that neurons and glia recover much more slowly in the distal apical layer.

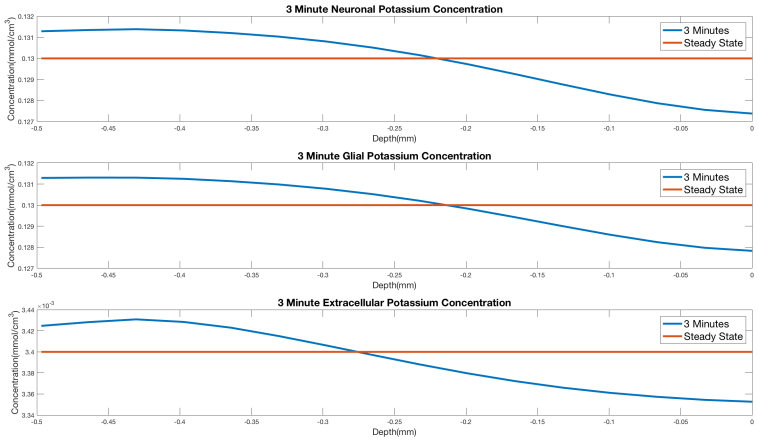

Figure 8.15: Potassium Concentrations across depth after the simulation has finished (3 minutes). At this point the voltages have recovered and the volumes have shrunk back down.

8.2.2 Heterogeneous Influence of Z Direction

We saw that the displacement of potassium is largely influenced by diffusion away from the apical dendrites, who release a large amount of potassium. So, we should look at how neuronal diffusion impacts this, as well as other dynamics. Throughout this section we will show contour plots of several specific layers: Distal apical, middle apical, proximal apical, soma, proximal basal, distal basal. For our 16 layers these correspond layer numbers: 1, 6, 12, 13, 14, 16, respectively. We first look at the glial potassium, Figure 8.17, we can see that the large amount of potassium released by the distal basal dendrites (seen in Figure 8.16) doesn't change as diffusion increases. Instead, time until it is cleared changes. For glia, we can see this influence in the slow peak that forms for low diffusion. Once this peak forms the glial diffusion allows it to be moved away, causing a dearth of potassium after a while. With, the increase of neuronal diffusion this process becomes less active as the glial uptake is passed upwards closer to the soma. On the opposite side of the domain, the apical dendrites release enough potassium and are far enough away, that this same process does not happen. Instead, the closer apical dendrites pass some potassium down and recover more quickly themselves and then help the apical layers above them.

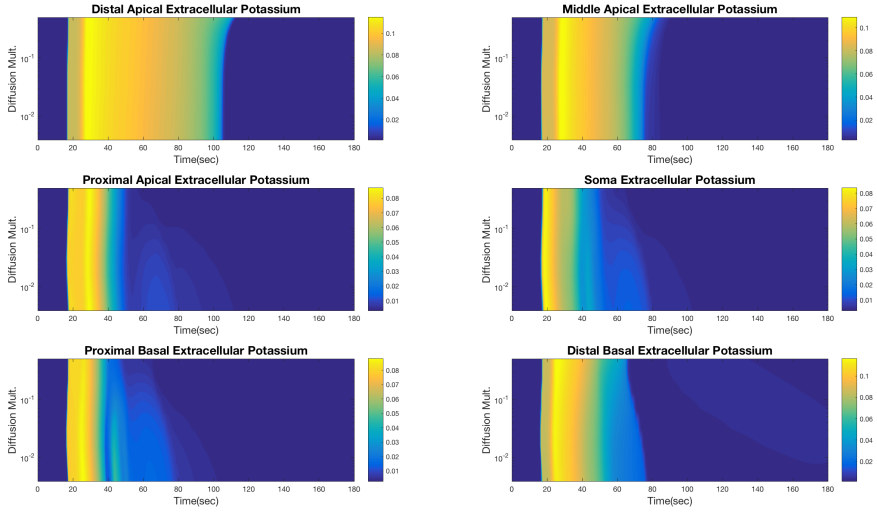

Figure 8.16: 6 layers dependence of extracellular potassium on neuronal z direction diffusion.

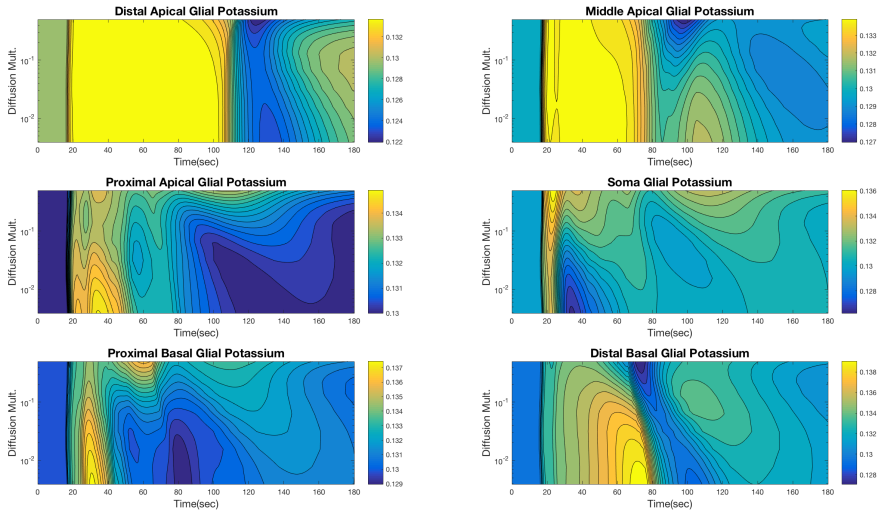

Figure 8.17: 6 layers dependence of glial potassium on neuronal z direction diffusion.

Neuronal sodium sees an interesting trend, Figure 8.18, adding neuronal diffusion shifts the peak to a lower value and moves it slightly in time for the top and bottom layers. It speeds up recovery significantly in the distal apical region and causes significantly more to be released in the soma. The extra released from the soma appears to diffuse down into the quickly recovering proximal basal layer. This change in the soma is related to a interesting dynamic that arises with the volume. The maximum neuronal volume fraction, for lower neuronal diffusion the basal and somatic regions are allowed to have much different neuronal volumes, Figure 8.19. For the soma and the basal regions the volume follows very closely, in shape, to the neuronal sodium graph, whereas the apical dendrites follow sodium and chloride more closely.

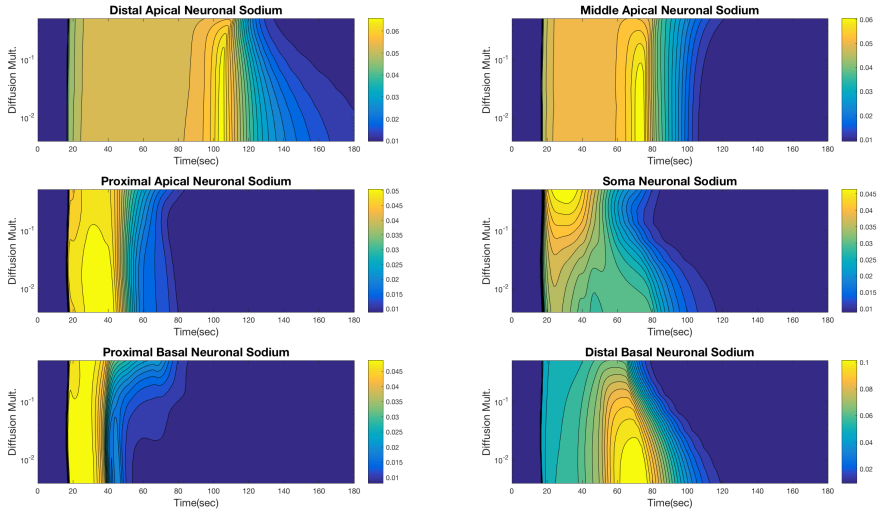

Figure 8.18: 6 layers dependence of neuronal sodium on neuronal z direction diffusion.

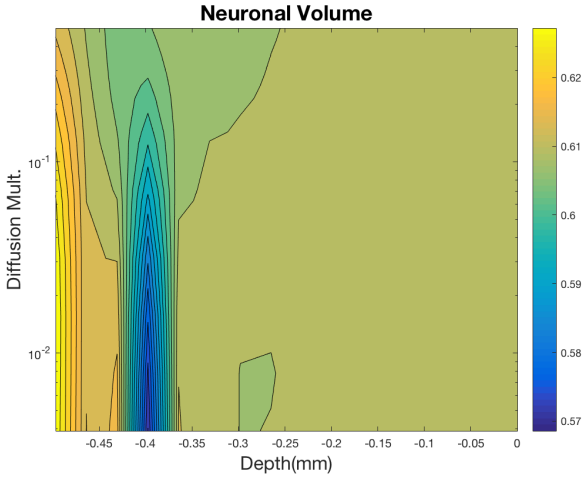

Figure 8.19: Maximal neuronal volume fraction over layers and diffusion coefficients.

Lastly, let us look at extracellular voltage's dependence of diffusion. We saw that it had a large impact on the magnitudes of changes in the homogeneous case. In this case, Figure 8.20, we see a less intense version of this. For higher diffusion we see the basal regions eventually becoming positively polarized, the soma does to a lesser extent. We see the increase in depth and width of the DC shift in the top layers. Interestingly, we can see the hint of multiple valleys in the soma and proximal basal regions. Figure 8.21 shows the DC shift seen in the soma for a separated layer simulation, low neuronal diffusion, and high neuronal diffusion. For the low neuronal diffusion 3 distinct DC shifts can be seen with a 4th very small one that occurs later. For higher diffusion the 3rd shift disappears and we see a larger positive polarization during recovery. If we simulate the soma as an individual layer we get only a single DC shift down to about -13 mV. This multiple shift that occurs in this layer model more closely fits the graphs seen in cell recordings [43](specifically the small dip down to -3mV, that occurs regardless of the size of the diffusion coefficient), which hints that a single set of parameters would not fit a model that tries to show this regional difference as a simple parameter change. It is the complex interaction between layers that gives this behavior.

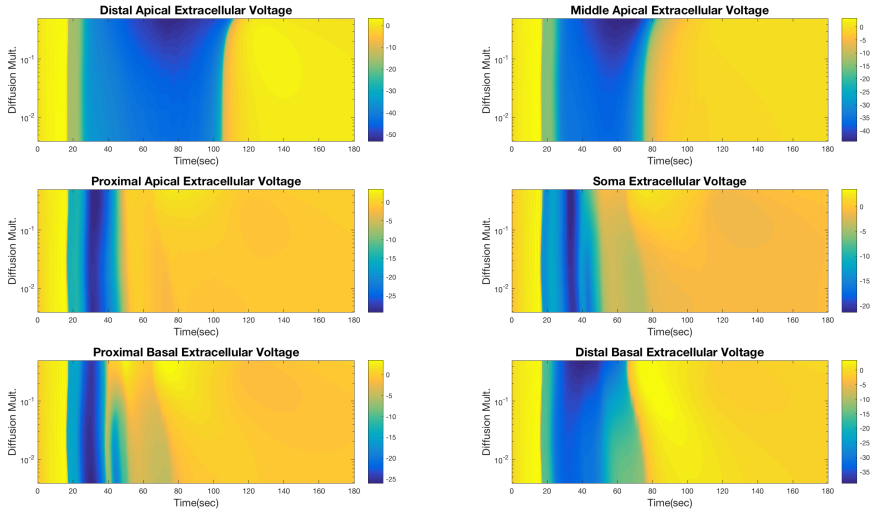

Figure 8.20: 6 layers dependence of extracellular voltage on neuronal z direction diffusion.

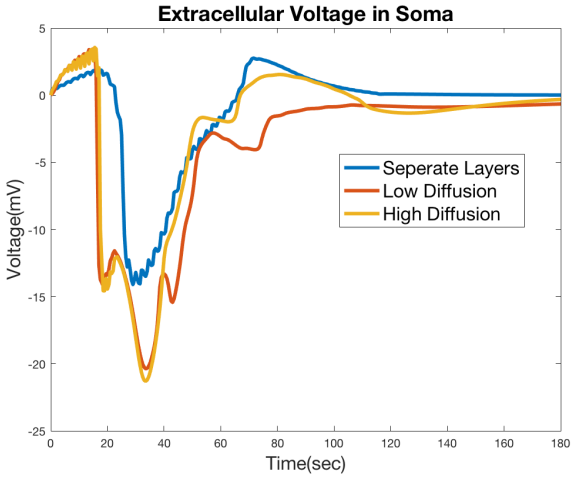

Figure 8.21: Sample of extracellular voltage in the soma for separate layers(1D simulations with these parameters), low neuronal diffusion, and high neuronal diffusion.

8.2.3 Shortcomings

There are several shortcomings of the simulations we have provided that could be improved upon. The general structure of the introduced layer model does not need modification, merely the parameter choices and ranges could use modification and refinement. First on these shortcomings is the DC shift, the apical dendrite region has possibly too large of a DC shift, however, the size of the DC shift is directly controlled by the strength of the NMDA receptor. Due to the lack of a good understanding of spatial dependence of the NMDA receptor, we operated on the assumption that the farthest regions had a large NMDA current/permeability ($5 \times 10^{-5} cm/s$) and the prevalence of NMDA scaled with synapses, which in general increase in number away from the soma. We also made the simplification of combining the expression of the NMDA receptor and the AMPA receptor since we lack the latter receptor. Since the AMPA receptor deactivates faster than the NMDA receptor, it's presence would likely shorten the duration and make the DC shift less pronounced.

One major problem that we have not mentioned up until now is the wave speed. It is much too fast. Figure 8.22 shows the impact diffusion has on velocity. With low or no neuronal diffusion the differences between layers is very large. The high prevalence of persistent sodium in the basal layer is why it is so much faster than the apical layers. As diffusion normalizes the speed we see a sharp decrease from $15 mm/min$ down to $12.5 mm/min$. While the decrease is a good thing, we need it to be lower. The speed of CSD is normally reported to be between $3 - 7 mm/min$, with a few people going up to $10 mm/min$.

Looking at a comparison with running a series of 2D simulations of each layer, Figure 8.23, we can see that the soma without the influence of the dendrites achieves a physiologically accurate speed of around $4 mm/min$. While it is a very useful observation that parameter regimes that would lead to large velocities in a $2D$ or $1D$ model can be mitigated by being linked together with a more detailed layer model, the mitigation in our current formulation is not enough. Where does the massive velocity difference come from? The cellular geometry, our model does not make detailed use of the structure of dendrites we work on an average bulk. The values of average surface area and volume

lead to membrane separation values of:

Region	Membrane Separation(cm)	Ion Permeability scale($1/cm$)
Soma	15.66×10^{-5}	6.38×10^{3}
Apical	2.6998×10^{-5}	3.70×10^{4}
Basal	1.9627×10^{-5}	5.09×10^{4}

The membrane separation is used to scale the ion channel fluxes by dividing (so the 2nd column of this table is that multiplying factor). As we can see the effective flux into the basal and apical compartments is 10-fold larger than the soma. We borrowed these values from [53], perhaps we should have had more refinement like [55] where the radius of the dendrites decreases as we moved along the soma, but it is unclear how to convert a single radius measurement to a surface area of a collection of dendrites. The simple idea of taking a linear increase of the soma measurement to both dendritic measurements leads to a velocity about $1mm/min$ smaller ($11mm/min$) across all the layers. If we look at the effect of just changing the membrane separation on a 1D wave, we see no shocking changes beyond the increased velocity. The main 2 effects are the velocity being significantly impacted(scaling slightly faster than quadratically) and the increase scaling of the ion channel fluxes making the NMDA receptor's longer duration, DC shift, and two hump behavior become pronounced for lower values of the NMDAR permeability.

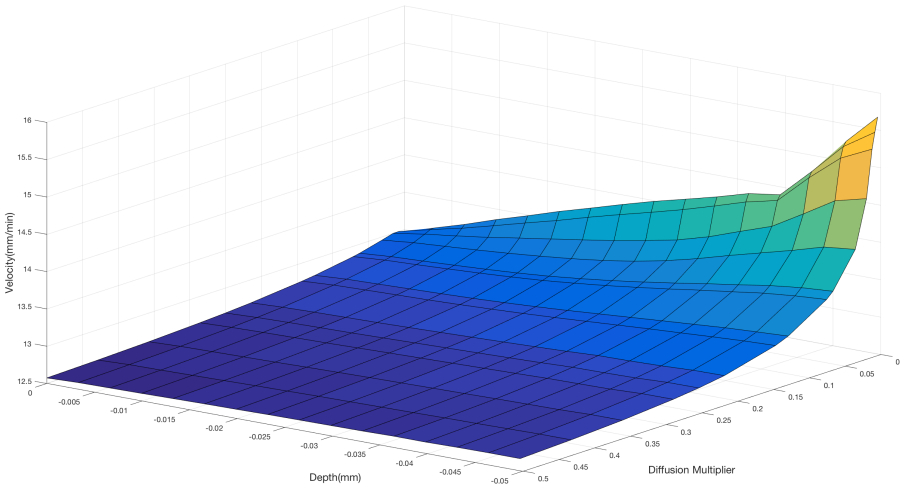

Figure 8.22: Velocity and duration dependence on neuronal z diffusion and depth. Lower diffusion allows for much larger velocity difference. And as higher diffusion normalizes velocity across layers the magnitude of velocity shifts downward.

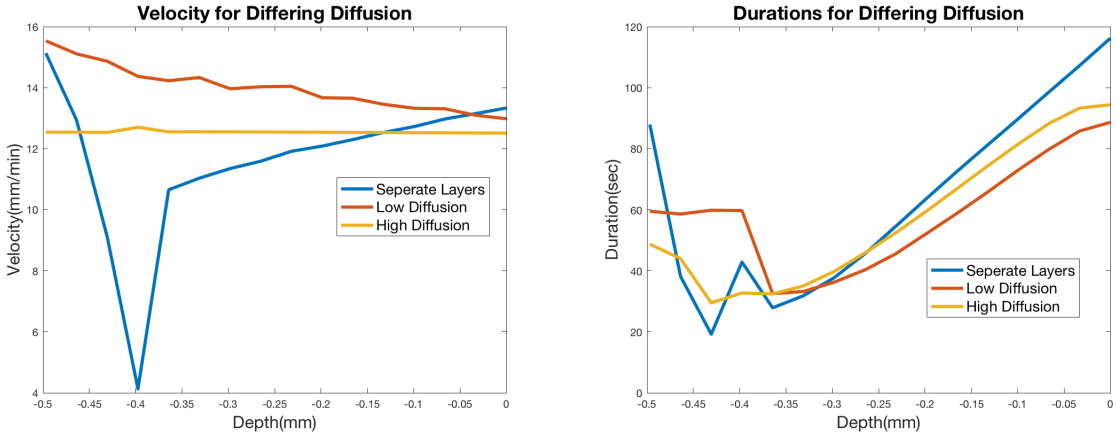

Figure 8.23: Comparison of velocities across layers for high neuronal diffusion, no neuronal diffusion, and completely seperate compartments.

Chapter 9

Conclusion and Discussion

9.1 Conclusion

We introduced an electrodiffusion model of cortical spreading depression that includes glutamate and NMDA receptor dynamics. We showed the capability of our simulation with 2D simulations of spirals and 3D spatially varying parameters. The inclusion of NMDAR allows us to adjust our model to more readily represent different regions of the brain(mainly focusing on differences between soma and dendrites). The combination of electrodiffusion and NMDA receptors allowed us to create the first mathematical model that can calculate extracellular voltage and show the two hump behavior seen in experiments[44, 89] and explain its cause.

We showed that propagation of CSD is influenced by both interstitial potassium and glutamate(summarized in Figs. 6.9 and 6.10). While both can act independently, details of the propagation change depending on which is dominant: NMDAR mediated propagation is significantly slower than persistent sodium driven propagation. While, persistent sodium channels recover much more quickly than NMDA receptors. This is due to the combination of slow deactivation of NMDA receptors and the sensitivity of the NMDA receptors to extracellular glutamate. We saw that extracellular volume suddenly becomes very important. When volume decreases concentrations increase. This increase causes a secondary activation of the NMDA receptor which, in turn, causes a second DC shift with a less extreme secondary depolarization. The secondary activation

of NMDA receptors and volume change causes the dynamics of the other ions become more change. We saw that, because of NMDARs, since potassium is released in tandem with sodium influx that extracellular voltage saw a positive polarization. Another consequence of this is that the neuronal and glial ion pumps have to work much harder to rebalance the sodium concentration in the cells than they did when there was little or no NMDA receptors.

We also generated spiral wave patterns and investigated their behavior as we modified the method of propagation. We saw that the increase in duration due to NMDAR was the primary factor in the shape and speed of the spiral. Compared to a plane wave, the spiral wave showed us that while the qualitative behavior of CSD stayed the same, the magnitude and shape of volume and ionic changes is dependent on having a non-recurrent spreading depolarization. We saw that recurrent spreading depolarizations causes less extreme deviations in voltage and volume. It's impact on ionic concentrations depends on the compartment. With neuronal ionic concentration being narrowly impacted, glial concentrations slightly more influenced, and extracellular concentrations being affected the most. We also saw that the speed of the depolarization is limited by the spiral(and as we saw in 6.3 for recurring waves). Since the state variables are not given enough time to fully recover, we see this impact how quickly a new wave can impact a recently recovered/recovering region, this effect changes depending on how close to the center of the spiral we are. Additionally, we investigated how much work the ion pumps are doing to try to maintain or recover homeostasis. We saw that the center of the spiral required more work on the part of the neurons, with less work for the glia. We also saw that increased NMDA receptor expression caused the neuronal ion pumps to work much harder. This effect is especially pronounced in the center of the spiral.

Our investigation has given modeling evidence to the idea that the spreading depression is not driven by one singular ion channel or ion. Only the coordinated effort of ions and channels can we create a model of CSD that appears to be faithful to the multiple different features seen in different regions of the brain. While we focused mainly on glutamate and potassium, we should make clear that sodium is equally important, its

ion channels are some of the strongest drivers of CSD, however its intimate linking to potassium through the NaK-ATPase and voltage activated potassium channels makes its role easy to ignore.

Lastly, we investigated the impact that the heterogeneous/layer structure of the brain can have on the wave. When parameters are constant across space the ionic changes mostly remain local(transferring among compartments), but with the differing structure along neurons we saw that ions become displaced. We saw that wildly different behaviors can be explained by the location from which we measure and that the interaction between differing regions can create dynamics that is not seen for a single set of parameters modeling a region. The large amount of potassium dumped by dendrites cannot recover as quickly if those dendrites existed in isolation. The dendrites are assisted by the rest of the domain that exists under them. Hence modeling a whole region by a single 1D or 2D wave will not reproduce behavior seen from the interaction of disparate regions. We also found that hard boundaries differentiating different regions can cause transitionary behaviors, in the simple case multiple spreading depressions passing through one region due to the influence of others, and in a more complex case a reversal of the direction of propagation.

There are two areas for improvement for this model. First, the glutamate dynamics we introduced were very simplistic. Since glutamate remains in the extracellular space, we had to introduce desensitization of the NMDA receptors. One method of combating this is to include a method for glia to synthesize glutamine. There are two issues that need to be addressed to come up with such a model. First is the lack of experimental data of these cycles outside of ordinary conditions(specifically short action potential depolarizations). The second difficulty is from the physiology, the glutamate-glutamine cycle is ATP dependent, and during CSD we have a possible lack of ATP that would have to be modeled. The second area of improvement for this model is the inclusion of calcium. NMDA receptors also allow the influx of calcium, granted only 5% of the current. More importantly, some mechanisms of glutamate release is calcium dependent [26], while other mechanisms exist that are calcium independent. For CSD, it is known that calcium plays a role, but that role is possibly unimportant as channels

blockers have little effect on preventing propagation [78]. One overarching problem in CSD modeling is time scales, many experiments that measure the ion channels we use provide good insight on the activation of channels (shorter time scale), but deactivation is less well known. Most experiments do not (and cannot) measure single channels at the prolonged time scale that CSD exists.

In the future, we can further refine the layered structure of the hippocampus or modify this to include different brain regions. Additionally, we have many parameters in this model that can be tweaked to see their influence, there is the open possibility for varying membrane stiffness, we also have the interaction with the fast sodium channel. While for computational ease (and because it only effects time just before onset and recovery) we set it to 0 for much of this work(everything besides the layer model), an interesting study could be performed in the realm of [99], where we allow for action potentials and thus tonic firing to occur just before onset. Lastly, two other hypothesis of propagation we did not mention are the neuronal or glial gap junctions Hypotheses[78]. While there is evidence that these are not the main drivers, further study of our model would allow us to investigate the effects these do have on the wave, we saw a taste of the effect neuronal diffusion has on the layer model and gap junctions would act similarly. Lastly, adding other ligand activated ion channels, AMPA or GABA receptors for example, can lead to interesting changes in dynamics since we have seen volume changes interact with these in non-trivial ways and would represent a wholly new use of previous models of these channels.

References

[1] P. Aitken, G. Tombaugh, D. Turner, and G. Somjen, *Similar propagation of sd and hypoxic sd-like depolarization in rat hippocampus recorded optically and electrically*, Journal of neurophysiology, 80 (1998), pp. 1514–1521.

[2] A.-C. G. Almeida, H. Texeira, M. A. Duarte, and A. F. C. Infantosi, *Modeling extracellular space electrodiffusion during lea/spl tilde/o's spreading depression*, IEEE transactions on biomedical engineering, 51 (2004), pp. 450–458.

[3] P. Andersen, R. Morris, D. Amaral, J. O'Keefe, T. Bliss, et al., *The hippocampus book*, Oxford university press, 2007.

[4] N. Astman, M. J. Gutnick, and I. A. Fleidervish, *Persistent sodium current in layer 5 neocortical neurons is primarily generated in the proximal axon*, Journal of Neuroscience, 26 (2006), pp. 3465–3473.

[5] S. Balay, S. Abhyankar, M. F. Adams, J. Brown, P. Brune, K. Buschelman, L. Dalcin, A. Dener, V. Eijkhout, W. D. Gropp, D. Kaushik, M. G. Knepley, D. A. May, L. C. McInnes, R. T. Mills, T. Munson, K. Rupp, P. Sanan, B. F. Smith, S. Zampini, H. Zhang, and H. Zhang, *PETSc Web page*. http://www.mcs.anl.gov/petsc, 2018.

[6] ——, *PETSc users manual*, Tech. Rep. ANL-95/11 - Revision 3.10, Argonne National Laboratory, 2018.

[7] S. Balay, W. D. Gropp, L. C. McInnes, and B. F. Smith, *Efficient management of parallelism in object oriented numerical software libraries*, in Modern

Software Tools in Scientific Computing, E. Arge, A. M. Bruaset, and H. P. Langtangen, eds., Birkhäuser Press, 1997, pp. 163–202.

[8] M. Balestrino and G. G. Somjen, *Chlorpromazine protects brain tissue in hypoxia by delaying spreading depression-mediated calcium influx*, Brain research, 385 (1986), pp. 219–226.

[9] E. Barreto and J. R. Cressman, *Ion concentration dynamics as a mechanism for neuronal bursting*, Journal of biological physics, 37 (2011), pp. 361–373.

[10] T. A. Basarsky, S. N. Duffy, R. D. Andrew, and B. A. MacVicar, *Imaging spreading depression and associated intracellular calcium waves in brain slices*, Journal of Neuroscience, 18 (1998), pp. 7189–7199.

[11] M. Bennett, L. Farnell, and W. Gibson, *A quantitative model of purinergic junctional transmission of calcium waves in astrocyte networks*, Biophysical journal, 89 (2005), pp. 2235–2250.

[12] M. R. Bennett, L. Farnell, and W. G. Gibson, *A quantitative model of cortical spreading depression due to purinergic and gap-junction transmission in astrocyte networks*, Biophysical journal, 95 (2008), pp. 5648–5660.

[13] A. Bikbaev, M. Duménieu, J. Lopez-Rojas, and M. Heine, *Localising receptors and channels across the dendritic arbour*, in Dendrites, Springer, 2016, pp. 387–424.

[14] B. Billups and D. Attwell, *Modulation of non-vesicular glutamate release by ph*, Nature, 379 (1996), p. 171.

[15] B. Bosche, R. Graf, R.-I. Ernestus, C. Dohmen, T. Reithmeier, G. Brinker, A. J. Strong, J. P. Dreier, and J. Woitzik, *Recurrent spreading depolarizations after subarachnoid hemorrhage decreases oxygen availability in human cerebral cortex*, Annals of neurology, 67 (2010), pp. 607–617.

[16] S. Canals, I. Makarova, L. Lopez-Aguado, C. Largo, J. M. Ibarz, and O. Herreras, *Longitudinal depolarization gradients along the somatodendritic*

axis of ca1 pyramidal cells: a novel feature of spreading depression, Journal of neurophysiology, 94 (2005), pp. 943–951.

[17] J. C. Chang, K. C. Brennan, D. He, H. Huang, R. M. Miura, P. L. Wilson, and J. J. Wylie, *A mathematical model of the metabolic and perfusion effects on cortical spreading depression*, PLoS One, 8 (2013), p. e70469.

[18] A. Charles and K. Brennan, *Cortical spreading depressionnew insights and persistent questions*, Cephalalgia, 29 (2009), pp. 1115–1124.

[19] A. C. Charles and S. M. Baca, *Cortical spreading depression and migraine*, Nature Reviews Neurology, 9 (2013), p. 637.

[20] J. Clements, *Transmitter timecourse in the synaptic cleft: its role in central synaptic function*, Trends in neurosciences, 19 (1996), pp. 163–171.

[21] B. W. Connors and M. A. Long, *Electrical synapses in the mammalian brain*, Annu. Rev. Neurosci., 27 (2004), pp. 393–418.

[22] C. Conte, R. Lee, M. Sarkar, and D. Terman, *A mathematical model of recurrent spreading depolarizations*, Journal of computational neuroscience, 44 (2018), pp. 203–217.

[23] M. A. Dahlem, R. Graf, A. J. Strong, J. P. Dreier, Y. A. Dahlem, M. Sieber, W. Hanke, K. Podoll, and E. Schöll, *Two-dimensional wave patterns of spreading depolarization: retracting, re-entrant, and stationary waves*, Physica D: Nonlinear Phenomena, 239 (2010), pp. 889–903.

[24] M. A. Dahlem and S. C. Müller, *Self-induced splitting of spiral-shaped spreading depression waves in chicken retina*, Experimental brain research, 115 (1997), pp. 319–324.

[25] N. Danbolt, D. Furness, and Y. Zhou, *Neuronal vs glial glutamate uptake: resolving the conundrum*, Neurochemistry international, 98 (2016), pp. 29–45.

[26] N. C. Danbolt, *Glutamate uptake*, Progress in neurobiology, 65 (2001), pp. 1–105.

[27] D. Debanne, E. Campanac, A. Bialowas, E. Carlier, and G. Alcaraz, *Axon physiology*, Physiological reviews, 91 (2011), pp. 555–602.

[28] A. Destexhe, Z. F. Mainen, and T. J. Sejnowski, *Synthesis of models for excitable membranes, synaptic transmission and neuromodulation using a common kinetic formalism*, Journal of computational neuroscience, 1 (1994), pp. 195–230.

[29] ——, *Kinetic models of synaptic transmission*, Methods in neuronal modeling, 2 (1998), pp. 1–25.

[30] J. P. Dreier, *The role of spreading depression, spreading depolarization and spreading ischemia in neurological disease*, Nature medicine, 17 (2011), p. 439.

[31] J. P. Dreier, N. Ebert, J. Priller, D. Megow, U. Lindauer, R. Klee, U. Reuter, Y. Imai, K. M. Einhäupl, I. Victorov, et al., *Products of hemolysis in the subarachnoid space inducing spreading ischemia in the cortex and focal necrosis in rats: a model for delayed ischemic neurological deficits after subarachnoid hemorrhage?*, Journal of neurosurgery, 93 (2000), pp. 658–666.

[32] J. P. Dreier, T. Isele, C. Reiffurth, N. Offenhauser, S. A. Kirov, M. A. Dahlem, and O. Herreras, *Is spreading depolarization characterized by an abrupt, massive release of gibbs free energy from the human brain cortex?*, The Neuroscientist, 19 (2013), pp. 25–42.

[33] J. P. Dreier and C. Reiffurth, *The stroke-migraine depolarization continuum*, Neuron, 86 (2015), pp. 902–922.

[34] R. Enger, W. Tang, G. F. Vindedal, V. Jensen, P. Johannes Helm, R. Sprengel, L. L. Looger, and E. A. Nagelhus, *Dynamics of ionic shifts in cortical spreading depression*, Cerebral Cortex, 25 (2015), pp. 4469–4476.

[35] I. A. Fleidervish, N. Lasser-Ross, M. J. Gutnick, and W. N. Ross, *Na+ imaging reveals little difference in action potential–evoked na+ influx between axon and soma*, Nature neuroscience, 13 (2010), p. 852.

[36] N. L. Golding, W. L. Kath, and N. Spruston, *Dichotomy of action-potential backpropagation in ca1 pyramidal neuron dendrites*, Journal of neurophysiology, 86 (2001), pp. 2998–3010.

[37] N. Gorelova and J. Bureš, *Spiral waves of spreading depression in the isolated chicken retina*, Journal of neurobiology, 14 (1983), pp. 353–363.

[38] B. Grafstein, *Mechanism of spreading cortical depression*, Journal of neurophysiology, 19 (1956), pp. 154–171.

[39] N. Hadjikhani, M. S. Del Rio, O. Wu, D. Schwartz, D. Bakker, B. Fischl, K. K. Kwong, F. M. Cutrer, B. R. Rosen, R. B. Tootell, et al., *Mechanisms of migraine aura revealed by functional mri in human visual cortex*, Proceedings of the National Academy of Sciences, 98 (2001), pp. 4687–4692.

[40] M. M. Haglund and P. A. Schwartzkroin, *Role of na-k pump potassium regulation and ipsps in seizures and spreading depression in immature rabbit hippocampal slices*, Journal of Neurophysiology, 63 (1990), pp. 225–239.

[41] N. B. Hamilton and D. Attwell, *Do astrocytes really exocytose neurotransmitters?*, Nature Reviews Neuroscience, 11 (2010), p. 227.

[42] A. V. Harreveld, *Compounds in brain extracts causing spreading depression of cerebral cortical activity and contraction of crustacean muscle*, Journal of neurochemistry, 3 (1959), pp. 300–315.

[43] O. Herreras and G. Somjen, *Propagation of spreading depression among dendrites and somata of the same cell population*, Brain research, 610 (1993), pp. 276–282.

[44] O. Herreras and G. G. Somjen, *Analysis of potential shifts associated with recurrent spreading depression and prolonged unstable spreading depression induced by microdialysis of elevated k+ in hippocampus of anesthetized rats*, Brain research, 610 (1993), pp. 283–294.

[45] L. Hertz and D. L. Rothman, *Glutamine-glutamate cycle flux is similar in cultured astrocytes and brain and both glutamate production and oxidation are mainly catalyzed by aspartate aminotransferase*, Biology, 6 (2017), p. 17.

[46] A. L. Hodgkin and A. F. Huxley, *A quantitative description of membrane current and its application to conduction and excitation in nerve*, The Journal of physiology, 117 (1952), pp. 500–544.

[47] D. A. Hoffman, J. C. Magee, C. M. Colbert, and D. Johnston, *K+ channel regulation of signal propagation in dendrites of hippocampal pyramidal neurons*, Nature, 387 (1997), p. 869.

[48] W. Hu, C. Tian, T. Li, M. Yang, H. Hou, and Y. Shu, *Distinct contributions of na v 1.6 and na v 1.2 in action potential initiation and backpropagation*, Nature neuroscience, 12 (2009), p. 996.

[49] N. Hübel and M. A. Dahlem, *Dynamics from seconds to hours in hodgkin-huxley model with time-dependent ion concentrations and buffer reservoirs*, PLoS computational biology, 10 (2014), p. e1003941.

[50] N. Hübel, E. Schöll, and M. A. Dahlem, *Bistable dynamics underlying excitability of ion homeostasis in neuron models*, PLoS computational biology, 10 (2014), p. e1003551.

[51] C. E. Jahr and C. F. Stevens, *Voltage dependence of nmda-activated macroscopic conductances predicted by single-channel kinetics*, Journal of Neuroscience, 10 (1990), pp. 3178–3182.

[52] ——, *Calcium permeability of the n-methyl-d-aspartate receptor channel in hippocampal neurons in culture*, Proceedings of the National Academy of Sciences, 90 (1993), pp. 11573–11577.

[53] H. Kager, W. Wadman, and G. Somjen, *Simulated seizures and spreading depression in a neuron model incorporating interstitial space and ion concentrations*, Journal of neurophysiology, 84 (2000), pp. 495–512.

[54] ——, *Conditions for the triggering of spreading depression studied with computer simulations*, Journal of neurophysiology, 88 (2002), pp. 2700–2712.

[55] ——, *Seizure-like afterdischarges simulated in a model neuron*, Journal of computational neuroscience, 22 (2007), pp. 105–128.

[56] P. Kalivas, *Extracellular glutamate: functional compartments operate in different concentration ranges*, Frontiers in systems neuroscience, 5 (2011), p. 94.

[57] W. Knowles, P. Funch, and P. A. Schwartzkroin, *Electrotonic and dye coupling in hippocampal ca1 pyramidal cells in vitro*, Neuroscience, 7 (1982), pp. 1713–1722.

[58] T. Kosaka and K. Hama, *Gap junctions between non-pyramidal cell dendrites in the rat hippocampus (ca1 and ca3 regions): A combined golgi-electron microscopy study*, Journal of Comparative Neurology, 231 (1985), pp. 150–161.

[59] M. Lauritzen, *Pathophysiology of the migraine aura: the spreading depression theory*, Brain, 117 (1994), pp. 199–210.

[60] M. Lauritzen, J. P. Dreier, M. Fabricius, J. A. Hartings, R. Graf, and A. J. Strong, *Clinical relevance of cortical spreading depression in neurological disorders: migraine, malignant stroke, subarachnoid and intracranial hemorrhage, and traumatic brain injury*, Journal of Cerebral Blood Flow & Metabolism, 31 (2011), pp. 17–35.

[61] A. A. Leao, *Spreading depression of activity in the cerebral cortex*, Journal of neurophysiology, 7 (1944), pp. 359–390.

[62] D. H. Leibowitz, *The glial spike theory. i. on an active role of neuroglia in spreading depression and migraine*, Proceedings of the Royal Society of London. Series B: Biological Sciences, 250 (1992), pp. 287–295.

[63] A. Lorincz and Z. Nusser, *Molecular identity of dendritic voltage-gated sodium channels*, Science, 328 (2010), pp. 906–909.

[64] J. C. Magee and D. Johnston, *Characterization of single voltage-gated na+ and ca2+ channels in apical dendrites of rat ca1 pyramidal neurons.*, The Journal of physiology, 487 (1995), pp. 67–90.

[65] V. Menon, T. F. Musial, A. Liu, Y. Katz, W. L. Kath, N. Spruston, and D. A. Nicholson, *Balanced synaptic impact via distance-dependent synapse distribution and complementary expression of ampars and nmdars in hippocampal dendrites*, Neuron, 80 (2013), pp. 1451–1463.

[66] M. Migliore and G. M. Shepherd, *Emerging rules for the distributions of active dendritic conductances*, Nature Reviews Neuroscience, 3 (2002), p. 362.

[67] R. M. Miura, H. Huang, and J. J. Wylie, *Cortical spreading depression: An enigma*, The European Physical Journal Special Topics, 147 (2007), pp. 287–302.

[68] H. Monyer, N. Burnashev, D. J. Laurie, B. Sakmann, and P. H. Seeburg, *Developmental and regional expression in the rat brain and functional properties of four nmda receptors*, Neuron, 12 (1994), pp. 529–540.

[69] Y. Mori, *A multidomain model for ionic electrodiffusion and osmosis with an application to cortical spreading depression*, Physica D: Nonlinear Phenomena, 308 (2015), pp. 94–108.

[70] C. Nicholson, *Diffusion and related transport mechanisms in brain tissue*, Reports on progress in Physics, 64 (2001), p. 815.

[71] T. P. Obrenovitch and E. Zilkha, *High extracellular potassium, and not extracellular glutamate, is required for the propagation of spreading depression*, Journal of neurophysiology, 73 (1995), pp. 2107–2114.

[72] R. O'Connell, *A computational study of cortical spreading depression*, PhD thesis, University of Minnesota, Twin Cities, 2016.

[73] R. OConnell and Y. Mori, *Effects of glia in a triphasic continuum model of cortical spreading depression*, Bulletin of mathematical biology, 78 (2016), pp. 1943–1967.

[74] M. P. Parsons and L. A. Raymond, *Extrasynaptic nmda receptor involvement in central nervous system disorders*, Neuron, 82 (2014), pp. 279–293.

[75] D. K. Patneau and M. L. Mayer, *Structure-activity relationships for amino acid transmitter candidates acting at n-methyl-d-aspartate and quisqualate receptors*, Journal of Neuroscience, 10 (1990), pp. 2385–2399.

[76] S. Pendyam, A. Mohan, P. Kalivas, and S. Nair, *Computational model of extracellular glutamate in the nucleus accumbens incorporates neuroadaptations by chronic cocaine*, Neuroscience, 158 (2009), pp. 1266–1276.

[77] G. C. Petzold, S. Haack, O. von Bohlen und Halbach, J. Priller, T.-N. Lehmann, U. Heinemann, U. Dirnagl, and J. P. Dreier, *Nitric oxide modulates spreading depolarization threshold in the human and rodent cortex*, Stroke, 39 (2008), p. 1292.

[78] D. Pietrobon and M. A. Moskowitz, *Chaos and commotion in the wake of cortical spreading depression and spreading depolarizations*, Nature Reviews Neuroscience, 15 (2014), p. 379.

[79] J. A. Reggia and D. Montgomery, *A computational model of visual hallucinations in migraine*, Computers in biology and medicine, 26 (1996), pp. 133–141.

[80] K. Revett, E. Ruppin, S. Goodall, and J. A. Reggia, *Spreading depression in focal ischemia: a computational study*, Journal of Cerebral Blood Flow & Metabolism, 18 (1998), pp. 998–1007.

[81] W. C. Risher, D. Ard, J. Yuan, and S. A. Kirov, *Recurrent spontaneous spreading depolarizations facilitate acute dendritic injury in the ischemic penumbra*, Journal of Neuroscience, 30 (2010), pp. 9859–9868.

[82] D. J. Rossi, T. Oshima, and D. Attwell, *Glutamate release in severe brain ischaemia is mainly by reversed uptake*, Nature, 403 (2000), p. 316.

[83] V. Savcenco, W. Hundsdorfer, and J. Verwer, *A multirate time stepping strategy for stiff ordinary differential equations*, BIT Numerical Mathematics, 47 (2007), pp. 137–155.

[84] M. M. Shah, M. Migliore, I. Valencia, E. C. Cooper, and D. A. Brown, *Functional significance of axonal kv7 channels in hippocampal pyramidal neurons*, Proceedings of the National Academy of Sciences, 105 (2008), pp. 7869–7874.

[85] B. E. Shapiro, *An electrophysiological model of gap-junction mediated cortical spreading depression including osmotic volume changes*, PhD thesis, University of California, Los Angeles, 2000.

[86] B. E. Shapiro, *Osmotic forces and gap junctions in spreading depression: a computational model*, Journal of computational neuroscience, 10 (2001), pp. 99–120.

[87] J. Shen, K. F. Petersen, K. L. Behar, P. Brown, T. W. Nixon, G. F. Mason, O. A. Petroff, G. I. Shulman, R. G. Shulman, and D. L. Rothman, *Determination of the rate of the glutamate/glutamine cycle in the human brain by in vivo 13c nmr*, Proceedings of the National Academy of Sciences, 96 (1999), pp. 8235–8240.

[88] G. Söhl, S. Maxeiner, and K. Willecke, *Expression and functions of neuronal gap junctions*, Nature reviews neuroscience, 6 (2005), p. 191.

[89] G. G. Somjen, *Mechanisms of spreading depression and hypoxic spreading depression-like depolarization*, Physiological reviews, 81 (2001), pp. 1065–1096.

[90] ——, *Ions in the brain: normal function, seizures, and stroke*, Oxford University Press, 2004.

[91] N. Spruston, P. Jonas, and B. Sakmann, *Dendritic glutamate receptor channels in rat hippocampal ca3 and ca1 pyramidal neurons.*, The Journal of physiology, 482 (1995), pp. 325–352.

[92] A. R. Stevens, I. Ng, A. Helmy, P. J. Hutchinson, D. Menon, and A. Ercole, *Glucose dynamics of cortical spreading depolarisation in acute brain injury: A systematic review*, Journal of neurotrauma, (2019).

[93] M. Szatkowski, B. Barbour, and D. Attwell, *Non-vesicular release of glutamate from glial cells by reversed electrogenic glutamate uptake*, Nature, 348 (1990), p. 443.

[94] A. Tottene, A. Urbani, and D. Pietrobon, *Role of different voltage-gated ca2+ channels in cortical spreading depression: specific requirement of p/q-type ca2+ channels*, Channels, 5 (2011), pp. 110–114.

[95] H. C. Tuckwell and R. M. Miura, *A mathematical model for spreading cortical depression*, Biophysical Journal, 23 (1978), pp. 257–276.

[96] G. Ullah, J. R. Cressman Jr, E. Barreto, and S. J. Schiff, *The influence of sodium and potassium dynamics on excitability, seizures, and the stability of persistent states: Ii. network and glial dynamics*, Journal of computational neuroscience, 26 (2009), pp. 171–183.

[97] A. Van Harreveld, *Two mechanisms for spreading depression in the chicken retina*, Journal of neurobiology, 9 (1978), pp. 419–431.

[98] W. Wadman, A. Juta, W. Kamphuis, and G. Somjen, *Current source density of sustained potential shifts associated with electrographic seizures and with spreading depression in rat hippocampus*, Brain research, 570 (1992), pp. 85–91.

[99] Y. Wei, G. Ullah, and S. J. Schiff, *Unification of neuronal spikes, seizures, and spreading depression*, Journal of Neuroscience, 34 (2014), pp. 11733–11743.

[100] T. Wolf, U. Lindauer, A. Villringer, and U. Dirnagl, *Excessive oxygen or glucose supply does not alter the blood flow response to somatosensory stimulation or spreading depression in rats*, Brain research, 761 (1997), pp. 290–299.

[101] W. Yao, H. Huang, and R. M. Miura, *A continuum neuronal model for the instigation and propagation of cortical spreading depression*, Bulletin of mathematical biology, 73 (2011), pp. 2773–2790.

[102] B.-J. Zandt, B. ten Haken, M. J. van Putten, and M. A. Dahlem, *How does spreading depression spread? physiology and modeling*, Reviews in the Neurosciences, 26 (2015), pp. 183–198.

[103] N. Zerangue and M. P. Kavanaugh, *Flux coupling in a neuronal glutamate transporter*, Nature, 383 (1996), p. 634.

[104] N. Zhou, R. L. Rungta, A. Malik, H. Han, D. C. Wu, and B. A. MacVicar, *Regenerative glutamate release by presynaptic nmda receptors contributes to spreading depression*, Journal of Cerebral Blood Flow & Metabolism, 33 (2013), pp. 1582–1594.

Appendix A

Glossary and Acronyms

For quick reference here is a small list of acronyms and terms used throughout this thesis. It is not an exhaustive list but contains many important phrases we use repeatedly.

A.1 Glossary

- **DC-Shift** – The characteristic shift in the extracellular potential from near 0 to a negative value (typically -10mV to -30mV).
- **Glia** – Glial cells. These are non-neuronal cells in the central nervous system. They act as helpers and inhibitors to neurons. Astrocytes are a particular type of these. There are many more.
- **Gap Junctions** – Connections between neurons are glia that are a direct form of connection. Electrical synapse is another term for this.
- **Soma** – The cell body. Most contexts in this thesis have this being specifically the cell body of the neuron.
- **Dendrite** – The branches that come off of the cell body. Specifically for this thesis, the neurons.
- **Pyramidal Cells** – A type of neuron that is the primary excitatory unit of the central nervous system (kind of).

- **stratum radiatum** – A subfield of the CA hippocampus regions that contains apical (receiving end) dendrites of the pyramidal neurons.
- **stratum pyramidale** – A subfield of the CA hippocampus regions that contains most of the pyramidal cell bodies.
- **stratum oriens** – A subfield of the CA hippocampus regions that contains inhibitive interneurons and the basal dendrites of the pyramidal cells (axons also travel through this region).

A.2 Acronyms

Table A.1: Acronyms

Acronym	Meaning
CSD	Cortical Spreading Depression
SD	Spreading Depolarization
NaP	Persistent Sodium Channel
NMDA (receptor)	N-methyl-D-aspartate (receptor)
NMDAR	N-methyl-D-aspartate Receptor
KDR	Potassium Delayed Rectifier
NaT	Transient Sodium Channel
KA	Transient/Active Potassium Channel
KIR	Potassium inward rectifier
NaK (ATPase)	Sodium-Potassium Ion Pump
ODE	Ordinary Differential Equation
PDE	Partial Differential Equation
ATP	Adenosine triphosphate
PETSC	Portable, Extensible Toolkit for Scientific Computation(software program)
KSP	Krylov Subspace Iterations

A.3 Velocity in 2 Dimensions

Velocity in 1 dimension is straight forward to calculate, take a cutoff level of your function. Then try to find the velocity v that minimizes the translation formulation of $f(x,t) = f(x-vt)$. For 2 dimensions it is a little more involved. First assume we have a function $F(x,y,t) : [0,L]^2 \times \mathbb{R}^+ \to \mathbb{R}$ that represents a spreading wave, this wave starts at a low value and reaches a maximum before returning back to a low value. Then for each point in the domain we define a T_{start} and T_{end} by:

$$T_{start}(x,y) = \left(t_1, t_2, \cdots, t_n \middle| F(x,y,t) = f_{cross} \text{ and } \frac{dF}{dt} > 0 \right)$$

$$T_{end}(x,y) = \left(t_1, t_2, \cdots, t_n \middle| F(x,y,t) = f_{cross} \text{ and } \frac{dF}{dt} < 0 \right)$$

which each denote the set of times that the wave starts and ends at each point. We can then define the unique point that a maximum value is attained in between each of these times (T_{peak}).

$$T_{peak}(x,y) = \left(t_1, t_2, \cdots, t_n \middle| \text{argmax}_{T_{start}(x,y)<t<T_{end}(x,y)} \left(F(x,y,t) \right) \right)$$

This is a function that takes multiple values. However, each value is a well defined strictly increasing sequence. For each of these values we can define the velocity of the wave that is passing at that time as:

$$v_{peak}(x,y) = \frac{1}{|\nabla(T_{peak}(x,y))|}$$

then for a domain with a constant set of parameters that generates the wave, the velocity is just the average of these over all the times and all of space.

A.4 Angular Velocity

In order to measure angular velocity we make an assumption: For a spiral wave, it's evolution in time can be describe by a rotation about some center point. Therefore, in order to find the angular speed we must also find this center point. To do this we

set up an optimization problem. Just like with velocity we assume we have a function $F(x, y, t)$. Define a rotation about a point (x_c, y_c) as $R(\theta, x_c, y_c)$. The action of this rotation on evaluating $F(x, y, t)$ under the rotation will be denoted $F(x_R, y_R, t)$. Now for our optimization problem. Under our assumption of how the spiral works, the angular velocity can be found by taking a small step Δt forward in time and finding the angle that equals that step.

$$F(x_R, y_R, t) = F(x, y, t + \Delta t)$$

(in full detail this looks like)

$$\begin{aligned} F\left(x, y, t + \Delta t\right) = F(&\cos(\theta)(x - x_c) + \sin(\theta)(y - y_c)) + x_c, \\ &- \sin(\theta)(x - x_c) + \cos(\theta)(y - y_0)) + y_0, \\ &t) \end{aligned}$$

For our simulations we have discrete sets of times and positions. To do this we interpolate our function in space, so that the rotations can be evaluated at the same sets of points. We then take all of our time points and pick a time step and calculate an objective function via a sum of squares of all of the differences of all the points choosing a fixed Δt. We then find the center : (x_c, y_c) and angle θ that minimizes all of them. An alternative method is to take sets of points in a smaller time interval and minimize those. This method can give us a set of centers and angles that change over time. The angular velocity can then be the average angle we rotate.

A.5 Energy Calculation

We will give a short detail of what the energy we are talking about is, for a more full discussion see [69]. Let G be the free energy, then we can write G as:

$$G = \int_\Omega \left(\mathcal{E} + \sum_{k=1}^{N} \left(RT \left(a_k \ln\left(\frac{a_k}{\alpha_k}\right) + \sum_{i=1}^{M} \alpha_k c_i^k \ln\left(c_i^k\right) \right) \right) + \sum_{k=1}^{N-1} \frac{1}{2} \gamma_k C_m \phi_{kN}^2 \right) dx \tag{A.1}$$

where $\mathcal{E}$ is the elastic energy, since we set the stiffness constant to zero in this paper, this term is zero. The free energy satisfies the equation:

$$\frac{dG}{dt} = -I_{bulk} - I_{mem}$$

where,

$$I_{bulk} = \int_\Omega \left(\sum_{k=1}^{N} \sum_{i=1}^{M} \frac{D_i^k c_i^k}{RT} |\nabla \mu_i^k|^2 \right) dx$$

$$I_{mem} = \int_\Omega \left(\sum_{k=1}^{N-1} \gamma_k \left(\psi_{kN} w_k + \sum_{i=1}^{M} \mu_i^{kN} g_i^k \right) \right) dx$$

where μ_i^{kN} is the chemical potential difference with $\mu_i^k = RT\left(\ln(c_i^k + 1) + z_i F c_i^k \phi_k\right)$. And ψ_k is the water potential with: $\psi_k = p_k - \pi_{wk} = p_k - RT\left(a_k/\alpha_k + \sum_{i=1}^{M} c_i^k\right)$, where p_k is the compartmental pressure (which is constant for no fluid flow). Reminder that g_i^k is the sum of all the ion channel fluxes for that compartment and ion. So, when we talk about work done by the ion pumps we are talking about only part of the sum in I_{mem}, that part is:

$$I_{mem}^{pumps} = \sum_{k=1}^{N-1} -\gamma_k \left(h_{Na}^{k,ATP} \left(RT \log\left(\frac{c_{Na}^k}{c_{Na}^N} \right) + F\phi_{kN} \right) + h_K^{k,ATP} \left(RT \log\left(\frac{c_K^k}{c_K^N} \right) + F\phi_{kN} \right) \right) \tag{A.2}$$

As an aside, we should mention here that the Figure **??** were created by looking at the unit-less quantity for NaK ATPase:

$$\frac{1}{\left(1 + m_k/c_K^N\right)^2 \left(1 + m_{Na}/c_{Na}^k\right)^3}$$

A.6 Figures

A.6.1 1 Dimension

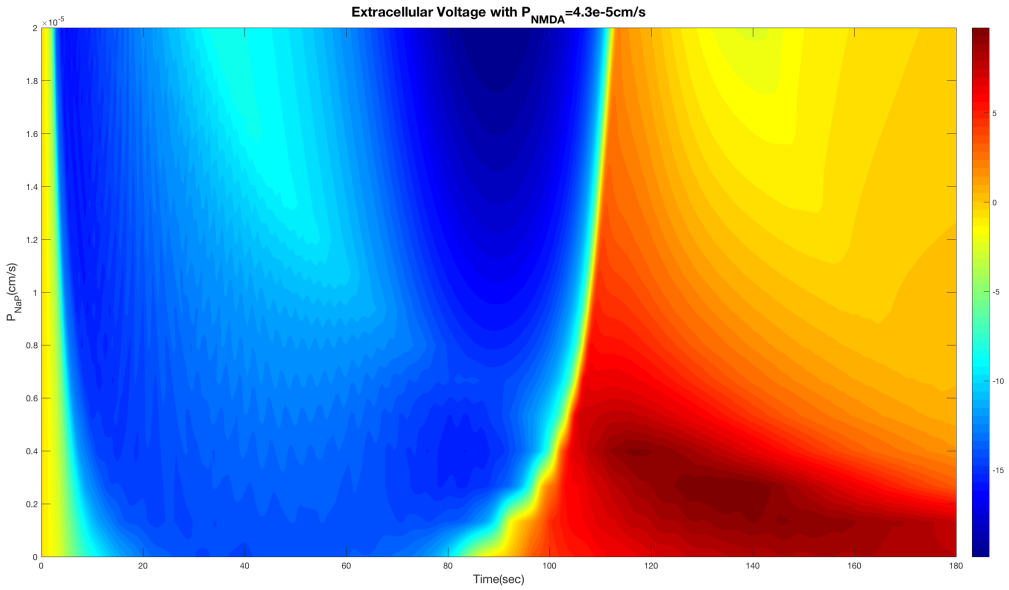

Figure A.1: Time profiles for a fixed P_{NMDA} and varying P_{NaP}. Notice that for a high enough NaP, we see an initial recovery that then becomes more polarized after. We can also see the clear increase in the over recovery that occurs as NMDA is left to act on it's own.

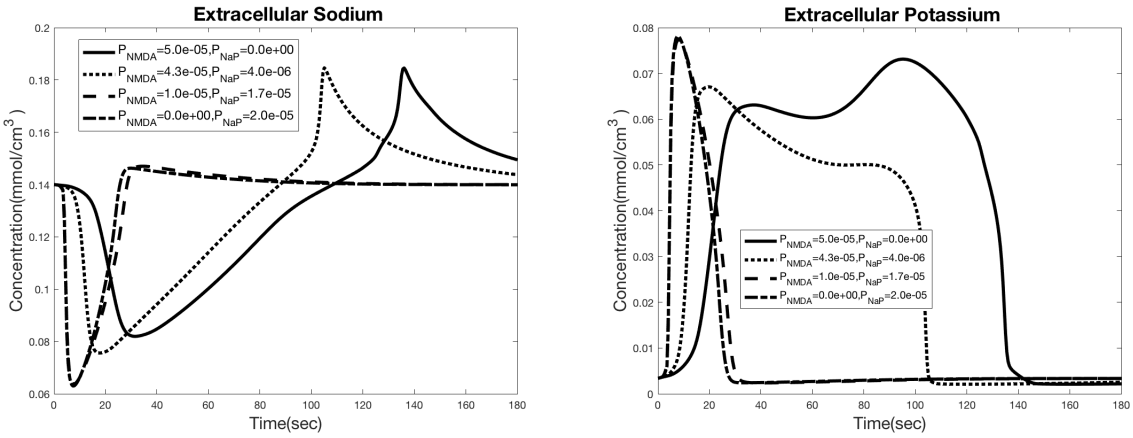

Figure A.2: Time profiles of extracellular sodium and potassium. The uptick in the sodium is due to NaK ATPase pumping sodium out of neurons and glia. The second increase in potassium is not immediately obvious in that context. But both sodium and potassium are still being released by the open NMDA channels.

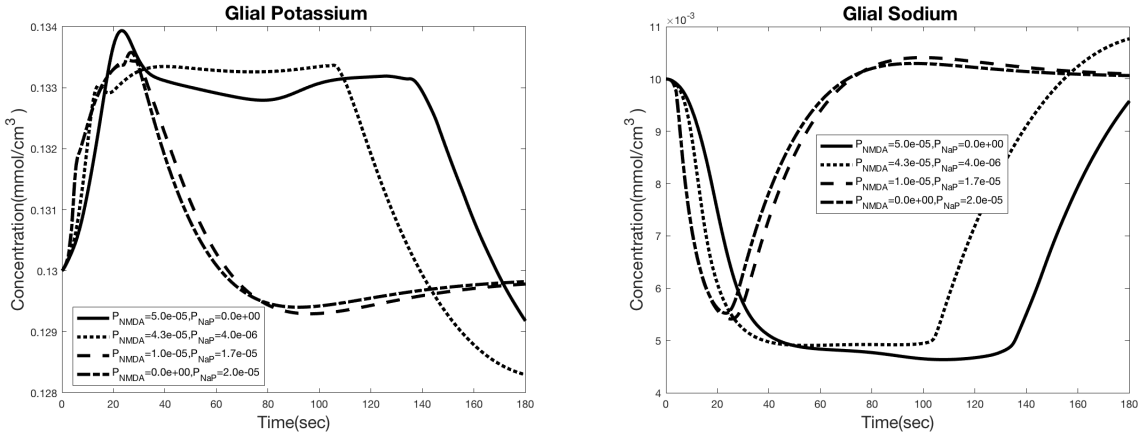

Figure A.3: Time profiles of glial potassium and sodium. Potassium uptake levels out and ceases to work as efficiently once enough potassium has been secreted by neurons. The counterbalancing sodium out pumping levels out as a consequence.

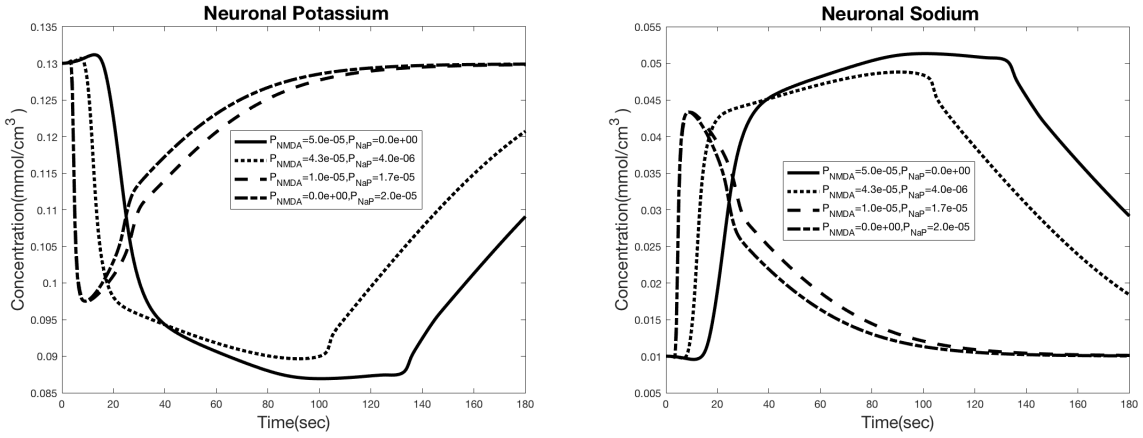

Figure A.4: Time profiles of neuronal potassium and sodium. Potassium leaking levels out and only grows mildly once the NMDA channels begin to shut. The counterbalancing sodium out pumping levels out as a consequence.

A.6.2 Spirals

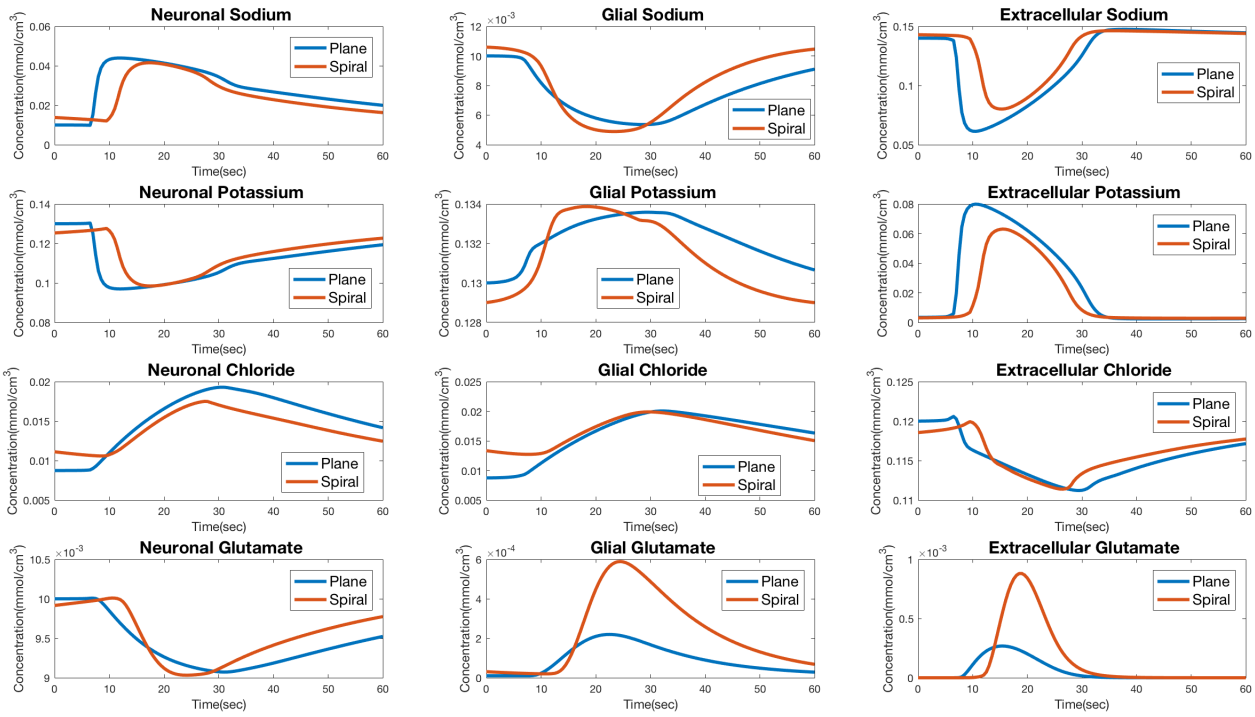

Figure A.5: Comparison between time slices for concentrations during a plane wave and a spiral wave. For the plane wave the results are identical to the 1D simulation except glial potassium attains a higher maximim due to the extra dimension potassium can diffuse in.

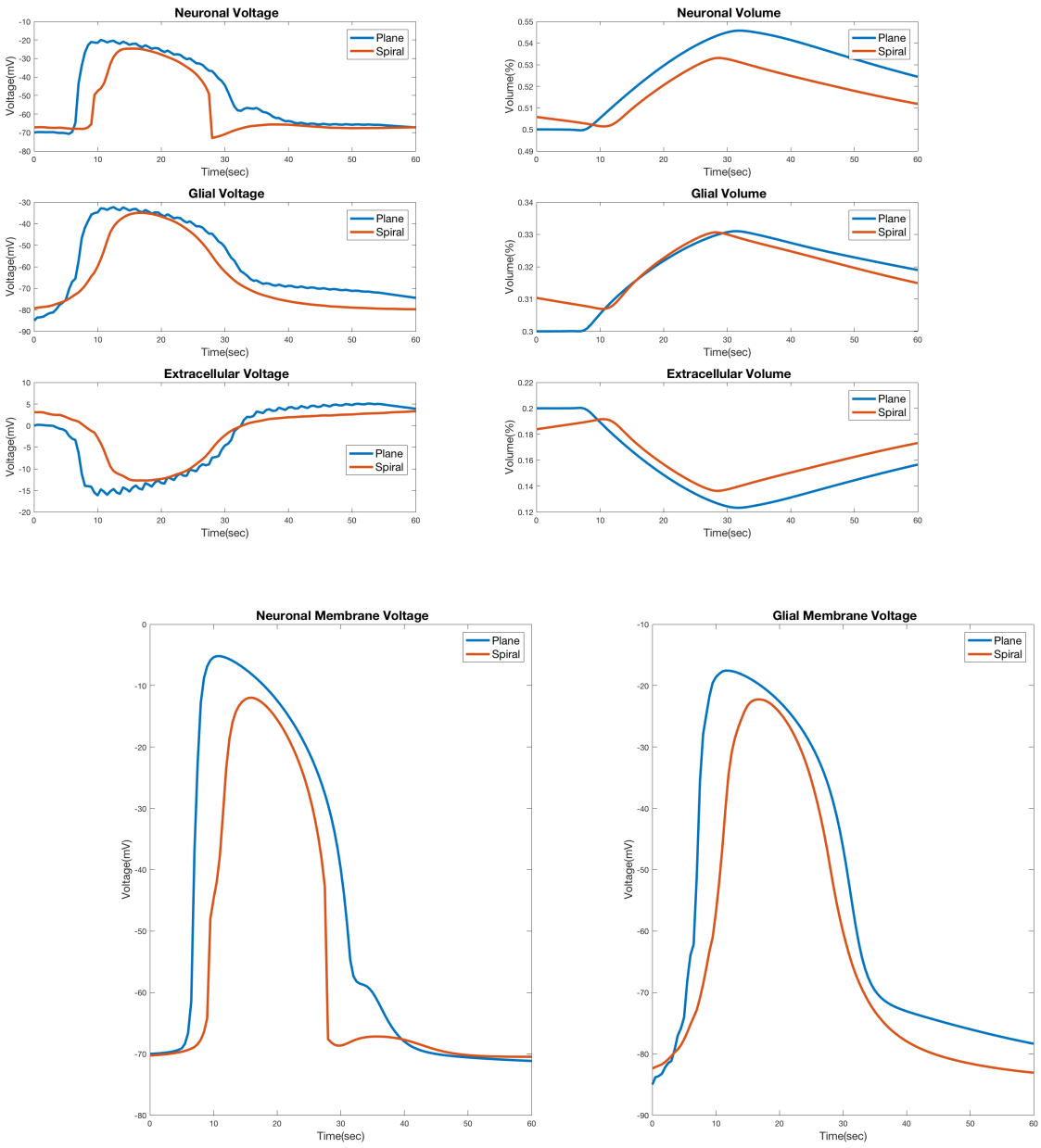

Figure A.6: Comparison between time slices for voltages and volume during a plane wave and a spiral wave.

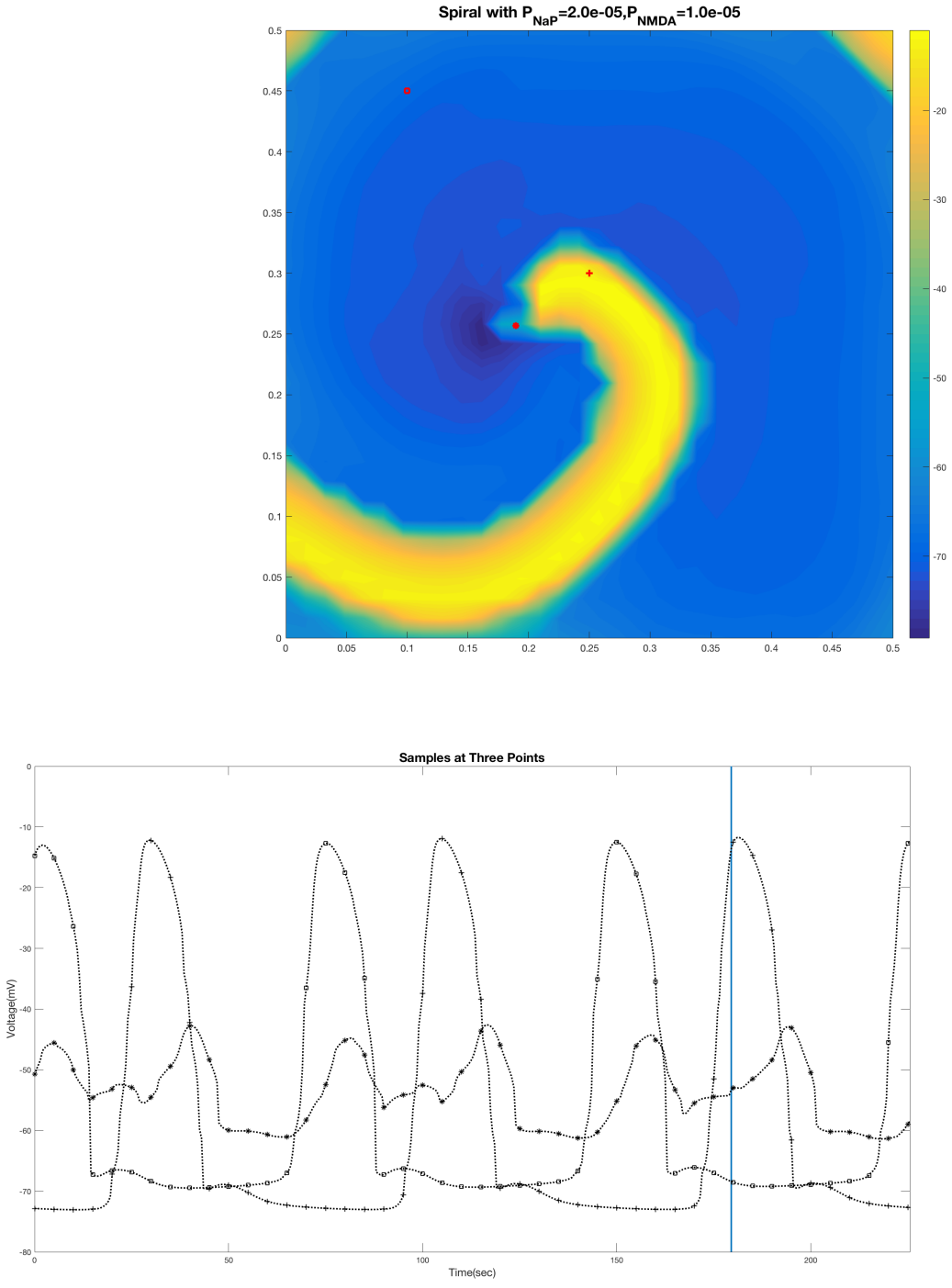

Figure A.7: Spiral driven by NMDA and NaP. Time profiles sampled at 3 points (calculated center, upper left side, and middle right side). Vertical line is the current time of the spiral shown.

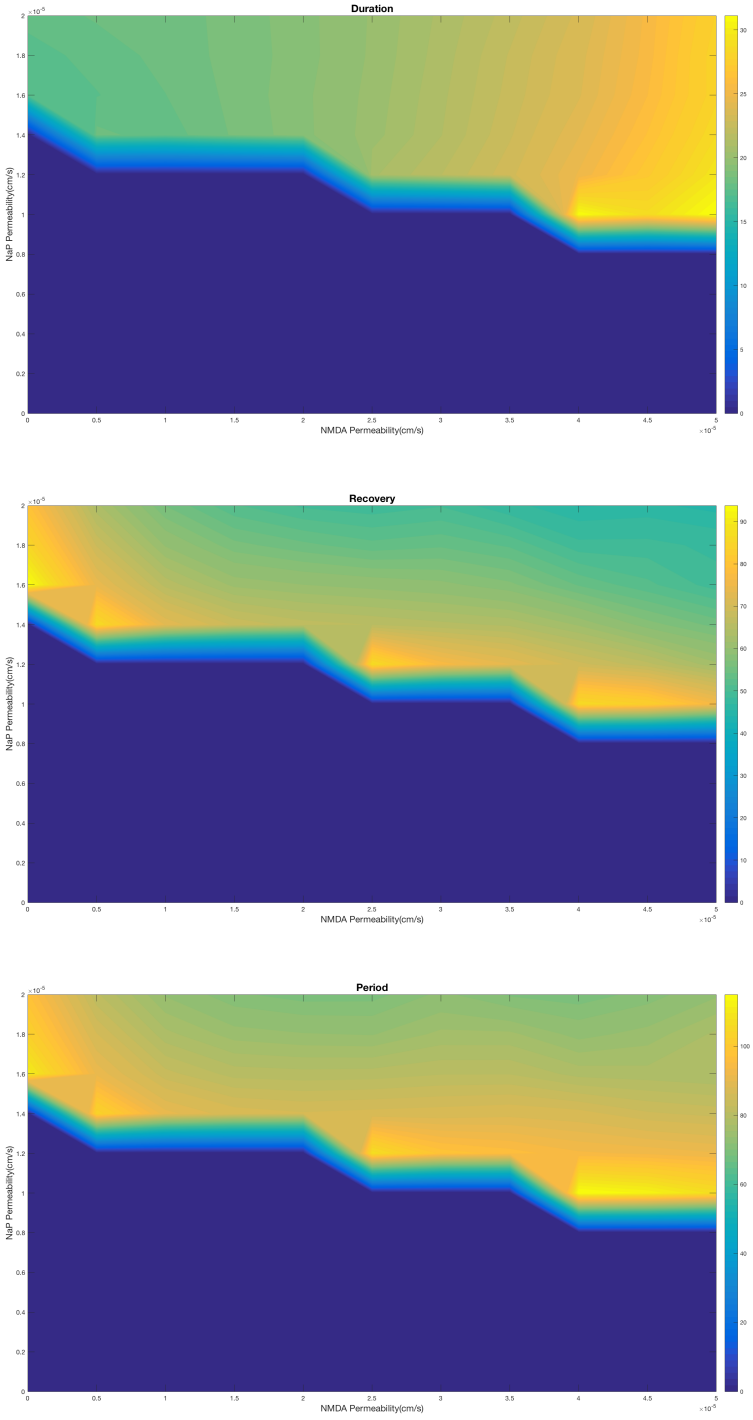

Figure A.8: Dependence of duration, recovery, and period of spirals on NMDA and NaP.